University of Nevada, Reno

Controls of High Grades within the Clementine Vein System in the Hollister Low-Sulfidation Epithermal Au-Ag Deposit, NV

A thesis submitted in partial fulfillment of the requirements for the degree of Master of Science in Geology

by

Joshua M. Smith

Dr. John L. Muntean/Thesis Advisor

December, 2014

THE GRADUATE SCHOOL

We recommend that the thesis
prepared under our supervision by

JOSHUA M. SMITH

Entitled

**Controls Of High Grades Within The Clementine Vein System In The Hollister
Low Sulfidation Epithermal Au-Ag Deposit, Nv**

be accepted in partial fulfillment of the
requirements for the degree of

MASTER OF SCIENCE

Dr. John L. Muntean, Advisor

Dr. Peter G. Vikre, Committee Member

Dr. Thom Seal, Graduate School Representative

David W. Zeh, Ph.D., Dean, Graduate School

December, 2014

Abstract

The Hollister gold-silver deposit is a very well preserved low-sulfidation epithermal system associated with middle Miocene bimodal volcanism related to the Northern Nevada Rift. Over 3,600 kg of gold were mined from volcanic rock-hosted, low-grade, disseminated ore from 2 open pits between 1990 and 1992. Later drilling led to the discovery of blind, high-grade vein systems in underlying Paleozoic rocks, which from 2007 to 2013 produced 10,668 kg (343,574 oz) of gold and 65,998 kg (2,121,555 oz) of silver from ore averaging about 34 g/t Au and 200 g/t Ag. Vein 18, the most productive vein of the Clementine vein system, was studied to document patterns of hydrothermal features around the vein and high-grade shoots within the vein, which can be applied to exploration for other high-grade veins at Hollister and in other epithermal districts. Geological, mineralogical, and geochemical features, including ore and gangue paragenesis; quartz textures; vein forms and structural data; concentrations of ore-related trace elements; and fracture-controlled and pervasive alteration in the surrounding Paleozoic wall rocks were logged from drill core and mapped onto a longitudinal section along, and a cross-section across Vein 18.

Vein 18 is a discrete, open-space filled vein, ranging from 0.15 – 1 meter thick, with local stockwork and breccia. Its paragenesis is characterized by 4 stages: 1) quartz-bladed calcite (replaced by quartz)-adularia-chlorite-pyrite-sphalerite-chalcopyrite-Ag selenides/sulfosalts-electrum; 2) quartz-pyrite-illite-ammonium illite-montmorillonite; 3) quartz-alunite-dickite-kaolinite-specular hematite-marcasite-siderite; and 4) quartz-pyrite veinlets related to a later hydrothermal event. Elevation exerts a strong control on the

gold and silver grades, with the highest grades occurring between 120 and 230 m below the current surface, which is very close to the original paleosurface and/or paleo-water table, as suggested by numerous mercury-bearing sinter and opalite bodies in the district. Boiling was likely the mechanism for ore formation, as evidenced by the strong spatial relationship between high grades and the distribution of bladed quartz after calcite, banded quartz, and adularia. Boiling and Stage 1 ore formation occur in repetitive cycles of pyrite→base-metal sulfides→Ag-selenides→electrum that commonly occur with banded and bladed quartz, separated by periods of largely barren massive quartz. Analyses of vein intercepts indicate a Au, Ag, Se, Cu, Pb, Zn, and Sb association for the ore. Stage 2 interlayered illite-montmorillonite commonly partially or completely replace adularia. Stage 3 is steam-heated alteration, which formed widespread kaolinite and a funnel-shaped zone of alunite±dickite alteration that rooted down on Vein 18, overprinting Stages 1 and 2, likely during lowering of the paleo-water table. $\delta^{34}S$ values of ore-stage pyrite in banded quartz veins range between 4.2 – 4.5‰, whereas those for late stage alunite are between 6.3 – 6.6‰, consistent with a steam-heated origin.

Features that suggest proximity to high-grade ore shoots include: 1) The presence of banded and bladed quartz and adularia; 2) A common paragenesis of quartz textures, which indicates multiple cycles of boiling; 3) Discrete veins that provide significant development of quartz textures; 4) Illite or illite-smectite zones that can reflect original distribution of adularia; 5) Discrete zones of steam-heated alunite, which can define high H_2S flux from underlying zones of upwelling, boiling fluid; and 6) Increases in Se and Cu concentrations.

Acknowledgments

I would like to thank Great Basin Gold (GBG) for granting access to the Hollister deposit and funding this study. GBG geologists and geotechs are greatly thanked for help in sample collection. Robin Solt provided excellent mentorship at Hollister and valuable input on this project. Thank you to Tommy Thompson who taught me the basics of fluid inclusion microthermometry, and to Jean Cline and Wyatt Bain, who provided access to and help with the UNLV heating-freezing stage. Thank you to Jeff Hedenquist, Stuart Simmons, and Jim Saunders, who provided helpful input. An SEG student research grant also partially funded this research. Thank you to my advisor, Dr. John Muntean, at the Nevada Bureau of Mines and Geology, for setting up this project and always pushing me to do my best. Thank you to Dr. Peter Vikre for acting as a second advisor, reviewing manuscripts, providing supportive conversations and suggestions, and sharing data from Hollister. Thanks to Dr. Thom Seal for reviews of manuscripts and providing my first experience with metallurgy. Lastly, thank you to Courtney Lafond and Mona Smith for constant support and encouragement.

Table of Contents

List of Tables:

List of Figures:

Introduction

Epithermal deposits are a major source of the world's gold and silver, accounting for approximately 6% of all gold and 16% of all silver that have been produced in the world (Singer, 1995). Epithermal deposits, including bonanza-grade vein deposits, have been important producers of gold and silver in Nevada since the discovery of the Comstock Lode in 1859. Since the 1970s, extensive studies of epithermal deposits and their modern geothermal analogues have lent great insight to their vertical and lateral extent, as well as processes and fluids controlling mineralization (e.g., Hedenquist and Browne, 1989; Simmons and Browne, 2000; Sillitoe and Hedenquist, 2003; Simpson and Mauk, 2007). Recently low-tonnage, high-grade vein deposits have become appealing exploration targets for junior mining companies in the Great Basin, due to the successful mining of the Midas low-sulfidation epithermal vein deposit over the last 15 years. This renewed interest in bonanza-grade vein systems led to the discovery of high-grade veins in other low-sulfidation systems in Nevada, such as at the Fire Creek and Hollister deposits.

Low- and intermediate-sulfidation epithermal deposits typically occur as quartz ± adularia veins with Au-Ag and base-metal sulfides, and are variably enriched in elements such as Te, Se, As, Sb, and Hg, in addition to others (Simmons et al., 2005; Sillitoe and Hedenquist, 2003). Low sulfidation deposits are commonly Au-Ag dominant with low base metal contents, and intermediate-sulfidation systems typically contain more Ag, Pb, and Zn, with lesser Au. High-grade vein deposits in low-and intermediate-sulfidation systems are typically hosted in high-angle faults with strike lengths of 500 to 3000 m, and

commonly extend 100 to 500 m down dip. Most examples are less than 10 m thick (Buchanan, 1981; Simpson and Mauk, 2007), although some world-class systems, such as the Veta Madre in Guanajuato, Mexico, can be up to 30 m thick (Moncada et al., 2012). Alteration commonly includes propylitic, argillic, advanced argillic, sericitic, and potassic assemblages, which commonly display zonation around hydrothermal fluid conduits. In the past, most deposits were discovered by encountering ore-grade mineralization at the surface; however, in recent decades discoveries of covered deposits have been made by identifying paleosurface manifestations of underlying epithermal mineralization, such as sinters, hydrothermal eruption breccias, and steam-heated alteration (Simmons et al., 2005; Sillitoe and Hedenquist, 2003; Hedenquist et al., 2000). In the future, exploration success will become increasingly dependent on blind discoveries, warranting an even better understanding of the lateral and vertical zonation of productive epithermal systems and the development of more effective tools that vector towards ore.

Classic examples of high-grade low-sulfidation vein deposits include Hishikari, Japan (~260 metric tons Au) (Izawa et al., 1990), Republic, Washington (~93 metric tons Au) (Fifarek et al., 1996), Cerro Vanguardia, Argentina, (~143 metric tons Au) (Zubia et al., 1999), and Waihi, New Zealand (~199 metric tons Au). The frequency, size, and worldwide distribution of low-sulfidation epithermal deposits warrant detailed study of controls on Au and Ag grades and identification of patterns that vector toward ore. Such detailed studies of low-sulfidation epithermal deposits in the Coromandel Peninsula (Hollinger and Mauk, 2001, 2002; Mauk and Simpson, 2007) and Japan (Shimizu et al.,

1998; Shimizu, 2014) have resulted in better understanding of controls on high-grades in epithermal vein deposits. In the Favona low-sulfidation veins in New Zealand, high Au and Ag grades are associated with the presence of banded and bladed quartz, vein breccias, and illite alteration (Hollinger and Mauk, 2001, 2002). At the Koryu low-sulfidation vein deposit, high-grade ore shoots are associated with a detailed vein "stratigraphy" and increasing textural complexity in banded quartz veins (Shimizu, 2014; Shimizu et al., 1998). Although the literature of Nevada epithermal deposits in the Great Basin of the western United States is extensive, studies on ore controls and vector patterns in geologic and geochemical features surrounding high-grade epithermal vein deposits in Nevada are lacking.

John (2001) pointed out that the types and characteristics of Neogene epithermal deposits in the Great Basin were likely influenced by the variations in the composition, tectonic setting, and eruptive style of the magmatic assemblages. Most low- and intermediate sulfidation epithermal deposits in the Great Basin are related to two magmatic assemblages (Figure 1). The first, referred to as the western andesite assemblage, is associated with stratovolcanoes, dome fields, and subvolcanic plutons formed by hydrous, high-K, calc-alkaline, and oxidized magmas of andesite to dacite composition. These magmas formed by subduction that gave rise to the ancestral Cascades in eastern California and western Nevada. The second assemblage is bimodal basalt-rhyolite magmatism that formed lava flows, dikes, cinder/spatter cones, shield volcanoes, domes and ash-flow calderas during continental rifting. The magmas, of dominantly basaltic or rhyolitic composition, were tholeitic, anhydrous, and reduced.

The objective of this paper is to present patterns of various geologic and hydrothermal features along the Clementine vein system at the low-sulfidation Hollister deposit, with the ultimate goal of developing the patterns into vectoring tools that can be applied to exploration for other high-grade Au-Ag veins on the Hollister property and other bonanza epithermal precious metal vein deposits throughout Nevada and the world. Using a combination of field and laboratory methods, several geologic features were mapped within Vein 18, the most productive vein in the Clementine system, and in the surrounding wallrock, including: 1) gold and silver grades, 2) vein ore and gangue mineralogy and paragenesis, 3) vein quartz textures, 4) vein forms, including strike, dip, and width data, 5) trace element concentrations in the vein, and 6) pervasive and fracture-controlled wallrock alteration. A secondary goal of this paper is to reconstruct in time and space the development of the Hollister epithermal system from new data presented here, as well as previously published data. Better understanding of the processes that formed the mapped features will lead to a better appreciation of which patterns are most valuable to exploration.
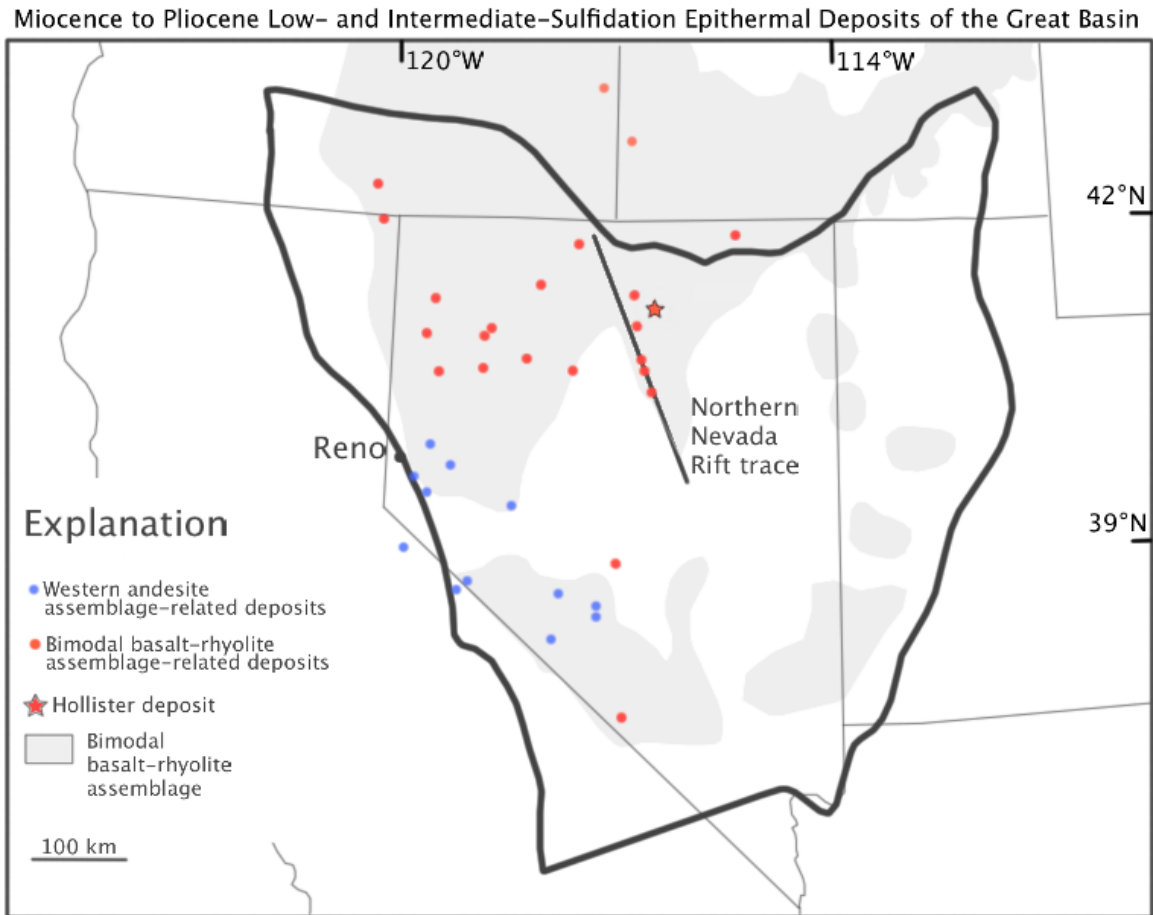
Fig. 1: Location map of the Hollister deposit and other low-sulfidation epithermal deposits of the Great Basin (dark outline). Modified from John (2001).

Hollister Deposit

Exploration and Mining History

The Hollister Au-Ag deposit, is located in the Ivanhoe mining district, in north-central Nevada, approximately 100 km east-northeast of the town of Winnemucca. It occurs along the northwest projection of the Carlin Trend, just outside the eastern margin of the Northern Nevada Rift (NNR). This area of the Great Basin hosts several other

low-sulfidation epithermal gold-silver deposits that are almost all of middle Miocene age (17.3 – 14.8 Ma) (John, 2001, and references therein). These deposits, are associated with bimodal basalt-rhyolite volcanism related to progression of the Yellowstone hot spot and the formation of the Northern Nevada Rift (John, 2001). Other middle Miocene, low-sulfidation epithermal deposits of the northern Great Basin include Midas (Leavitt et al., 2000; Goldstrand and Schmidt, 2000), Sleeper (Nash and Trudel, 1996), Buckskin-National (Vikre, 1985), DeLamar (John, 2001), Mule Canyon (John et al., 2003), Hog Ranch (Halsor et al., 1988), and Jarbidge (Coats, 1964).

Mercury mining in the Ivanhoe district began in 1915, and continued periodically until 1943. This work focused on mercury-bearing sinter and replacement bodies and produced 2,180 flasks of Hg from the Butte #1, Butte #2, Velvet, and Clementine mines (Wallace, 2003). Total production through 1943 was approximately 3000 flasks (Bartlett et al., 1991). Exploration resumed in the 1960s, initially for Hg, then for uranium and porphyry molybdenum in the 1970s and early 1980s, and then for gold deposits, beginning with exploration by Homestake Mining in 1979. Between 1980 and 1986, US Steel Corporation (USSC) extensively explored the property for epithermal mineralization, which included an extensive drill program between 1982 and 1986 (Bartlett et al., 1991). Through a joint venture, Cornucopia and Galactic acquired the property by 1987, and soon defined a resource of ~18 Mt, averaging 1.2 g/t Au as open-pittable volcanic rock-hosted mineralization. From 1990 to 1992, two open pits in the USX zone produced > 115,000 oz of gold (Wallace, 2003). From 1992 to 1997, Newmont Mining explored the area for epithermal veins and intercepted a number of

high-grade epithermal Au-Ag veins in Paleozoic rocks underlying the Miocene volcanic rocks, but these intercepts were not followed up (Oelofse et al., 2011).

In 1997, Great Basin Gold, Ltd. acquired the property and focused on exploring for and developing these blind, high-grade vein systems (Oelofse et al., 2011). From 1997 to 2001, Great Basin Gold successfully delineated the Clementine and Gwenivere vein systems, after turning drill rigs to explore for WNW trending vein systems, rather than for NNW veins parallel to the axis of the NNR. By October 2001, Great Basin defined a vein deposit of 719,000 metric tons of ore, averaging 40.3 g/t Au and 240 g/t Ag (press release Great Basin Gold, October, 2001). Between 2002 and 2007, Hecla undertook an underground drill program of several hundred core holes. In 2007 Hecla relinquished its option, and beginning in that year Great Basin Gold mined the Hollister vein systems, producing nearly 345,000 ounces of Au and 2.1 million ounces of Ag until mining ceased in 2013 when Waterton Global Mining acquired Hollister. Proven and probable reserves at the beginning of 2013 stood at 516,000 tons of ore at average grades of 0.882 opt Au and 2.9 opt Ag.

Pre-Miocene District Geology

The geology of the Ivanhoe district was most recently described by Wallace (2003) (Figure 2). The oldest rocks exposed in the Ivanhoe District are Ordovician basinal siliciclastic rocks of the Vinini Formation, one of the formations that comprises the upper plate of the Roberts Mountain thrust fault. During the late Devonian to early Mississippian Antler Orogeny (Roberts et al., 1958), basinal rocks were thrust eastward over younger slope to shelf facies carbonates. The Vinini Formation hosts the high-grade

Hollister vein systems. In the Ivanhoe district, it is composed of isoclinally folded argillite, siltstone, and quartzite. The deformed Vinini Formation was subsequently folded to form a crescent-shaped anticline, which trends NE-SW in the Hollister area and NW-SE in the northern portion of the district (Bartlett et al., 1991). Two deep core holes pierced the Roberts Mountain thrust and intercepted variably calcareous mudstones and sandstones of the Devonian Rodeo Creek Formation in the lower plate at a depth of ~300 m. One of the holes was drilled through the Rodeo Creek, into muddy carbonates of likely the Devonian Popovich Formation, and into the silty carbonate rocks of the Devonian-Silurian Roberts Mountain Formation and Silurian-Ordovician Hanson Creek Formation, in which the hole was stopped at a depth of 2,115 m (Oelofse et al., 2011).

Intruding the Vinini Formation is a granodiorite porphyry stock of Eocene age, known as the Hatter stock. The stock crops out in a small area east of the Hollister deposit, and exceeds 1.8 km by 1 km in the subsurface. The stock contains plagioclase, quartz, and bioitite phenocrysts in a fine-grained groundmass of quartz and alkali feldspar. It has been dated by K-Ar at 39 Ma (Oelofse et al., 2011). The stock locally hosts epithermal veins similar to those in the Hollister deposits.

Miocene volcanism, hydrothermal activity, and faulting

Middle Miocene volcanic rocks dominate the surface exposures in the Ivanhoe district, including basaltic andesite lavas and dikes, and rhyolitic lavas, domes, and tuffs. Igneous activity at Hollister occurred between 16.5 – 14.0 Ma (Wallace, 2003) and is part of the bimodal basalt-rhyolite assemblage related to the Northern Nevada Rift. However, Hollister is situated outside of the rift several kilometers east of the rift margin. Wallace

(2003) described in detail the Miocene rocks in the Hollister area and summarized new and previously published $^{40}Ar/^{39}Ar$ and K-Ar dates on adularia, sanidine, and plagioclase. The Miocene history outlined in Wallace (2003) is summarized here.

Lacustrine sedimentation in the northern Ivanhoe district began 16.5 – 16.0 Ma, forming a thick sequence of volcaniclastic sedimentary rocks, known as the lower tuff. This was followed by eruption of the Rock Creek flow-banded rhyolite in the western and northwestern portions of the Ivanhoe district, at about 16 Ma, which created a subaerial topographic high along the western margin of the lake. Continued sedimentation expanded the margins of the lake, south to the area of the Hollister mine, where thinning of the lower tuff to 0-30 m suggests the mine area was a topographic high. Around 15.4 Ma andesitic flows erupted in the western part of the Ivanhoe district. These flows were deposited subaerially on both the lower tuff unit and the Vinini Formation.

After eruption of andesite, continued widespread lacustrine sedimentation formed what is locally referred to as the middle tuff. The middle tuff locally contains siliceous sinter deposits. At 15.1 Ma, a 10 m thick vitric tuff was deposited subaerially over much of the Ivanhoe district, forming a distinct marker unit. Eruption of the vitric tuff was followed by another episode of lacustrine sedimentation. In addition, several local volcanic and hydrothermal events occurred in the Hollister area between 15.2 and 15.0 Ma. Starting at 15.16 and continuing to 14.92 Ma, voluminous rhyolite flows, including the Craig and Velvet rhyolite were emplaced east and southeast of Hollister. Adularia from a high-grade vein in the Hollister deposit indicates mineralization began by 15.19 Ma (Peppard, 2002). Silicification and mercury mineralization in portions of the middle

and vitric tuffs indicate mineralization occurred at least periodically through 15.1 Ma. Adularia from disseminated mineralization hosted by the middle tuffs in the open pits at Hollister was dated at 15.1 ± 0.4 Ma, indicating the disseminated deposit and high-grade veins formed from the same hydrothermal system (Wallace, 2003). East of Hollister, the Velvet rhyolite and upper tuffs are also silicified and make up the Upper Silicified Zone, which postdates vein and disseminated mineralization at Hollister (Peppard, 2002).

Minimal offset, high-angle normal faults, which host the Hollister vein systems, began to form by at least 15.2 Ma. These faults initially left the paleosurface undisturbed. Between 15.1 and 14.4 Ma, significant faulting began to affect the paleosurface, which was tilted up to 25° (Wallace, 2003). Sedimentation continued until at least 14.4 Ma, but under increasing fluvial rather than lacustrine conditions. At 14.92 Ma, rhyolite porphyry domes erupted north of the Hollister area. Thus, between 15.1 and 14.4 Ma, the Ivanhoe district had lakes, streams, and highlands underlain by Vinini Formation, Craig and Velvet rhyolite, tuffaceous sediments, and rhyolite porphyry domes.

The interpreted volcanic and hydrothermal history is similar to the history of the Midas district and its high-grade veins located ~20-25 km northwest of Hollister. Lacustrine sediments, referred to as the Esmeralda formation at Midas (Wallace, 1993: Goldstrand and Schmidt, 2000), likely represent the fringe of the Ivanhoe paleo-lake. At both Midas and Hollister, rhyolite flows and domes erupted during mineralization, though high-grade vein mineralization and rhyolitic volcanism at Midas occurred between 15.6 and 15.2 Ma (Leavitt, et al., 2004).

Geologic Map of the Hollister Deposit
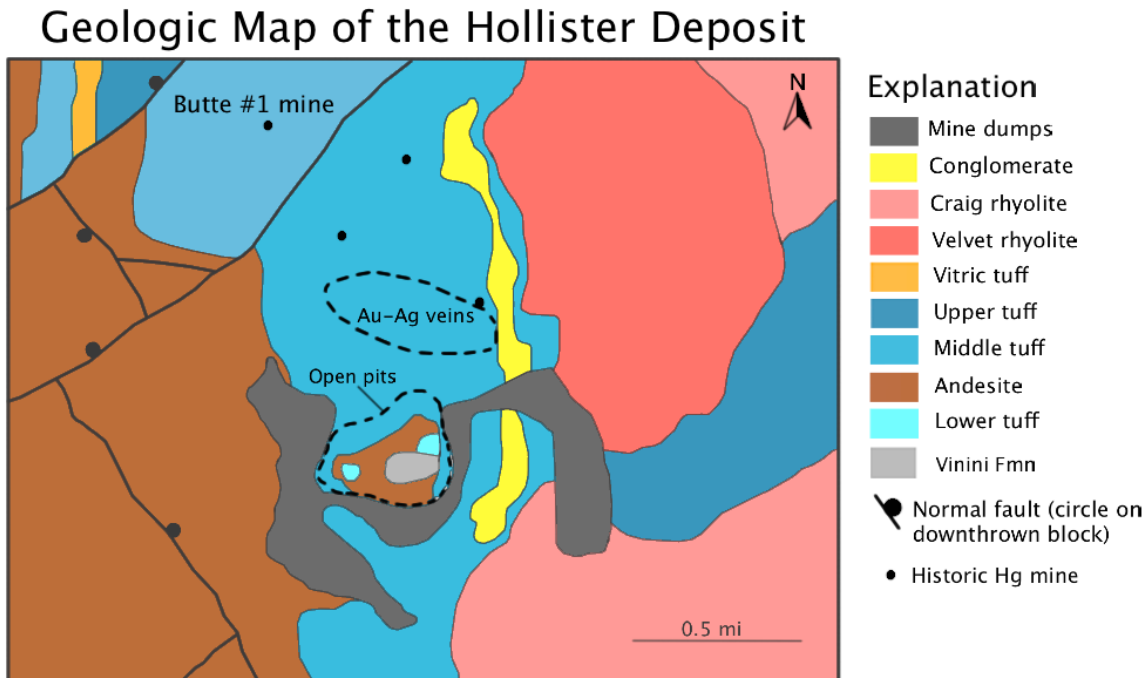
Fig. 2: Geologic map of the Hollister deposit and surrounding area. Modified from Wallace, 2003.

Volcanic-hosted Au-Hg mineralization

The Hollister open pits to the south of the known vein systems (Figs. 2,3) represent the discovery defined by U.S. Steel Corporation in the 1980s (Bartlett et al., 1991). In the pits, the deposit shows a vertical zonation from the gold deposit to overlying Hg replacement deposits. Disseminated Au mineralization likely occurred at and below the paleowater table, while sinter deposits formed from the same ore-bearing fluid at groundwater outflow points. Replacement Hg deposits, on the other hand, formed above the paleowater table in a vapor-rich, steam-heated environment (Hollister et al., 1992). Such deposits are also reported in the Sulphur district, and likely formed from the same mechanism (Ebert and Rye, 1997). Replacement deposits typically

underlie sinter at Hollister, which likely reflects a drop in the paleowater table (Wallace, 2003).

Mercury deposits are hosted in sinter and underlying silicified horizons. These zones consist of cinnabar, quartz, chalcedony, and opal (Peppard, 2002). Surface vents associated with bedded sinter deposits have been identified at the old Butte #1 Hg mine (Fig. 2) (Wallace, 2003). Replacement Hg deposits are present in the upper portions of the middle tuff and are associated with a laterally extensive silicified horizon. This horizon hosts Hg mineralization at the Butte #1, Butte #2, Velvet, and Clementine Hg mines, north of the Hollister pits (Wallace, 2003).

Disseminated gold mineralization occurs in altered Miocene volcanic units beneath Hg-bearing silicified zones in the Hollister open pits. Other zones of volcanic-hosted, disseminated gold are also known to exist beneath near-surface Hg mineralization at the Clementine, Velvet, and Butte #1 mines, north of the Hollister pits. Average grades in the Hollister open pits were ~1.2 g/t Au (Bartlett et al., 1991). The Hollister disseminated gold deposit underlies a silicified horizon of the middle tuff, which is associated with replacement Hg mineralization (Bartlett et al., 1991; Hollister et al., 1992). Gold in the Hollister disseminated deposit is hosted in the middle and lower tuff units and locally extends downward into the Vinini Formation. In the open pits, the lower tuff hosts much of the disseminated gold ore. Shallow, mineralized tuffs are generally oxidized, while preserved unoxidized parts of the ore body are typically restricted to andesite flows. Unoxidized mineralization in the open pit is characterized by electrum, pyrite, quartz, chalcedony, and adularia (Deng, 1991). Adularia from this

mineralization was dated by K-Ar at 15.1 ± 0.4 Ma (Bartlett et al., 1991). Alteration of

the volcanic sequence produced adularia, montmorillonite, nontronite, chalcedony,

chlorite, pyrite, and marcasite, with lesser sericite, kaolinite, and alunite. Silicification is

observed along faults and fractures, although open space-filled quartz veins in the

Miocene rocks are uncommon (Bartlett et al., 1991). The disseminated gold ore body is

largely coincident with the broad, crescent-shaped paleotopographic ridge developed at

the top of the Vinini Formation. Most high-grade zones are hosted at fault intersections

or in favorable volcanic units (Bartlett et al., 1991).

Fig. 3: Perspective view of the USX East and West pits, looking WSW. Modified from
Oelofse et al., 2011. Buried vein systems are to the right of the open pits and off the
photograph.

Basement-hosted quartz vein mineralization

As pointed out above, Au and Ag production from 2007 to 2013 was predominantly from high-grade, Au-Ag bearing quartz-adularia veins of the Vinini Formation, which intersect the base of the Miocene volcanic sequence (Oelofse et al., 2011), where some Au grades have been encountered as high as 2,500 opt (Great Basin Gold, press release, 2010). A $^{40}Ar/^{39}Ar$ date on adularia from one of the high-grade veins is 15.19 ± 0.05 Ma (Peppard, 2002), within error of the K-Ar date on adularia from the open pit. The main vein systems, the Clementine and Gwenivere systems, are ~ 1 km north of the Hollister open pits. Great Basin Gold and Touchstone Resources have also shown that the Tertiary volcanic rocks are anomalously elevated with respect to Au content where they directly overlie the high-grade veins.

Methods

Vein material and immediate wallrocks along Vein 18 were investigated by first logging ~ 200 m of vein intercepts from 37 holes drilled along eleven cross-sections spaced ~100 m apart. The elevation of the sampled vein intercepts ranges from 1446 to 1687 m. From those sections, 149 samples of vein material and adjacent wallrock from the 37 intercepts of Vein 18 were described with a binocular microscope. Along a separate cross-section, drill core from the entire length of five core holes were logged, and from which 581 samples of hanging wall rocks, vein material, and footwall rocks were collected. From the samples, 97 polished thin sections were prepared and inspected.

Also, doubly polished fluid inclusion plates were prepared from 3 samples of quartz vein material from a single cross-section of Vein 18.

In addition, 25 remaining pulps from the 37 vein intercepts were analyzed for 48 elements by ALS Minerals using a four-acid digestion followed by ICP-MS. Peter Vikre analyzed two serially cut sinter samples, perpendicular to bedding, for 17 elements using LA-ICP-MS at the U.S. Geological Survey laboratories in Denver, Colorado. Whole rock analyses were performed on two sinter samples. Three samples of pyrite and three samples of alunite were separated for sulfur isotope analyses, performed at the Nevada Stable Isotope Laboratory at the University of Nevada, Reno. Furthermore, 289 samples of vein material and wallrock were analyzed with an ASD Terraspec reflectance spectrometer to identify clay and sulfate minerals detectable in the SWIR range of wavelengths.

Description of the Clementine Vein System

The most strongly developed vein systems at Hollister are the Clementine and Gwenivere systems. Veins occur in both the Tertiary volcanic rocks and the underlying Ordovician Vinini formation, where they are better developed. They have an average strike of ~ 280°; are continuous for at least 1,400 m along strike; are 0.1 – 1 m thick; have near-vertical dips; and extend at least 450 m down dip. Veins have been encountered between 1720 m and 1297 m elevation. Limited drill data indicate weakly mineralized veins are open at depth. The Clementine system commonly consists of thin,

discrete veins and vein breccias, whereas the Gwenivere system is commonly characterized by anastamosing zones of stockwork. The western part of the Gwenivere system converges with the veins of the Clementine system. Prior to mining stopping, the cut-off grade was 8.5 ppm Au, while average ore grades were approximately 34 ppm Au and 200 ppm Ag.

The Clementine vein system consists of veins 14 – 22, with Vein 18 having been the most productive vein at Hollister. It strikes 280°, dips nearly vertical, and typically is 0.15 – 1 meter wide (Figures 4, 5). Vein 18 is dominantly hosted in the Vinini Formation and is comprised of discrete veins, vein breccias, and, less commonly, stockworks. Minor replacement structures represent the extension of Vein 18 into the volcanic rocks (Figure 6). These replacement structures consist dominantly of quartz, which replaces and floods into volcanic rocks. These replacement veins have approximately the same strikes and dips as the underlying veins and are confined to one to two meter wide intervals at the bottom of the volcanic sequence and transition into the silicified horizons and disseminated gold deposits in the shallower parts of the volcanic sequence. Vein 20 has also been a significant Au producer and shares textural, mineralogic, and structural characteristics with Vein 18 (Figure 5). Vein 17 is also part of the Clementine system and is commonly found within meters of, or anastamosing with, Vein 18 (Figures 5, 7, 8); However, it contains significantly less Au and Ag mineralization than Vein 18. The Clementine vein system partially underlies the original Hollister open pit resource, which was never mined (Bartlett et al., 1991).
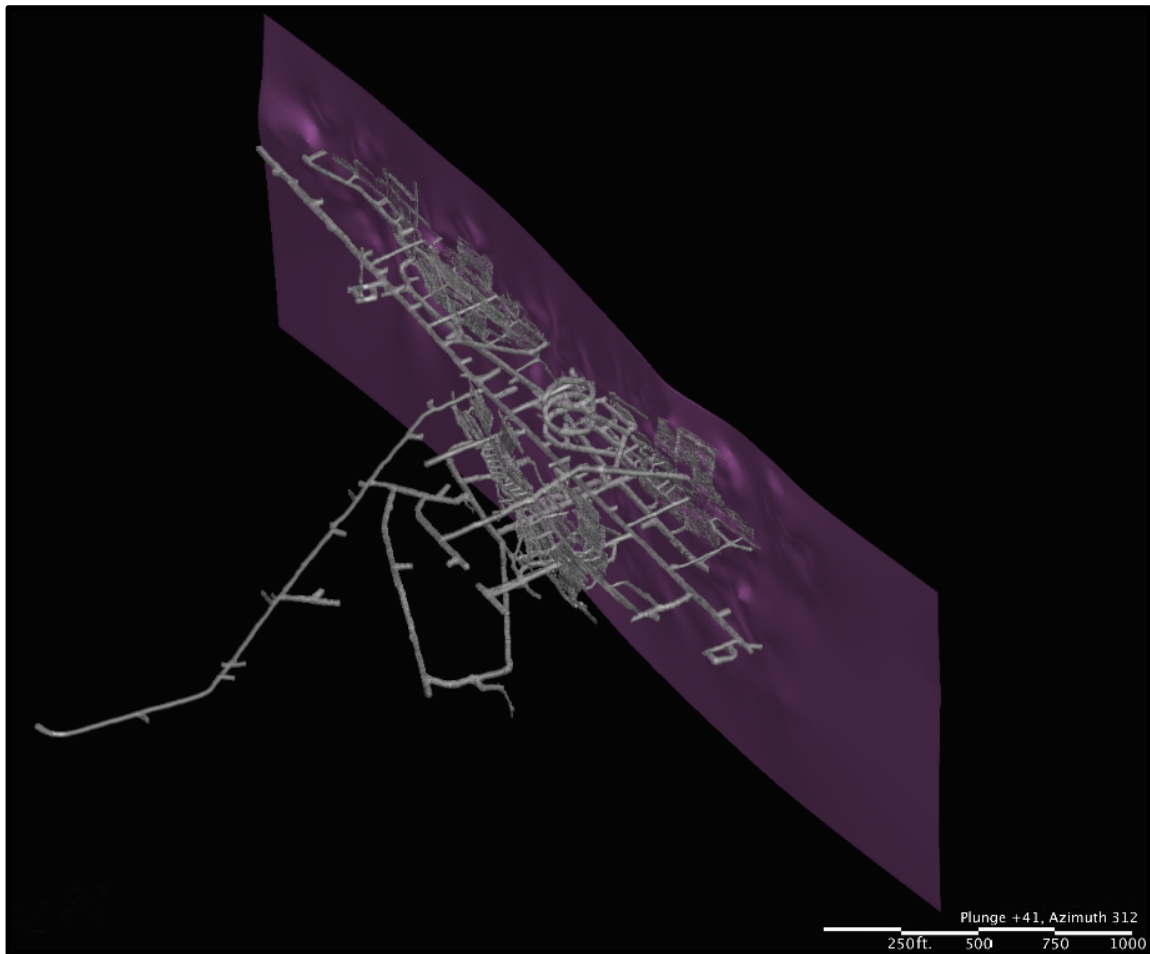
Fig. 4. Oblique view of Vein 18 (purple) and current underground workings (gray) looking down to the northwest, as modeled by Great Basin Gold, Ltd using Leapfrog software.

Fig. 5: Geologic cross-section through the Hollister deposit, based on five underground drill holes. Vein 18 likely transects the Tertiary-Ordovician unconformity based on modeling and other drill hole data.
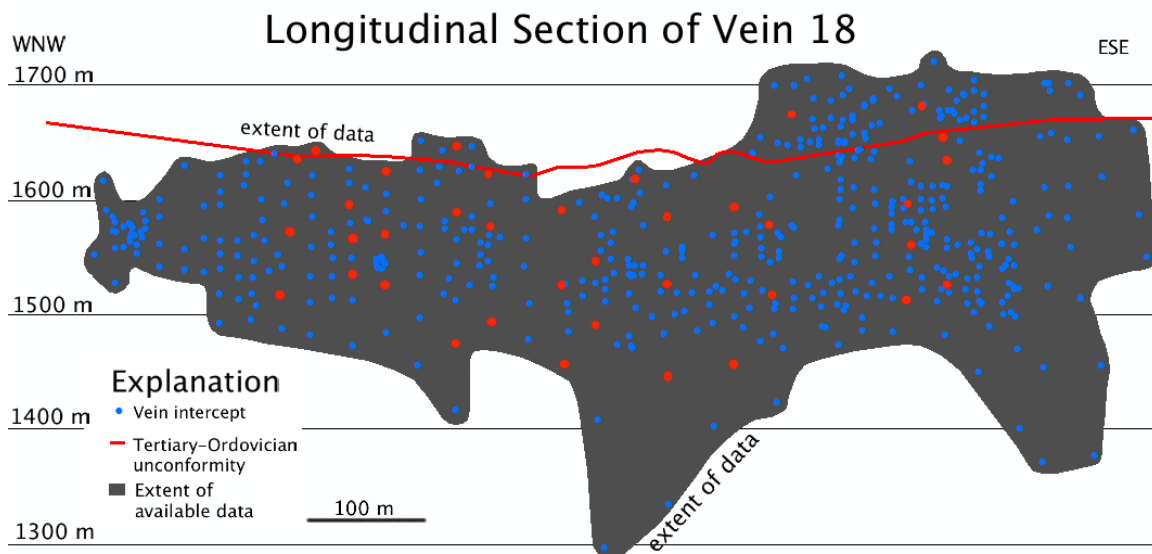
Fig. 6: Longitudinal section of Vein 18 from the Clementine vein system. Red dots represent intercepts sampled in this study. The current extent of Vein 18 data is defined by available drilling, and is likely open at depth and to the east and west.
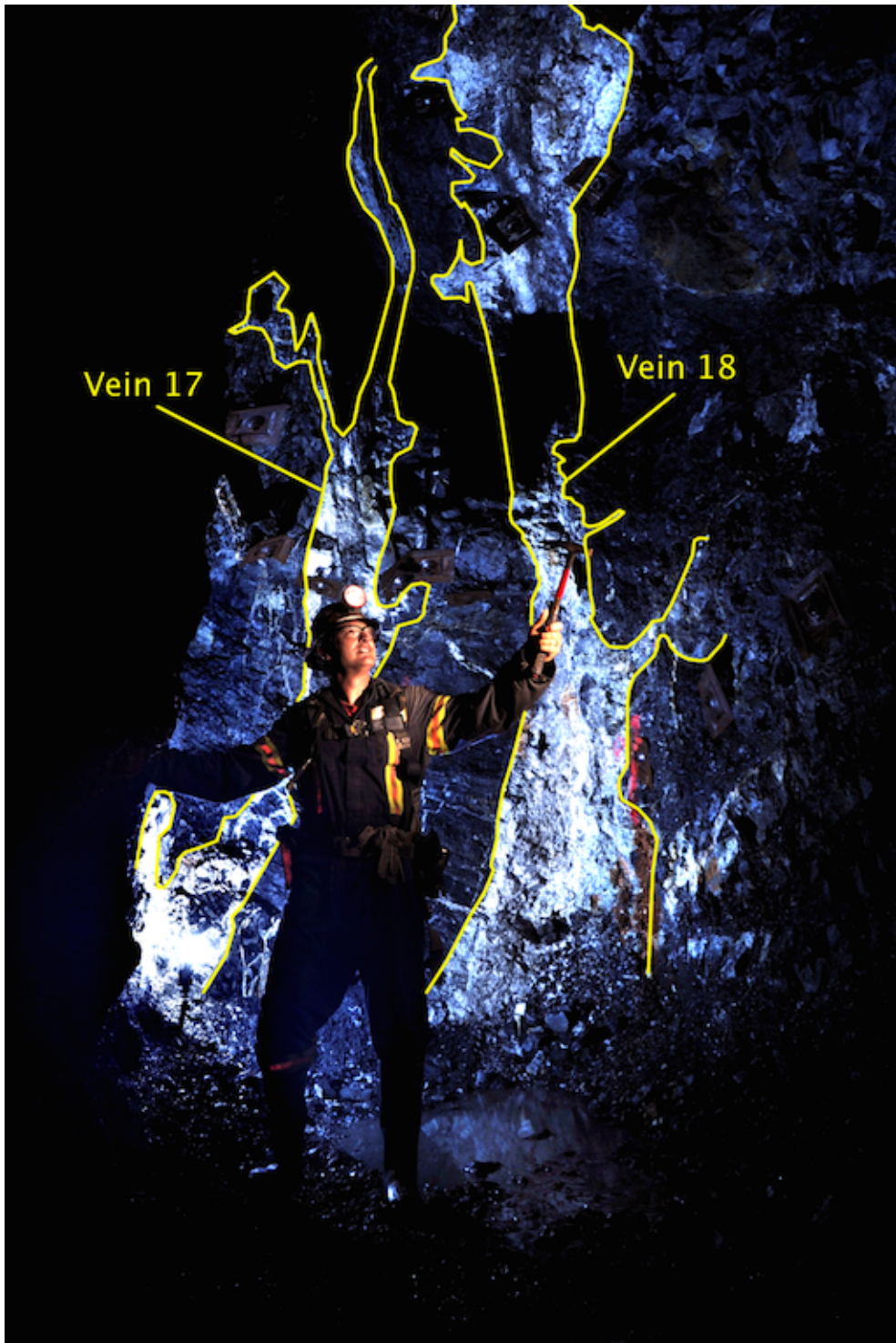
Fig. 7: Underground image of Veins 17 and 18 at Hollister.

Fig. 8: Underground image of Vein 18 with Vein 17 to the left. Note the brecciation throughout the right part of Vein 18.

Description of Wall Rock

The Clementine vein system is almost entirely hosted by the Vinini Formation, which can be characterized by two lithologic sequences – a quartzite dominant sequence and an argillite-dominant sequence composed of predominantly of interbedded argillite and argillaceous siltstone (Figures. 5, 9). Siltstone occurs locally in both sequences. Bedding thicknesses range from millimeters to meters in thickness.

Unaltered quartzites are composed of 90 – 95% rounded, detrital quartz grains ~ 0.1 to 0.3 mm in diameter. Interstices are filled with dark clay and framboidal pyrite (5 –

10%). Siltstones are mineralogically and texturally similar to quartzites, but with finer grained quartz (~50-100 μm). Argillites are mudstones and shales composed of dark clays and carbonaceous material. Argillaceous siltstones are composed of ~60 % clays and 40 % detrital quartz silt. Both argillite and argillaceous siltstone contain significant amounts of framboidal, diagenetic pyrite (1 – 2 %).

Fig. 9: Drill core showing quartzite and argillite of the Vinini Formation.

Description of Vein Mineralization

At least 4 stages of vein mineralization can be identified in Vein 18 (Table 1),
each of which display a variety of hydrothermal quartz textures. Mineral paragenesis,
quartz textures, and vein forms are described below.

Stage 1 is characterized by quartz-bladed calcite-adularia-chlorite-pyrite-
sphalerite-chalcopyrite-Ag selenides/sulfosalts-electrum. Bladed calcite has
subsequently been replaced by microcrystalline quartz during stages 1 or 2. Adularia is
found as alternating bands with quartz and ore minerals, filling and lining cavities in
bladed quartz, and filling and lining vugs in other quartz textures. Textures indicate ore
minerals were deposited in cycles of pyrite (oldest) → chalcopyrite/sphalerite → Ag-
selenides/sulfosalts → electrum (youngest); however, cycles commonly vary in the
amount of Au and Ag deposition. Cycles are hosted as bands of ore minerals separated
by bands of quartz-adularia without ore minerals; encrustations on bladed quartz after
calcite; and pods in quartz veins and vein breccias (Figure 10). Similar ore-stage
parageneses have been documented at Guanajuato in Mexico (Petruk and Owens, 1974),
Camoola Reef in New Zealand (Main et al., 1972), and Koryu in Japan (Shimizu et al.,
1998). Microprobe analyses of ore minerals by Peppard (2002) also identified the minor
phases argentotennantite $[(Ag,Cu)_{10}(Zn,Fe)_2(As,Sb)_4S_{13}]$, arsenopyrite $[FeAsS]$,
tetrahedrite $[(Cu,Fe)_{12}Sb_4S_{13}]$, aguilarite $[Ag_4SeS]$, clausthalite $[PbSe]$, and giraudite
$[(Cu,Zn,Ag)_{12}(As,Sb)_4(Se,S)_{13}]$, which are part of Stage 1 mineralization. Peppard
(2002) reported high Se concentrations in many ore-stage sulfides, including pyrite (1.05
wt % Se), sphalerite (1.32 wt % Se), and tetrahedrite (1.42 wt % Se). Stage 1 accounts

for nearly all Au-Ag mineralization in the Clementine system and occurs throughout the known vertical extent of the vein (~1297 – 1720 meters).

Stage 2 is characterized by granular and drusy quartz, pyrite, and illite, ammonium illite, and minor montmorillonite, in which illite and montmorillonite formed by replacement of adularia (Figure 11). Fine-grained bands of quartz-adularia are typically replaced by illite with minor pyrite. Drusy quartz lines vugs and other open spaces formed during Stage 1, with individual quartz crystals ranging from 0.5 – 1 mm in length. Stage 2 occurs throughout the vertical extent of Vein 18, but there is no evidence for additional Au-Ag during Stage 2.

Stage 3 is vertically zoned and consists of quartz – alunite – dickite – specular hematite – marcasite – siderite (± kaolinite ± electrum ± Ag-selenides) (Fig. 12). Above the Tertiary unconformity, Miocene volcaniclastic rocks are replaced by quartz and minor alunite, dickite, and kaolinite. Larger volcanic fragments have been leached and replaced by alunite and minor dickite ± kaolinite. In the Vinini Formation, the extent of Stage 3 progressively becomes more restricted to Vein 18 with depth. In Vein 18, quartz-alunite veinlets cross-cut Stage 1 (Figure 21B), and vug-filling alunite postdates Stage 2 drusy quartz (Figure 14). Alunite has also locally replaced adularia. Sulfides near alunite are typically oxidized, but earthy and specular hematite, marcasite, naumannite, and electrum locally occur with alunite. In thin section, the ore minerals are surrounded by quartz, alunite, and minor kaolinite. Stage 3 marcasite is uncommon, but where it occurs, is typically intergrown with kaolinite and only minor alunite. Quartz-alunite wallrock alteration is observed in the upper parts of the Vinini Formation and throughout the

Tertiary volcanic rocks. Quartz-alunite alteration in the Vinini formation is typically limited to the contact between Vein 18 and wallrock, where primary argillite clays are altered to alunite with minor kaolinite and dickite. Below an elevation of 1508 m, alunite was not observed. Rather, late quartz and siderite are commonly present at depth. The deep siderite is commonly found as fine-grained, botryoidal overgrowths on Stage 2 drusy quartz crystals. Where quartz-siderite veinlets are hosted in quartzites, they are commonly associated with planar to oval-shaped dissolution features.

Stage 4 consists of quartz – pyrite veinlets, which cross-cut all the previous stages in the Clementine system, including alunite-bearing Stage 3 mineralization (Fig. 13). Veinlets are typically < 1 cm thick and are composed of drusy and granular quartz with slightly later pyrite. These quartz-pyrite veinlets are present throughout the known vertical extent of the Clementine vein system, and cross-cut both Vein 18 and vein structures in the overlying volcanic rocks.

Stage 1 veins with mineralized bands, encrustations, and vugs; occurs as repetitive cycles	quartz, calcite, adularia, pyrite, sphalerite, chalcopyrite, naumannite, electrum, Ag-sulfosalts, chlorite
Stage 2 adularia altered to illite and pyrite; quartz, illite, pyrite veinlets cross-cutting stage 1	quartz, illite, ammonium illite, montmorillonite, pyrite
Stage 3 quartz-alunite replaced volcaniclastic rocks and vein adularia; quartz-alunite veins (<3 cm) cross-cut Vein 18; open spaces filled with drusy quartz and botryoidal siderite	quartz, alunite, dickite, kaolinite, naumannite, electrum, siderite, marcasite,
Stage 4 quartz-pyrite veins (< 3 cm thick) cross-cut all other assemblages	quartz, pyrite

Table. 1: Mineralization stages observed in Vein 18.
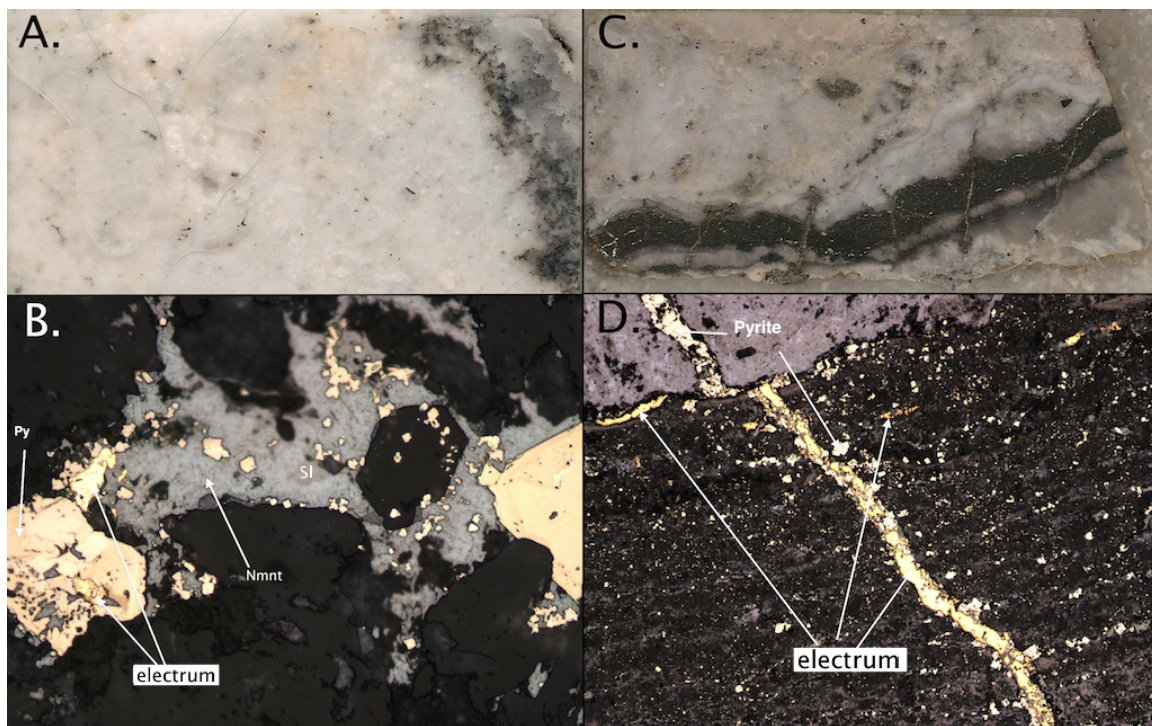
Fig. 10: Thin section billet (A) and photomicrograph (B) of sample 44-QV3, displaying and single cycle of typical stage 1 paragenesis (pyrite → sphalerite → Ag selenides/sulfosalts → gold/electrum) (FOV: 0.54 mm). On the right is a billet (C) and photomicrograph (D) of sample 29-QV5, displaying multiple mineralized bands (FOV: 4.32 mm). Both samples represent typical Stage 1 mineralization. FOV = Field of view.
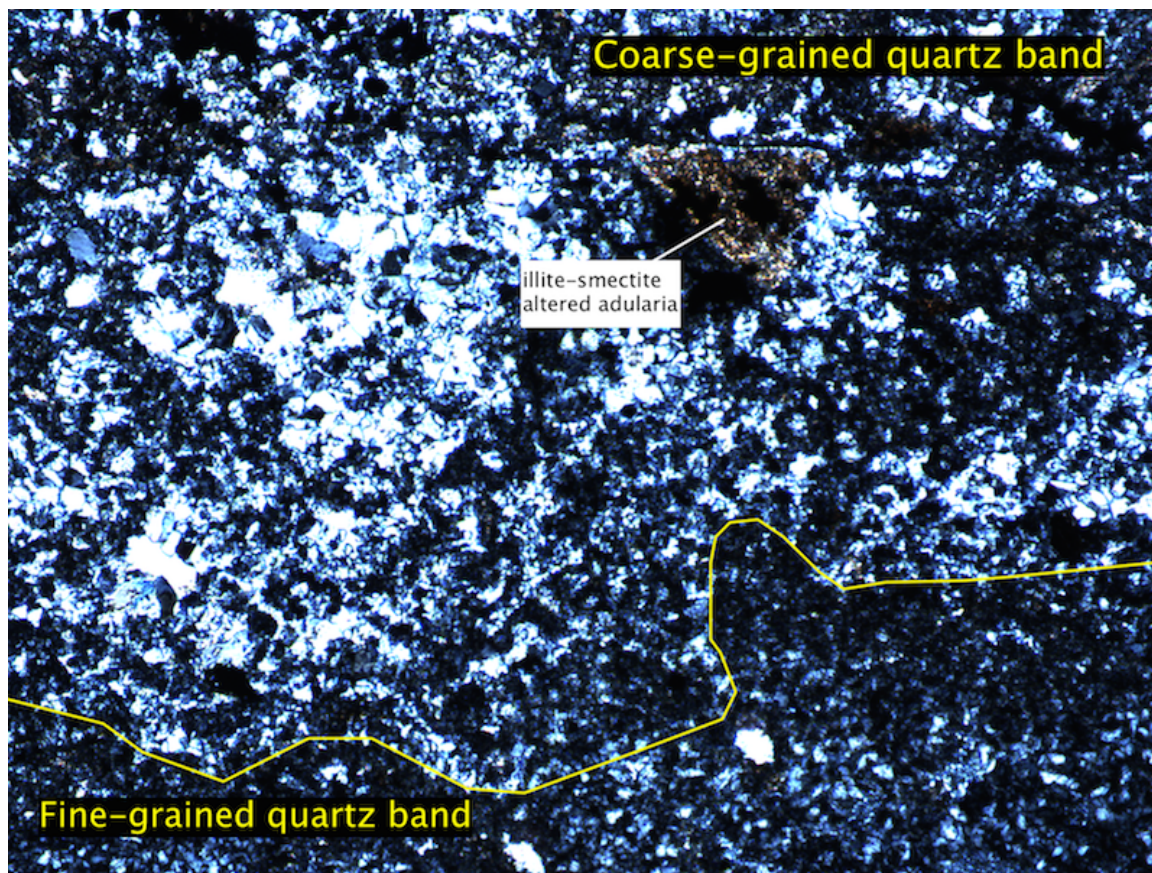
Fig. 11: Adularia rhomb replaced by Stage 2 illite-smectite (likely montmorillonite) and pyrite, in a band of coarser-grained quartz (FOV: 4.32 mm).
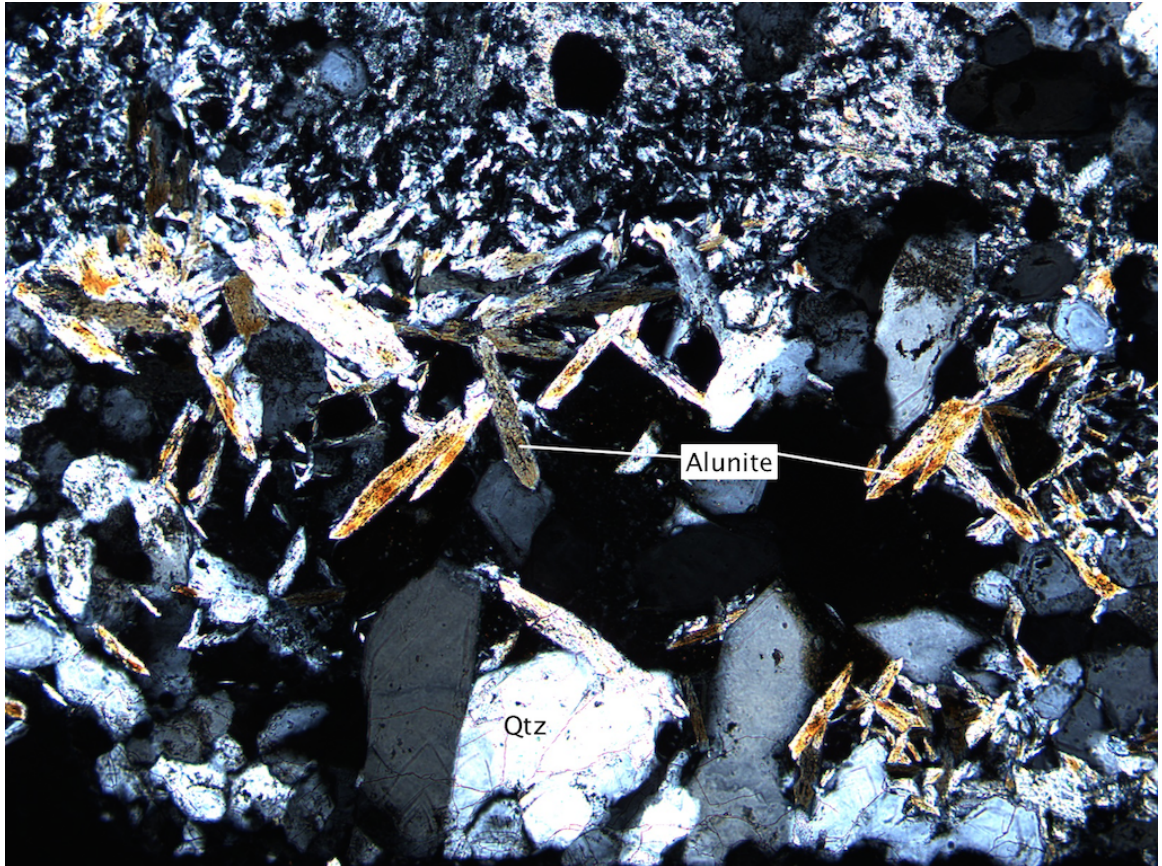
Fig. 12: Stage 2 drusy quartz overgrown by stage 3 alunite in vug (FOV: 1.7 mm).
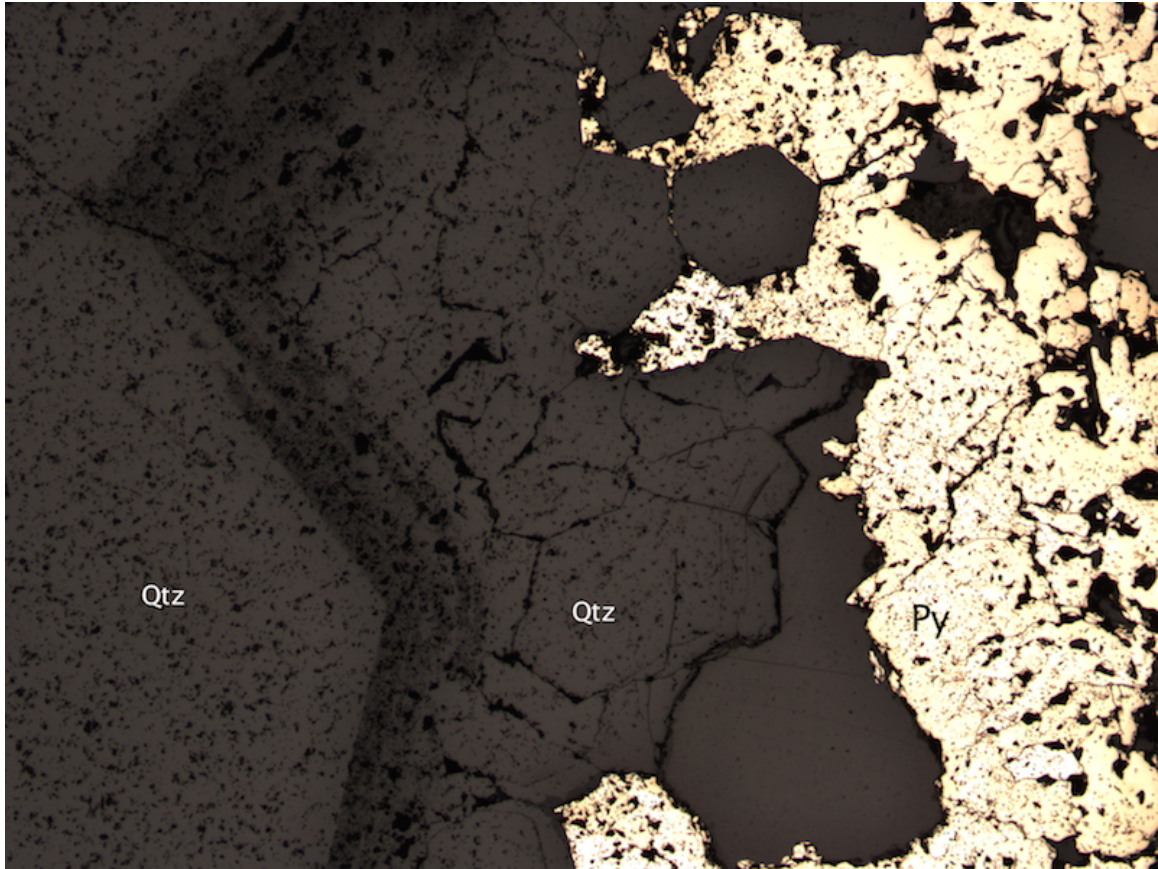
Fig. 13: Late, stage 4 quartz pyrite veinlet (FOV: 4.32 mm).

Quartz vein textures

Quartz textures in Vein 18 at Hollister are described here based on 37 drill core intercepts of Vein 18. Much attention has been paid to characterizing quartz textures in low-sulfidation epithermal systems. Quartz textures in Vein 18 are mostly similar to those described by Dong et al. (1995); Moncada et al. (2012); and Shimizu (2014). To maintain continuity with the exploration program at Hollister, the textural nomenclature utilized by Great Basin Gold was used in this study. For this reason some textural terms

may be slightly modified from those reported in the literature. The textures described here are massive quartz, banded quartz, bladed quartz, chaotic quartz, vuggy quartz, and cockade quartz, and also includes vein breccias, which are illustrated in Figures 14 and 15. Though quartz is the dominant gangue mineral, adularia is also common, comprising up to 10 volume percent of veins. It occurs with banded, bladed, chaotic, and cockade quartz, as well as vein breccias.

In hand sample, massive quartz has a homogeneous texture characterized by a milky, white appearance (Figure 15A). It is composed of granular crystals between 20 and 100 microns in size. It locally hosts disseminations of pyrite, chalcopyrite, and sphalerite, and less commonly electrum and silver selenides. Small, circular to oval-shaped vugs (0.5 mm – 1 cm) are fairly common in massive quartz (< 15 volume %) and are generally lined or filled with stage 2 drusy quartz (up to 500 μm) and minor pyrite euhedra. Adularia has not been observed in massive quartz.

In hand sample, banded quartz (Figure 15B) comprises alternating, parallel bands of crustiform quartz or botryoidal colloform bands of quartz (Dong et al., 1995). Bands are typically 0.5 – 2 mm wide, and are commonly defined by alternating bands of grey, white, and tan quartz and adularia. Bands are differentiated in thin section by alternating layers of coarser-grained (~100-600 μm) and finer-grained (~10-90 μm), interlocking quartz and adularia. Gray and white bands contain variable amounts of illite, adularia, base-metal sulfides, Ag-selenides, and electrum. In hand sample, darker bands typically correspond to finer-grained bands in thin section.

Bladed quartz in hand sample is characterized by elongate, 2-3 cm long, platy aggregates of quartz (Figure 15C). In cross-polarized light, the centers of blades are made of linear "seams" (Dong et al., 1995), which are overgrown by fine-grained (~50 – 200 μm), granular quartz crystals, which have grown symmetrically around, and perpendicular to the seams by replacement of original bladed calcite. The variety of bladed quartz at Hollister is known as lattice bladed quartz (Dong et al. 1995), which is characterized by networks of intersecting quartz blades. These blades at Hollister are commonly overgrown with pyrite, sphalerite, chalcopyrite, silver selenides, and electrum. Most cavities between the blades are lined with drusy to granular quartz, adularia and minor pyrite. Samples of lattice bladed quartz, in which cavities are completely filled with quartz and pyrite, make the texture less conspicuous in hand sample. Some samples of bladed quartz show ore minerals preferentially deposited along one side of quartz blades. Such textures are referred to as "sluice box textures" and have previously been described at Hollister and the Sleeper deposit by Saunders et al. (2011), who interpreted such features as evidence of physical transport of gold and naumannite.

Chaotic quartz texture (Figure 15D) in hand sample is characterized by intermixed, white to yellow quartz with minor dark nodules. In thin section, features include interlocking to granular quartz, radiating chalcedonic nodules, disseminated sulfides, and less commonly, electrum and selenides. Chaotic quartz is composed of granular quartz crystals that show a bimodal size distribution. The radiating, chalcedonic nodules are more commonly present in zones of coarser-grained quartz. Chaotic quartz is

analogous to flamboyant quartz, as identified in Dong et al. (1995) and Moncada et al. (2012). Only minor adularia has been identified in samples with chaotic quartz.

Vuggy quartz is very similar to massive quartz in grain size, crystal shape, and mineralogy (Figure 15E). It is differentiated from massive quartz by a high density of vugs (> ~15 volume %), which are commonly lined with drusy quartz crystals, minor pyrite, and tan-orange botryoidal siderite overgrowths on drusy quartz crystals.   Hand samples are milky white to grey. Quartz is granular with grain sizes ranging from 20 – 100 μm, while drusy quartz crystals are up 500 μm long. Within granular quartz there are often small amounts of disseminated sulfides, dominantly pyrite.

Cockade quartz is characterized in hand sample by clasts of wallrock and/or vein material, which are surrounded by bands of gray or white quartz (Figure 15D). In thin section, the bands are composed of feathery quartz and adularia. This texture is described by Dong et al. (1995) as a sub-type of banded quartz, and is considered to have formed similarly to banded quartz.

Vein breccia is a broad term used for any sample containing angular to subrounded clasts of quartzite or argillite or vein material that is cemented with white-grey quartz, and less commonly, adularia. Fragments are angular to sub-rounded and can range from 2 mm to 5 cm in length. Both matrix- and clast-supported breccias occur.
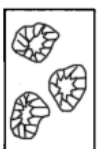
Quartz Texture	Banded (BD) quartz	Bladed (BL) quartz	Chaotic (CH) quartz	Massive (MS) quartz	Vuggy (VGG) quartz	Cockade (CC) quartz	Vein Breccia (VNBX)
Description	Alternating bands of fine- and coarse-grained, interlocking and granular quartz crystals; some bands have significant adularia or sericiticezed adularia; Grain sizes: 10 - 600 microns	Granular quartz grains replacing lattice-work calcite blades; lattice is frequently lined with drusy quartz and adularia or filled with granular quartz; Grain sizes: 50 - 200 microns	Bimodal distribution of grain sizes of both interlocking and granular quartz; Zones of coarser-grained quartz appear cemented by finer grained quartz and may indicate brecciation. Coarser- and finer-grained quartz both display feathery spheres of recrystallized silica; Grain sizes: 10 - 600 microns	Granular quartz grains, generally with similar grain sizes in each sample; Grains sizes: 20 - 100 microns	Similar in appearance to MS quartz with a high percentage of vugs. Vugs are consistently lined or filled by drusy quartz and are frequently filled by later-stage minerals; Grain sizes: 20 - 500 microns	Has a banded appearance around clasts of vein and wallrock material, while the rest of the cement consists of similar-sized, granular crystals similar to MS quartz; Grain sizes: 10 - 600 microns	Typically consists of brecciated wallrock cemented by MS quartz. Vein segments must be completely occluded with clasts in order to qualify as VNBX texture; Grain sizes: 20 - 100 microns
Schematic Diagram							

Fig. 14 (Above): Summary diagram of quartz textures observed in Vein 18. From left to right: banded quartz, bladed quartz, chaotic quartz, massive quartz, vuggy quartz, cockade quartz, and vein breccia. Modified from Dong et al., 1995 and Moncada et al., 2012.
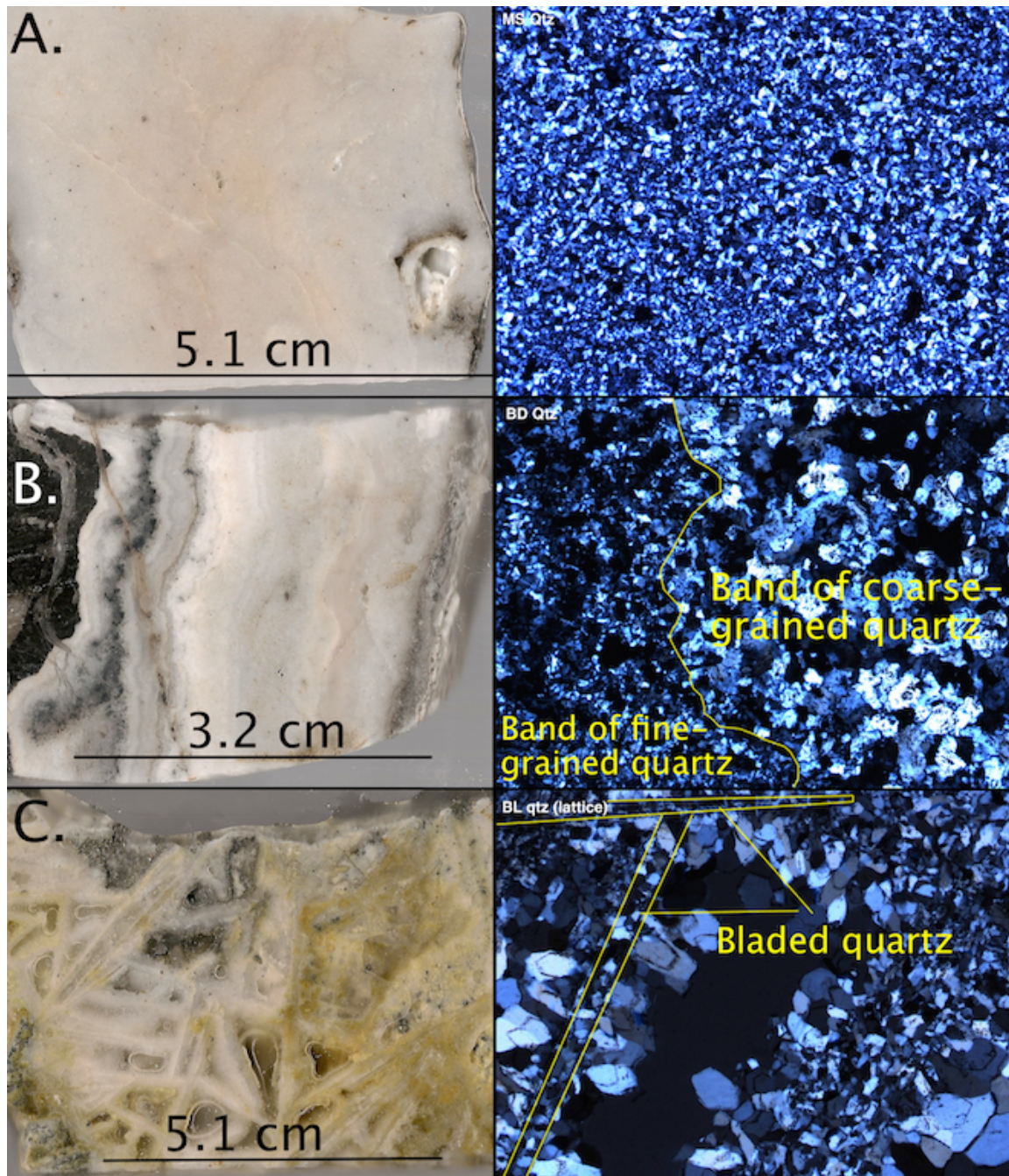
Fig. 15: Hand sample photographs and thin section photomicrographs (crossed polars) of quartz textures seen at Hollister. A. massive quartz. B. banded quartz. C. bladed quartz. FOV for each photomicrograph is 4.32 mm.
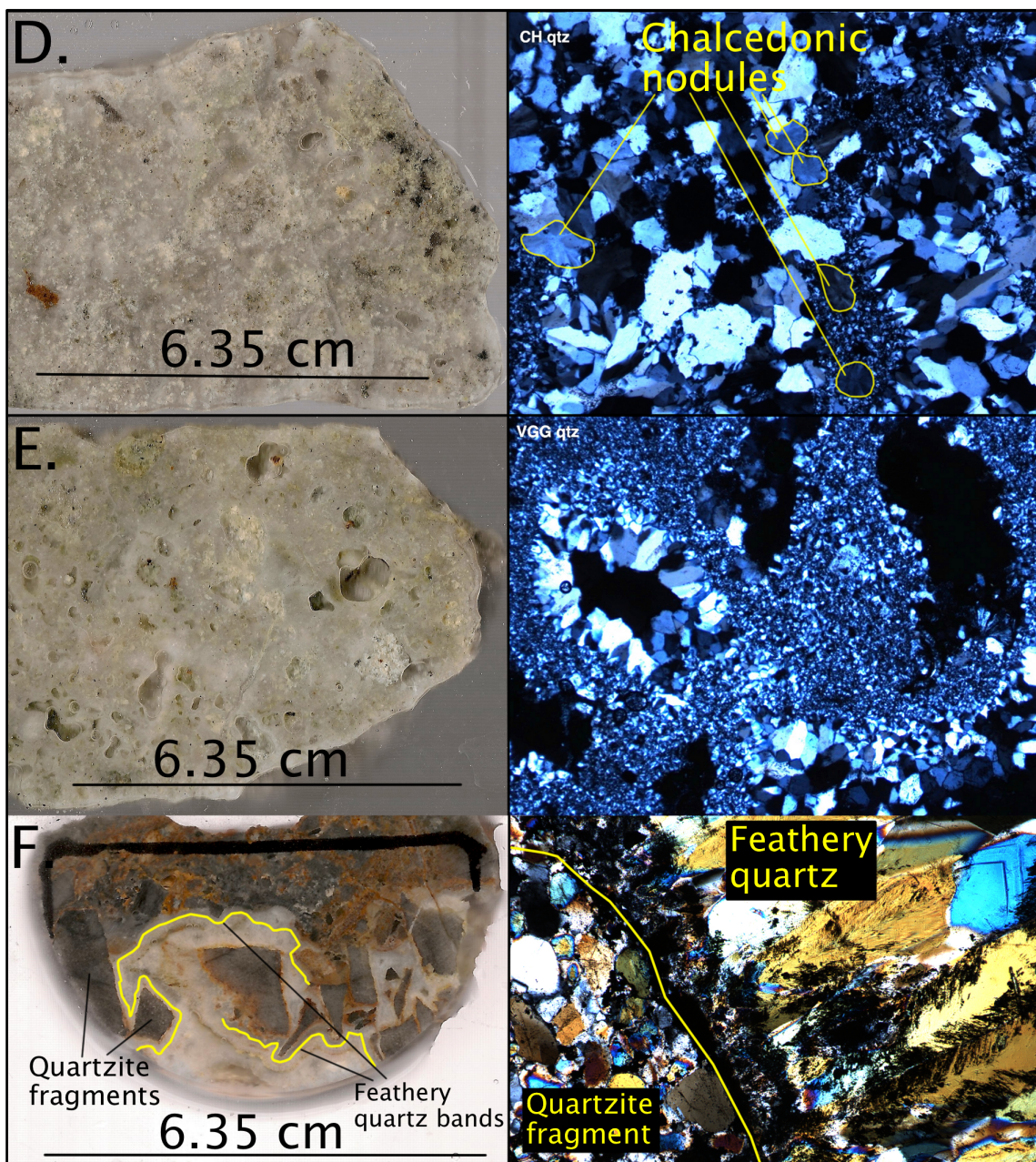
Fig. 15 (con't): D. chaotic quartz. E. vuggy quartz. F. cockade quartz. FOV for each photomicrograph is 4.32 mm.

Ambiguity commonly exists among geologists regarding use of the term "banded quartz" in epithermal veins. For example, Figure 16 shows mm-sized bands of quartz, whereas Figure 17 shows a vein with cm-sized bands of alternating massive and vuggy

quartz. The two veins both have some degree of layering, which is concordant with vein

strikes and dips; however, millimeter-scale, rhythmic-like banding is considered here to

be a diagnostic characteristic of banded quartz in the epithermal environment. When

making genetic interpretations, scale is of paramount importance, and the two varieties

must not be confused.
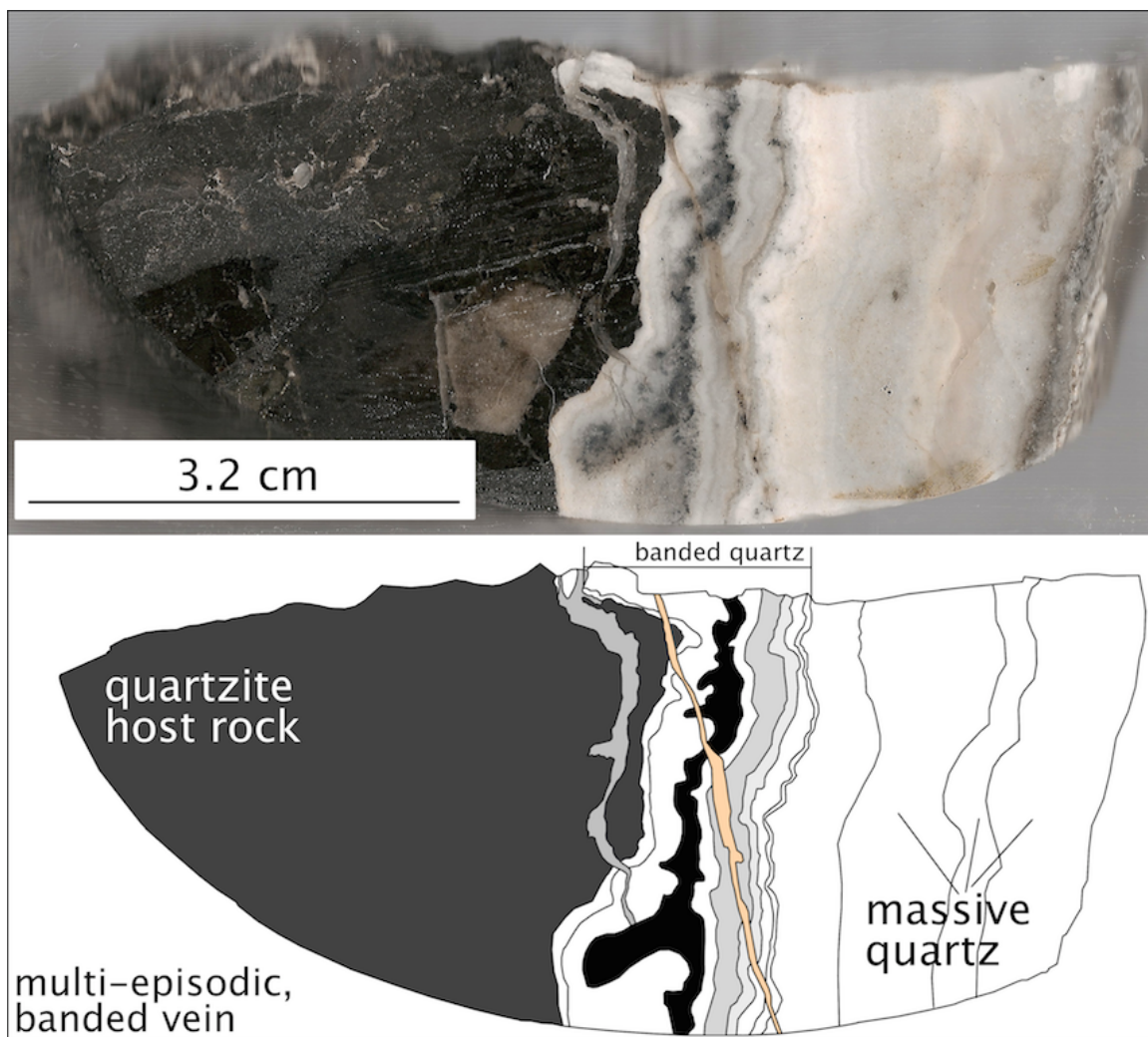
Fig. 16 (above): Multi-episodic, banded vein. As seen in sample 29-QV5. Black band
represents naumannite, electrum, and quartz, with minor chalcopyrite and sphalerite.
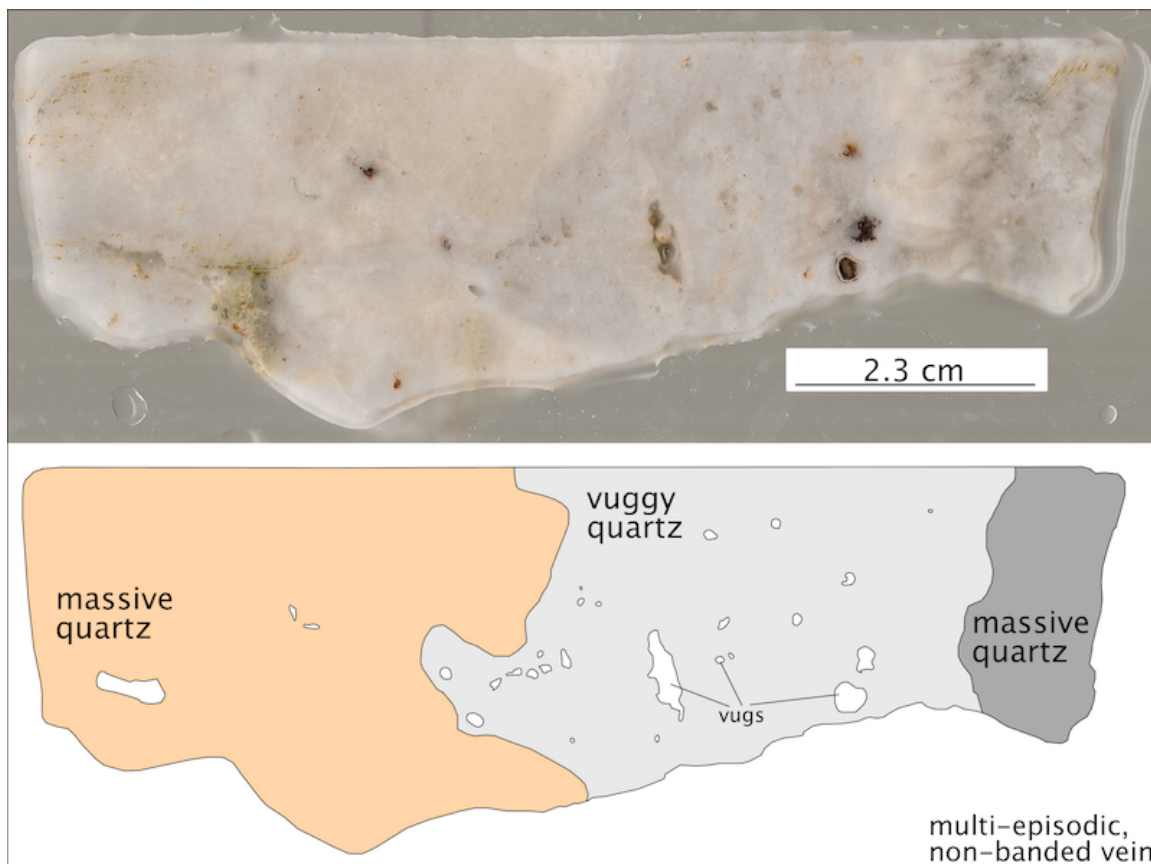
Fig. 17: Multi-episodic, non-banded vein. As seen in sample 150-QV4. Multiple textures are present and display a centimeter-scale layering, which should not be confused with true banded quartz.

Vein Forms

Four vein forms are observed in Vein 18 (Fig. 18), three of which, discrete veins, stockwork, and breccia, represent open space filling and commonly exhibit all the quartz textures described above. The fourth vein form represents replacement of volcanic host rocks and typically contains massive, banded, and vuggy quartz and other gangue minerals, mainly clays.

Discrete veins are veins that show a defined area of hydrothermal quartz between two distinct vein walls. In this study, classification as discrete was limited to veins with widths of greater than 3 cm. Vein walls are sharp and fairly straight. Discrete veins typically host multiple quartz textures and display the best examples of multi-stage silica deposition. Veins of this nature are most commonly found in quartzites and argillites of the Vinini formation.

Stockwork veins are comprised of networks of thin, commonly anastamosing, quartz veinlets, typically less than 3 cm wide. Banded, massive, bladed, chaotic, and vuggy quartz, and vein breccia textures have been observed in stockwork. Stockworks occur in both the Vinini Formation and the overlying Miocene volcanic rocks.

Vein breccia include planar and pipe-shaped bodies, which contain fragments of immediate wallrock or vein material. The matrix is composed of predominantly hydrothermal quartz. These can range from cm-scale bodies, to larger, meter-scale veins. These show a lack of textures except for rare cockade quartz and massive quartz, which commonly make up the matrix of the vein breccia. Vein breccias predominantly occur in the Vinini Formation.

Replacement bodies form portions of the upper part of Vein 18, where it transects Miocene volcanic rocks and directly overlies the vertical projection of Vein 18. Rather than open space fillings, they are characterized by irregular bodies of quartz with minor adularia or alunite that have replaced tuffaceous rocks. These bodies are related to the propagation of Vein 18 into the overlying volcanic sequence. Widths range from a few centimeters to about 1.5 meters. At the Ordovician-Miocene unconformity, veins fan out

from discrete veins in the Vinini formation and "flood" into the volcanic rocks, becoming

thicker than discrete veins. As mentioned above, replacement bodies along the

unconformity locally have extremely high grades.
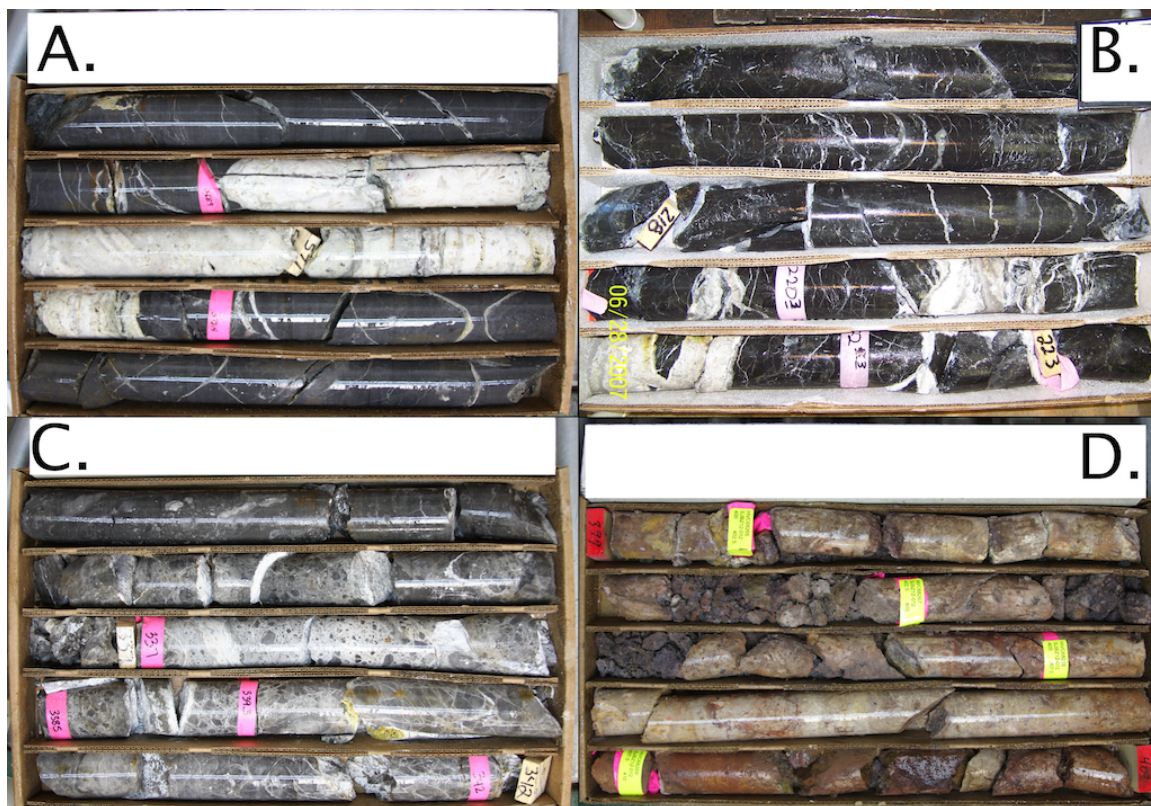
Fig. 18: Representative examples of vein geometries observed at Hollister. A: Discrete vein B. Stockwork C. Vein breccia D. Replacement structure. Core boxes are 2 feet long (~0.6 m).

Fluid Inclusion Studies

Fifteen fluid inclusion plates of vein intercepts from Vein 18 were examined to determine the origin (primary vs. secondary vs. uncertain), contents (L/V ratios), and morphologies of fluid inclusions found in quartz veins. Microthermometric measurements were performed on two fluid inclusion plates with primary inclusions, in order to determine minimum temperatures and place constraints on the depths of formation and the salinities of the fluids. Fluid inclusion homogenization temperatures were measured on a FLUID INC.-adapted USGS gas-flow heating system at the University of Nevada, Reno. Final ice melting temperatures were measured using a LINKAM LNP 95 cooling system at the University of Nevada, Las Vegas.

Petrographic studies showed Stage 2 drusy quartz crystals in veins with vuggy, massive, and bladed quartz textures contain primary inclusions up to 15 µm in diameter, which occur along growth zones (Figure 19). The primary inclusions were relatively equant, two-phase, liquid-dominant, Type I inclusions. Bladed quartz and vein breccias host moderate amounts of large, Type I, equant fluid inclusions; however, the origin of inclusions in quartz after bladed calcite is uncertain. Most inclusions hosted in vein breccias were irregular, necked inclusions in feathery quartz crystals, which likely formed by recrystallization of chalcedony or amorphous silica (Sander and Black, 1988).
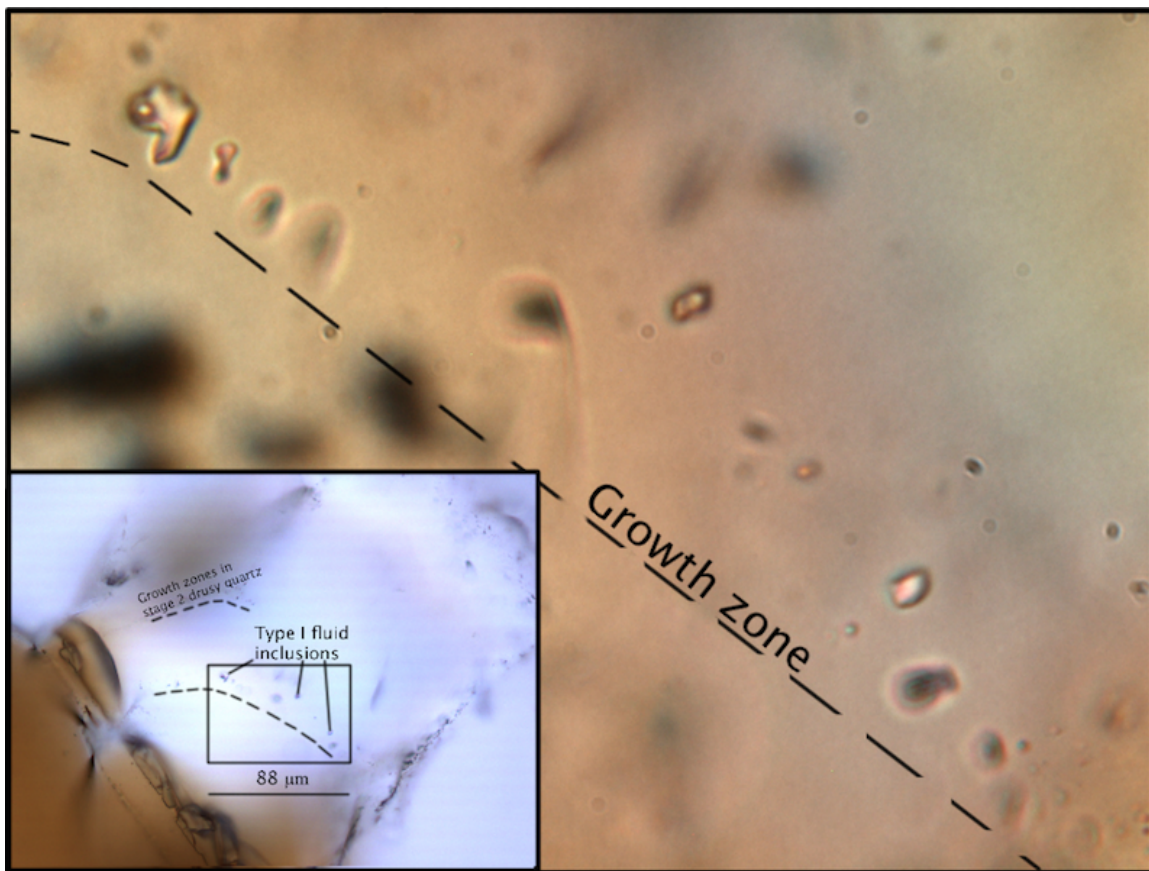
Fig. 19: Thin section images of samples 524-239, displaying non-necked, type I fluid inclusions in growth zones in drusy quartz. Field of view for close-up is 88 μm.

Homogenization temperatures of seven inclusions from a single growth zone in sample 524-239 (1510 m elevation) ranged from 196° – 209°C, with an average of 203°C. The average final ice melting temperature from five inclusions was -0.82°C, indicating salinities of 1.3 wt% NaCl equivalent (Potter et al., 1978). Nine inclusions from sample 542-244 (1530 m elevation) homogenized between 190° - 205°, with an average of 198°C. The average final ice melting temperature from 7 inclusions was -0.66°C, indicating salinities of 1.0 wt% NaCl equivalent. Inclusions in both samples were also cooled to -100°C. In two inclusions, subsequent heating to -56.6°C indicated

melting of minor CO_2; however, no clathrate was recognized upon further heating, indicating CO_2 concentrations below ~ 3.6 wt % (Hedenquist and Henley, 1985).

Peppard (2002) measured homogenization and freezing temperatures in similar Type 1 fluid inclusions of primary and secondary origin, hosted in quartz veins from the Clementine vein system. Primary fluid inclusions were also from growth bands in drusy quartz crystals, whereas the secondary inclusions occurred along planes that cut multiple quartz grains. Homogenization temperatures of primary inclusions ranged between 170° and 245°C, with an average of 210°C; secondary inclusions homogenized between 255° and 280°C, and are likely part of stage 4, as part of a younger hydrothermal system. Drusy quartz-hosted fluid inclusions, which were spatially associated with minor silver selenides and electrum yield homogenization temperatures between 174° and 189°C. Primary fluid inclusion assemblages containing both Type I and Type II, non-necked inclusions, and, thus, indicative of boiling, homogenized at an average of 220°C. Final ice melting temperatures ranged from 0° to -1.5°, which correspond to salinities of 0 to 2.6 wt % NaCl equivalent. Peppard (2002) did not report clathrates during freezing runs. The salinities determined by Peppard (2002) and this study are similar to those reported for Midas (Goldstrand and Schmidt, 2000), Bullfrog (Eng et al., 1996), National (Vikre, 1985), and Sleeper (Nash and Trudel, 1996) (0.5 – 2.0 wt% NaCl equivalent).

Stable Isotope Data

Stage 1 and Stage 2 vein pyrite and Stage 3 vein alunite were measured for $\delta^{34}S$ values, in order to constrain the processes responsible for alunite formation. Pyrite samples were sawed, crushed, panned, and hand-picked to obtain a pyrite separate. Alunite was separated from three samples by drilling fracture and vug fillings and hand-picking alunite. The $\delta^{34}S$ of stage 1 and 2 pyrite range between 4.2 – 4.5‰, and $\delta^{34}S$ values of stage 3 alunite range between 6.3 – 6.6‰ (Table 2). These results are consistent with a steam-heated origin for the alunite and inconsistent with supergene or magmatic-hydrothermal origins (Rye et al., 1992).

In steam-heated alunites, $\delta^{34}S$ values will usually be the same as H_2S boiled off the hydrothermal fluid, assuming $\delta^{34}S_{sulfides}$ is the same as $\delta^{34}S_{H2S}$; however, given enough time at steam-heated temperatures, aqueous sulfate can exchange with H_2S to yield higher $\delta^{34}S$ values in the oxidized state (Rye et al., 1992). At Crofoot-Lewis, ore-stage sulfides ranged from -15.0 to -11.0 ‰, while steam-heated alunite was between -14.0 and -2.2 ‰ (Ebert and Rye, 1997). At Buckskin Mountain, vein and disseminated sulfides ranged from -8.8 to -5.1 ‰, and steam-heated alunite was between -4.5 and -2.8 ‰ (Vikre, 2007).

$\delta^{34}S$ values for both pyrite and alunite are slightly elevated in comparison to volcanic-hosted low-sulfidation epithermal systems at Crofoot-Lewis and Buckskin, displaying steam-heated alteration (Ebert and Rye, 1997; Vikre, 2007). Ore-stage pyrite of volcanic-hosted epithermal systems worldwide are largely below 0‰. Higher overall

δ^{34}S values at Hollister indicate diagenetic pyrite in Paleozoic sedimentary rocks may have exchanged heavy sulfur with the hydrothermal fluid.

Sample	Location	Mineral	Stage	Description	δ^{34}S
29-QV3	Vein 18	Pyrite	1	Quartz vein with pyrite, gold, and naumannite bands	4.5
29-QV5	Vein 18	Pyrite	1	Quartz vein with pyrite, gold, and naumannite bands	4.2
11-474-CV1	Vein 18	Pyrite	2	Clay/quartz vein with kaolinite, muscovite, quartz and pyrite	4.2
79-QV1	Vein 18	Alunite	3	White alunite vug in quartz vein; minor quartz	6.4
79-QV2	Vein 18	Alunite	3	Pink alunite filling vein with naumannite, gold, and pyrite bands	6.3
171-QV2	Vein 18	Alunite	3	White alunite filling vein with naumannite, gold, and pyrite bands	6.6

Table 2: Table of δ^{34}S values from 3 samples of pyrite and 3 samples of alunite from Vein 18.

Peppard (2002) measured δ^{18}O values for quartz in silicified deposits, sinter deposits, and veins. Similarities in calculated δ^{18}O$_{fluid}$ values between the silicified zone in the Miocene volcanic rocks (-6.3‰), sinter (-4.4‰), and the South Clementine (-7.0‰) vein system suggest they formed from the same hydrothermal fluid. Slightly higher δ^{18}O values in the stratigraphically higher LSZ and sinter are likely attributed to evaporation, steam loss, and wall-rock interaction.

Metal Associations in Vein 18 and Sinter

Drill pulps from 25 vein intercepts were analyzed by four-acid digestion and ICP-MS in order to determine the trace element associations in Vein 18. Elements of interest, based on previous studies (Bartlett et al., 1991; Deng, 1991), included Au (range of values: 0.04 – 463 ppm), Ag (0.63 – 2720 ppm), Cu (7.6 – 440 ppm), Pb (1.5 – 54.5 ppm), Zn (2 – 2560 ppm), Se (2 – 789 ppm), Hg (cold vapor atomic absorption, <0.1 – 4.51 ppm), As (23 – 1510 ppm), Sb (5.97 – 290 ppm), Tl (0.3 – 5.51 ppm), Mo (0.39 –

6.52), W (0.2 – 4.4 ppm), Bi (0.02 – 11.05 ppm), and Te (<0.05 – 0.88). Spearman rank correlation matrices and principal component analysis for these 25 vein intercepts were completed for Au, Ag, and 28 other elements. Gold and silver correlate well ($R^2 = 0.94$). For 515 gold and silver assays of vein 18 intercepts provided by Great Basin Gold, the association was somewhat lower ($R^2 = 0.75$), but still very significant given the large number of samples. Au and Ag for the 25 vein intercepts also strongly correlate with Se (0.89; 0.96), consistent with the association of electrum with naumannite and other Ag-selenides. Au and Ag also correlate well with Bi (0.56; 0.68), Cd (0.59; 0.6), Cu (0.66; 0.75), Ge (0.93; 0.95) Pb (0.73; 0.78), Sb (0.73; 0.76), Te (0.42; 0.55), U (0.53; 0.55), and Zn (0.56; 0.62).

Principal component analysis using ioGAS software identified four factors accounting for 69.2% of the variance in the data. The four factors and the elements with high loadings that strongly influence them, in order of decreasing amount of variance are listed below:

1. Factor 1 (Stage 1 Vein Factor) (32.2%): Au, Ag, Cd, Co, Cu, Ge, Hg, Ni, Pb, Sb, Sc, Se, Sr, Te, W, and Zn

2. Factor 2 (15.7%): As, Be, Co, Li, Sb, and Tl

3. Factor 3 (Gold Factor) (11.7%): Au, Ag, Cu, Ge, Sb, Se, and Zn

4. Factor 4 (9.6%): Bi, Cd, Cr, Mo, and Te

Factor 1 likely represents stage 1 mineralization in Vein 18. Factor 3 represents a gold factor and likely represents the base metal sulfide/sulfosalt, naumannite, and electrum parts of the stage 1 cycles.

In addition, LA-ICP-MS traverses were performed on two samples of sinter collected from the Butte #1 mine, located about 1 km northwest of the Clementine vein system (Figure 2) (P. Vikre, personal commun.). Analyses were performed to test whether the sinter and veins had similar metal associations, which would permit them to have formed from a similar parental fluid, which was suggested by the calculated $\delta^{18}O_{H2O}$ values of vein material and sinter done by Peppard (2002). .

Sinters are found at multiple historic mine sites in the Ivanhoe district and in drill core, typically in the middle tuff. Sinters are characterized by layering of microcrystalline quartz, chalcedony, opal, and drusy quartz with cinnabar and trace sulfides. Sinter is up to 3 m thick and grades downward into a lower silicified zone in the Miocene volcanic sequence (Peppard, 2002). Locally, hydrothermal eruption breccias are associated with sinter deposits (Wallace, 2003).

LA-ICP-MS traverses of the sinters were oriented perpendicularly to bedding in the samples. This method provided data in counts per second, meaning only relative amounts of elements were measured. Although semi-quantitative, this method is valuable in understanding spatial relationships between elements (Vikre, 2007). In addition, conventional whole rock XRF and ICP-MS analyses (after a four acid digestion) were also performed on 3 sinter samples collected from the Butte #1 mine (Table 3).

In red to pink sinter beds, cinnabar is associated with Au, Ag, Se, Pb, As, Tl, Ba, and Sb (see Figure 20). Elements that were found to be elevated in whole-rock sinter samples included Hg, Ba, Mo, Pb, Sb, Se, Sn, Zr, +/- Au, Ag, and Cu. Likewise, Vein 18 is elevated in regards to Au, Ag, As, Ce, Co, Cr, Cu, La, Li, Mo, Ni, Rb, Sb, Se, Sr, V, Zn +/- Pb, and Te. A schematic elemental zoning profile (Figure 21) summarizes these associations, along with metal associations reported by Bartlett et al. (1991) and Deng (1991) from the volcanic hosted disseminated gold ore. Elemental analyses, combined with the documented mineralogy of the Buckskin sinters, suggest the presence of cinnabar, electrum, Ag selenides, Ag-Pb sulfosalts, and potentially base-metal sulfides in red to pink sinter beds (Roberts, 1940; Vikre, 2007).

At Hollister, banded quartz veins and red-pink bedded sinter deposits have similar thicknesses. Mineralized sinter beds and vein bands, containing Au, Ag, Se, Pb, Sb, associations, rhythmically alternate with unmineralized beds and bands. Feeder conduits for sinter have been identified at the Butte #1 mine and are associated with hydrothermal eruption breccias (Wallace, 2003). These observations and associations support deposition of sinter and veins from the same ore fluid, as was documented at Buckskin (Vikre, 2007). Hollister sinter samples carry up to 1.5 ppm Au, 327 ppm Ag, and 1490 ppm Hg. With the exception of volatile Hg, steam-heated and silicification zones at the groundwater-table typically do not contain strong metal anomalies (Sillitoe, 1993; Hedenquist et al., 2000). Furthermore, these high gold and silver grades in these sinters support discharge of a metal-rich liquid at a groundwater outflow point (Hedenquist et al., 2000).
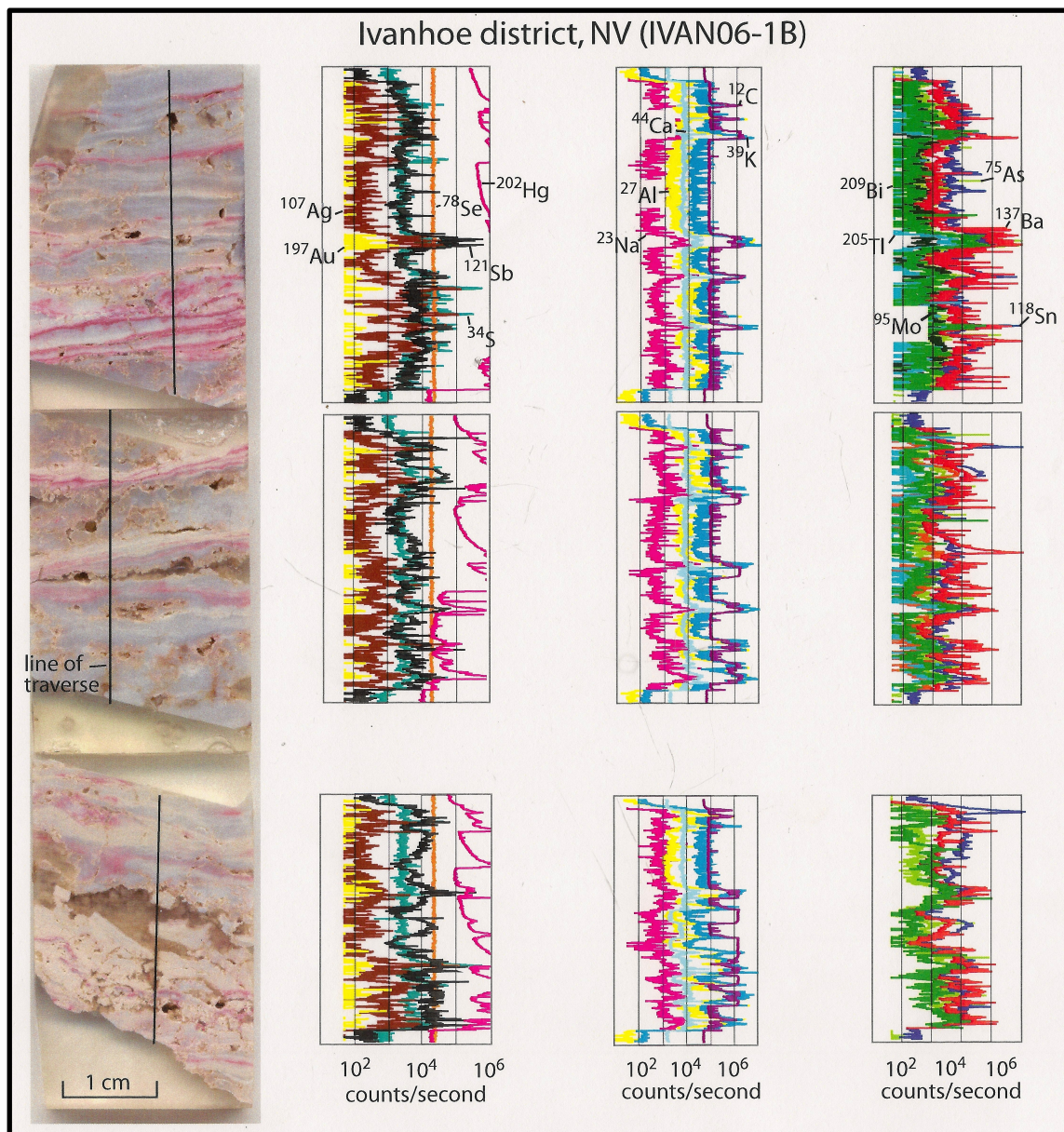
Fig. 20: LA-ICP-MS analyses for sinter sample IVAN06-1B. Dark line in sample marks the laser ablation traverse.

SAMPLE	DESCRIPTION	Au PPB	Pd PPB	Pt PPB	Hg PPM	Al %	Ca %	Fe %	K%	Mg %	Mn%
IVAN06-1A	Whole rock, sinter	479	<1	<0.5	1490	0.13	0.03	0.03	<0.01	<0.01	<0.01
IVAN06-1B	Whole rock, sinter	80	<1	<0.5	1350	0.25	0.01	0.1	0.02	0.02	<0.01
IVAN06-1C	Whole rock, sinter	1510	<1	<0.5	30.4	0.22	0.01	0.17	<0.01	<0.01	0.02

SAMPLE	DESCRIPTION	P%	Ti%	Ag PPM	As PPM	Ba PPM	Be PPM	Bi PPM	Cd PPM	Ce PPM	Co PPM
IVAN06-1A	Whole rock, sinter	<0.01	0.28	327	<30	3450	<5	0.1	<0.2	0.5	<0.5
IVAN06-1B	Whole rock, sinter	<0.01	0.22	17	<30	58.4	<5	<0.1	<0.2	1.1	2.8
IVAN06-1C	Whole rock, sinter	<0.01	0.08	13	<30	425	<5	<0.1	<0.2	0.5	1.5

SAMPLE	DESCRIPTION	Cr PPM	Cs PPM	Cu PPM	Dy PPM	Er PPM	Eu PPM	Ga PPM	Gd PPM	Ge PPM	Hf PPM
IVAN06-1A	Whole rock, sinter	<10	0.2	37	0.75	0.65	<0.05	2	0.41	3	19
IVAN06-1B	Whole rock, sinter	<10	0.3	17	0.24	0.16	0.06	<1	0.18	<1	8
IVAN06-1C	Whole rock, sinter	<10	<0.1	5	0.11	0.09	<0.05	<1	0.1	1	5

SAMPLE	DESCRIPTION	Ho PPM	In PPM	La PPM	Li PPM	Lu PPM	Mo PPM	Nb PPM	Nd PPM	Ni PPM	Pb PPM
IVAN06-1A	Whole rock, sinter	0.17	<0.2	0.3	<10	0.19	5	56	0.4	<5	78
IVAN06-1B	Whole rock, sinter	<0.05	<0.2	0.9	<10	0.14	3	36	0.9	<5	11
IVAN06-1C	Whole rock, sinter	<0.05	<0.2	0.4	<10	<.05	3	18	0.4	<5	<5

SAMPLE	DESCRIPTION	Pr PPM	Rb PPM	Sb PPM	Sc PPM	Se PPM	Sm PPM	Sn PPM	Sr PPM	Ta PPM	Tb PPM
IVAN06-1A	Whole rock, sinter	0.08	0.8	37.8	<5	132	0.2	10	12.6	3.4	0.09
IVAN06-1B	Whole rock, sinter	2.3	2.3	5.9	<5	2.2	0.2	9	1.2	2	<0.05
IVAN06-1C	Whole rock, sinter	1	1	6.9	<5	0.6	<.1	3	0.3	1	<0.05

SAMPLE	DESCRIPTION	Te PPM	Th PPM	Tl PPM	Tm PPM	U PPM	V PPM	W PPM	Y PPM	Yb PPM	Zn PPM	Zr PPM
IVAN06-1A	Whole rock, sinter	<0.5	3.1	<0.5	0.1	15.3	10	3	3.9	0.8	52	592
IVAN06-1B	Whole rock, sinter	<0.5	0.5	<0.5	<0.05	6.45	11	2	1.5	0.2	6	225
IVAN06-1C	Whole rock, sinter	<0.5	0.4	<0.5	<0.05	8.08	8	2	0.8	0.1	<5	150

Table 3: Whole rock analyses for 3 sinter samples collected from the Butte #1 mine.

Sinter deposits: Hg, Ba, Mo, Pb, Sb, Se,
Sn, +/– Au, Ag, and Cu

0 m

Disseminated epithermal mineralization:
Au, Ag, Sb, As, Ba, Cd,
Co, Cu, Pb, Mn, Hg,
Mo, Te, Tl, Zn

Epithermal vein mineralization:
Au, Ag, Cd, Co, Cu,
Ge, Hg, Ni, Pb, Sb, Sc,
Se, Sr, Te, W, and Zn

300 m
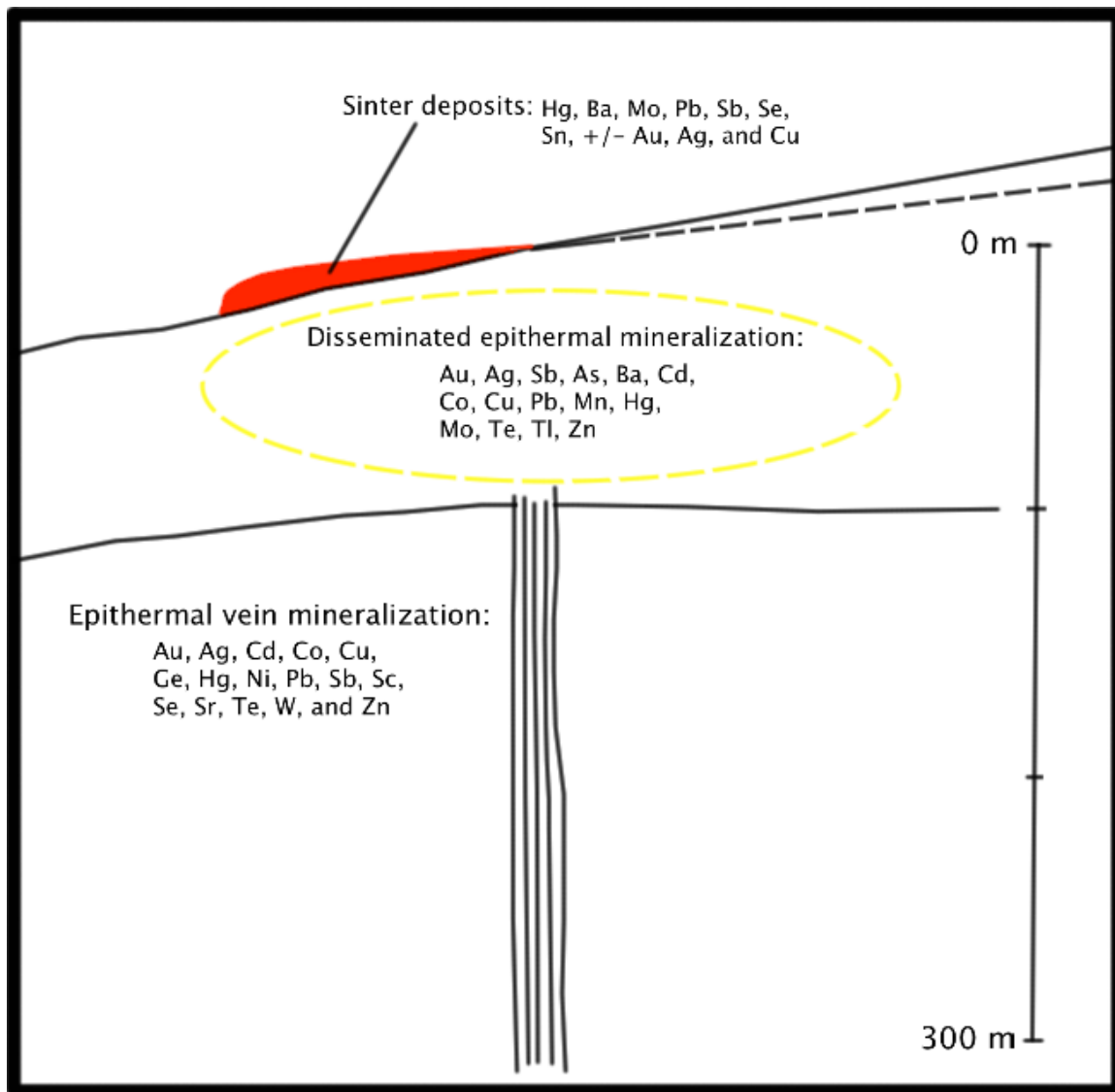
Fig. 21: Elemental zoning profile through the Hollister deposit.

Controls on High Gold-Silver Grades in the Clementine System

In order to identify controls on the locations of high-grade, Au-Ag ore shoots

along Vein 18, data sets presented above were plotted on longitudinal sections of Vein 18

to assess the relationship between geological, mineralogical, and geochemical features

and Au and Ag grades. Data sets include quartz textures, mineralogy, vein geometry,

trace element data, and structural data.

Gold and silver grades

Longitudinal sections of Au and Ag grades clearly show an elevation control on

ore-grade mineralization in Vein 18 (Fig. 22). The elevation control is shown even better

in elevation vs. grade plots (Fig. 23). Three large ore shoots, the west, central, and east

shoots, are defined by relatively large, continuous zones of > 40 ppm Au and > 200 ppm

Ag. These shoots extend 75 to 150 m along strike and 75 to 100 m down dip. The east

shoot is the most noticeable and forms a vertical plume. The central ore shoot forms an

elongate lens of high grades, with a more limited vertical extent. The west shoot rakes up

the vein from the WSW to ENE.

Gold grades greater than 8.5 ppm are found in a 265 m vertical interval, from

elevations of 1445 m to 1710 m. Silver grades greater than 40 ppm occur between 1402

m and 1710 m. High Au grades (> 40 ppm) are restricted to a 225 m vertical interval

from elevations between 1485 m and 1710 m, with most of the highest gold grades (>80

ppm) concentrated in a 107 m vertical interval, between 1508 m and 1615 m, which is

also where the highest Ag grades occur (>535 ppm). The available data display no

vertical pattern in the Ag:Au ratios (Fig. 24).

Select trace element data were displayed on longitudinal-sections (APPENDIX

A34 and A35). High grade ore shoots (> 40 ppm Au; > 200 ppm Ag) are only found

where Se is greater than 150 ppm. These high-grade ore shoots also coincide with zones

of > 250 ppm Cu. Patterns seen in longitudinal sections are consistent with results from

Spearman correlation matrices and principal component analysis.
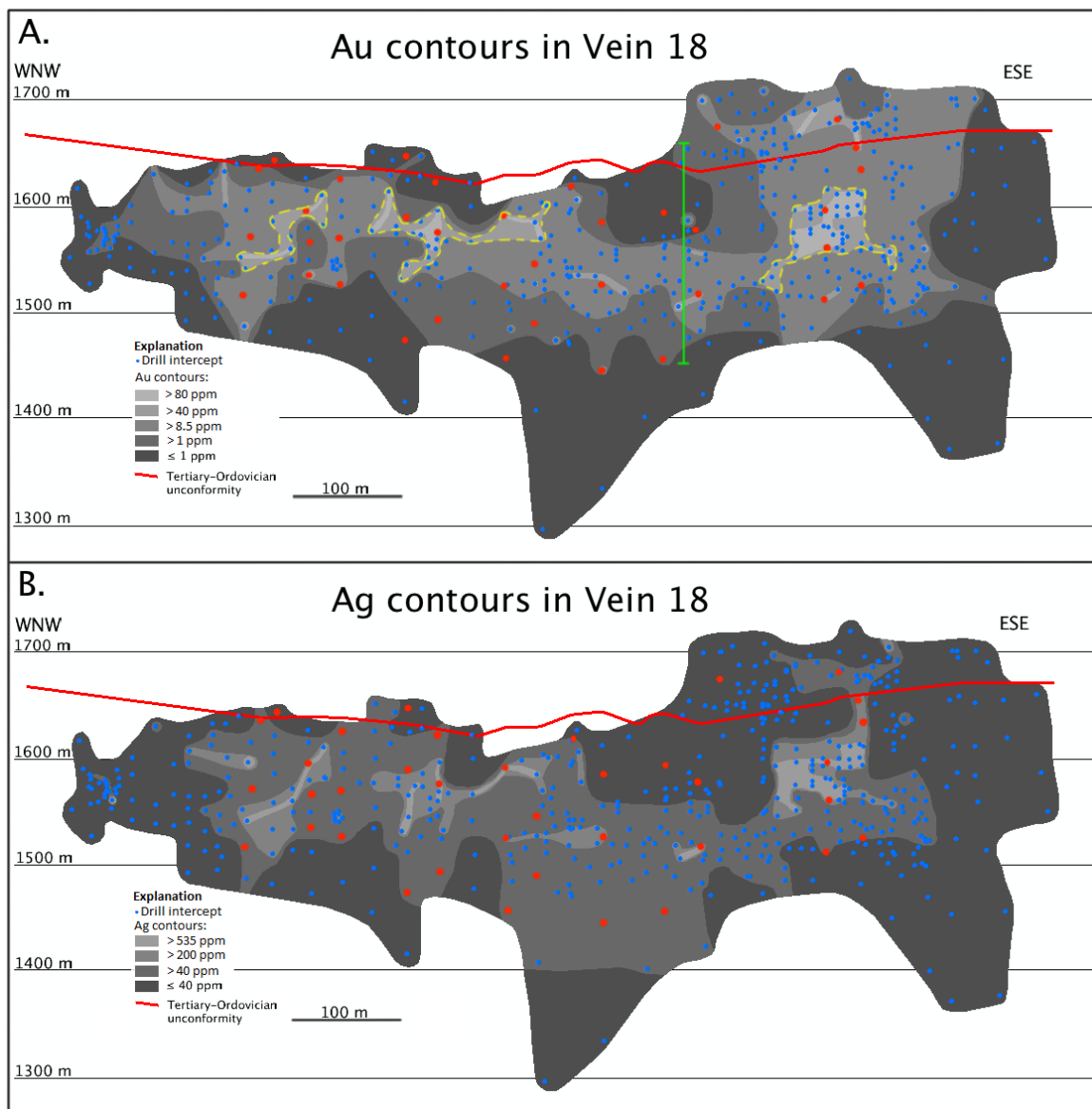
Fig. 22: Longitudinal sections of Vein 18 showing: A. Contoured gold grades. Green line represents axis of cross-sections in Figs. 37, 40, 42, and 43. From left to right, the west, central and east ore shoots are outlined in yellow dashed lines. B. Contoured silver grades. Contours at < 1 ppm Au and < 40 ppm Ag represent the extent of available drill data. Red dots represent vein intercepts sampled in this study.
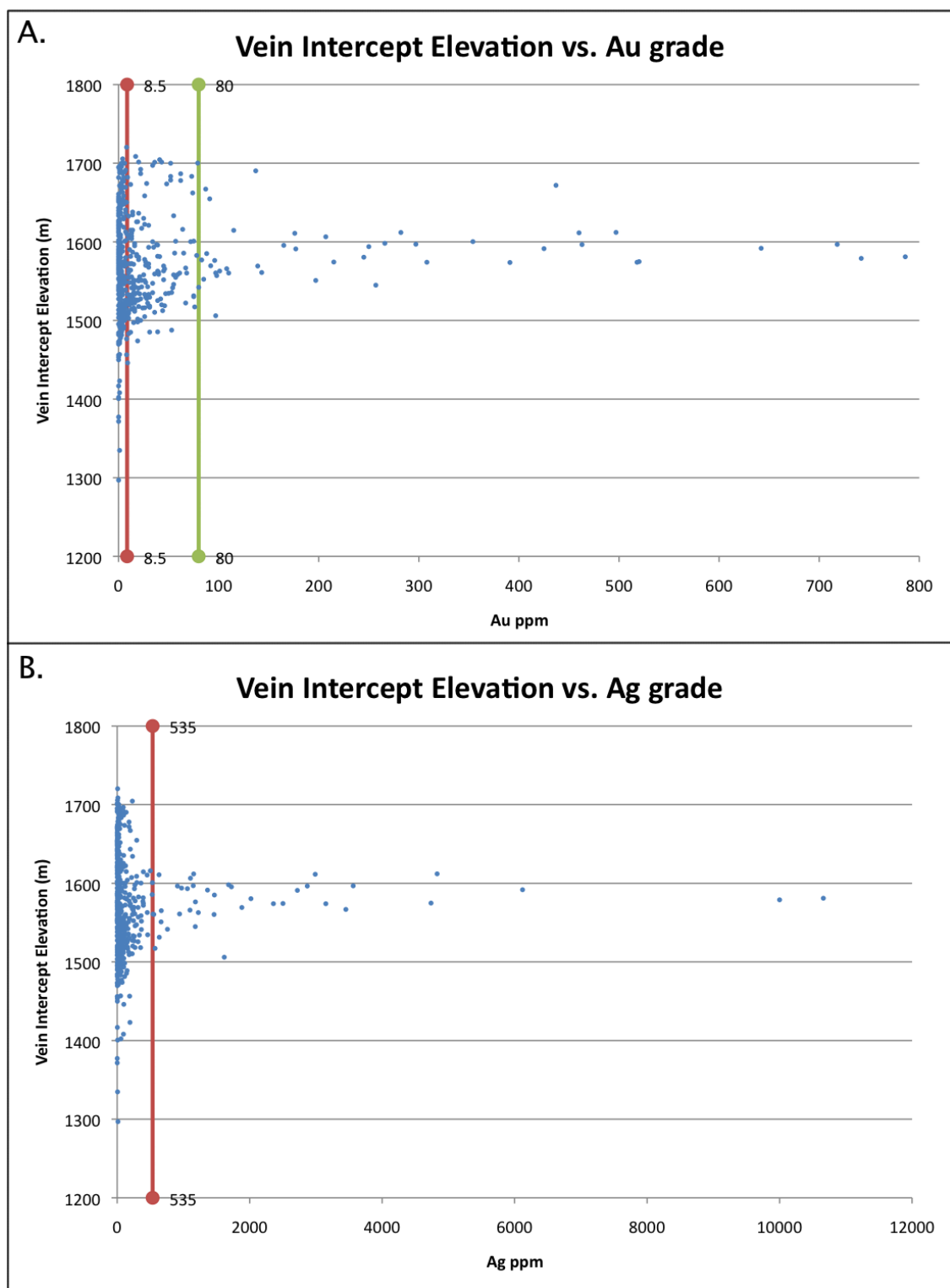
Fig. 23. Plots of elevation versus grades of Vein 18 drill intercepts for A. Au, and B. Ag.
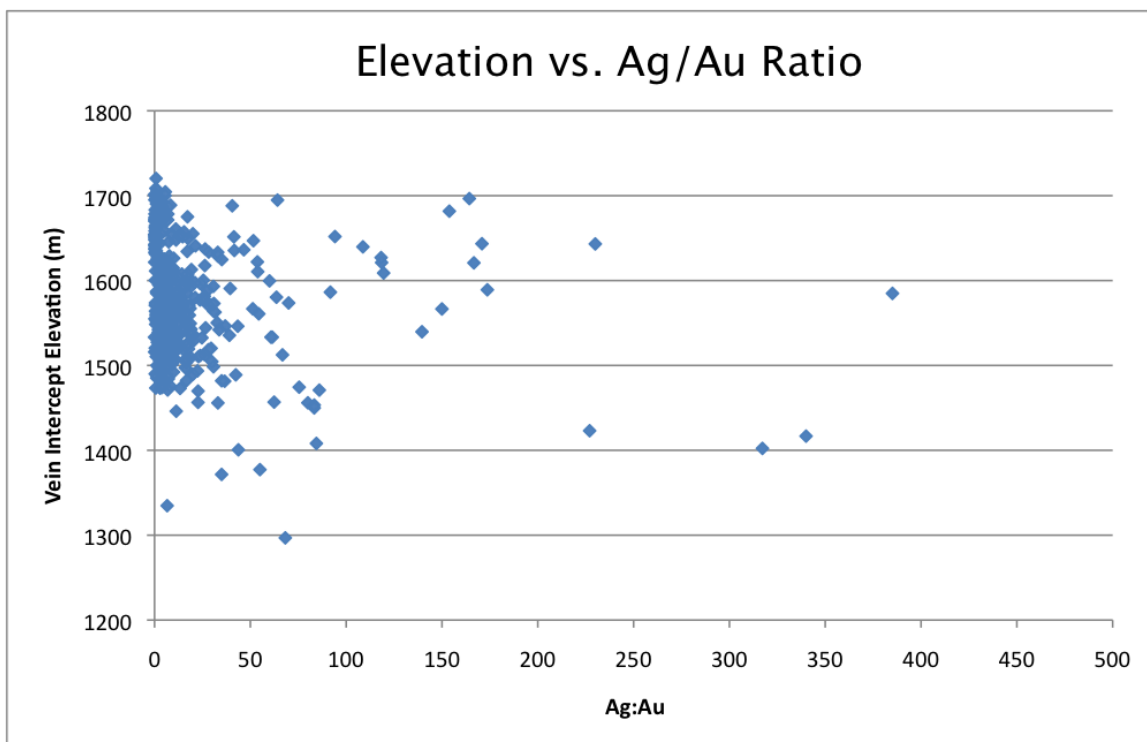
Fig: 24. Plots of elevation versus Ag/Au ratios for Vein 18 drill intercepts.

Relationship between quartz textures and gold and silver grades

Quartz textures, as described above, were recorded from 435 drill intercepts of Vein 18 based on examination of hand samples, polished thin sections, and drill core photos. The most common quartz texture is massive (MS) quartz, occurring in 371 out of 435 intercepts (86%). The second most common quartz texture is banded (BD) quartz (290, 67%), followed by vein breccia (VNBX, 188, 43%), bladed (BL) quartz (71, 16%), vuggy (VGG) quartz (57, 13%), chaotic (CH) quartz (45, 10%), and cockade (CC) quartz (4, 1%). Bar and whisker diagrams comparing distributions of Au and Ag grades in the presence or absence of six of the quartz textures are shown in Figure 25. The most

pronounced increase in the distribution of Au and Ag grades is where banded, bladed, and chaotic quartz are present.   Where vuggy quartz and vein breccia are present, median Au and Ag grades are lower than where they are absent.
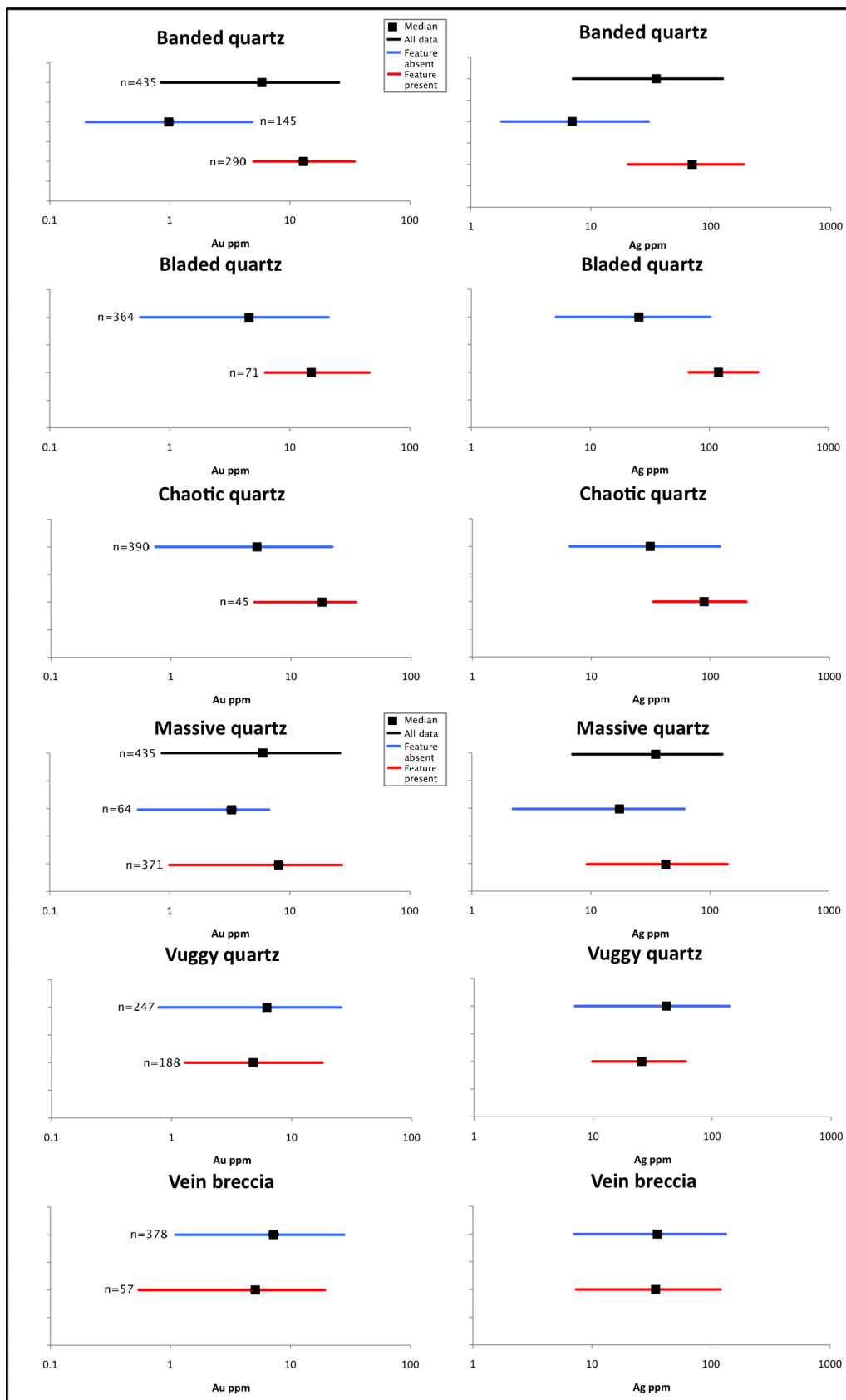
Fig. 25 (above): Bar and whisker plots comparing distributions of Au and Ag grades (log scale) for banded quartz, bladed quartz, chaotic quartz, massive quartz, vuggy quartz, and vein breccia when those quartz textures are present (red lines) to when they are absent (blue lines). Blue lines represent the absence of that texture, while red lines represent presence of that texture. The black lines in the top diagrams represent all Au and Ag data, respectively. The black square represents the medians of the data in the populations, and the ends of the lines represent the middle fifty percent (2nd and 3rd quartiles) of the data populations.

The distribution of quartz vein textures versus elevation is shown in Figure 26. Massive quartz, vein breccia, banded quartz, and chaotic quartz cover nearly the entire elevation range of data (1297 to 1720 m) and extend to the bottom of the known extent of Vein 18. Massive quartz is found throughout the known vertical extent of Vein 18. Bladed and vuggy quartz do not extend as deep, extending down to elevations of 1446 m.
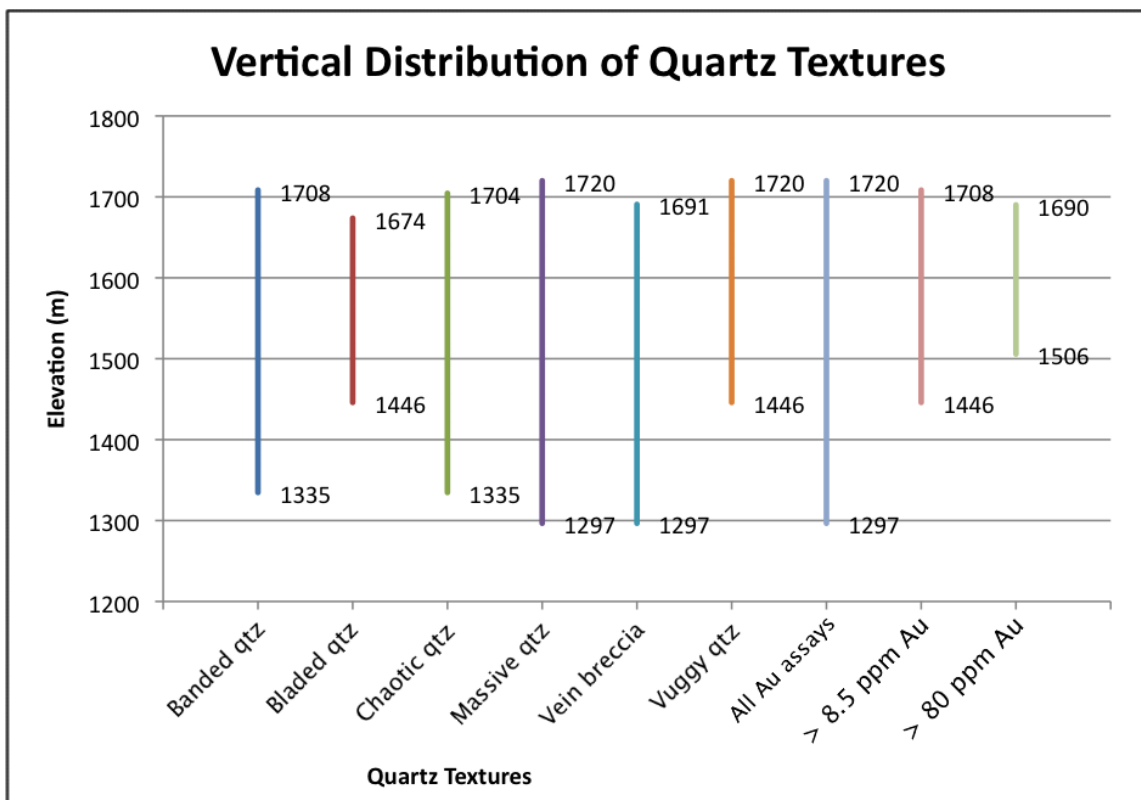
Fig. 26 (above): Plot of the vertical distribution of quartz textures in Vein 18. Vertical intervals of > 8.5 ppm Au and > 80 ppm Au are also plotted for comparison.

When plotted on the longitudinal section of Vein 18, bladed, banded, and chaotic quartz correlate best with Au and Ag grades (Fig. 27). Bladed quartz and chaotic quartz have similar spatial distributions and are almost entirely confined to zones of >8.5 ppm Au. Bladed quartz, occurring between 1446 and 1674 m, corresponds best with the vertical range containing the highest grades, > 40 ppm Au and > 200 ppm Ag. Banded quartz is more widespread and is mainly confined to zones of >1 ppm Au. Banded quartz is also present in 74 of 84 intercepts that assayed greater than 40 ppm Au and 33 of 36 that assayed > 80 ppm Au. Spatial relationships between massive quartz, vuggy quartz, and vein breccia textures and Au and Ag grades are not apparent. Massive quartz and vein breccia are found throughout Vein 18, whereas vuggy quartz occurs mostly in the upper parts of Vein 18 and above the Tertiary unconformity.

Fig. 27 (below): Longitudinal section of Vein 18 showing gold grades distribution of massive, banded, bladed, and chaotic quartz. Contour at < 1 ppm Au represents the extent of available drill data.

Au grades vs. quartz texture distribution
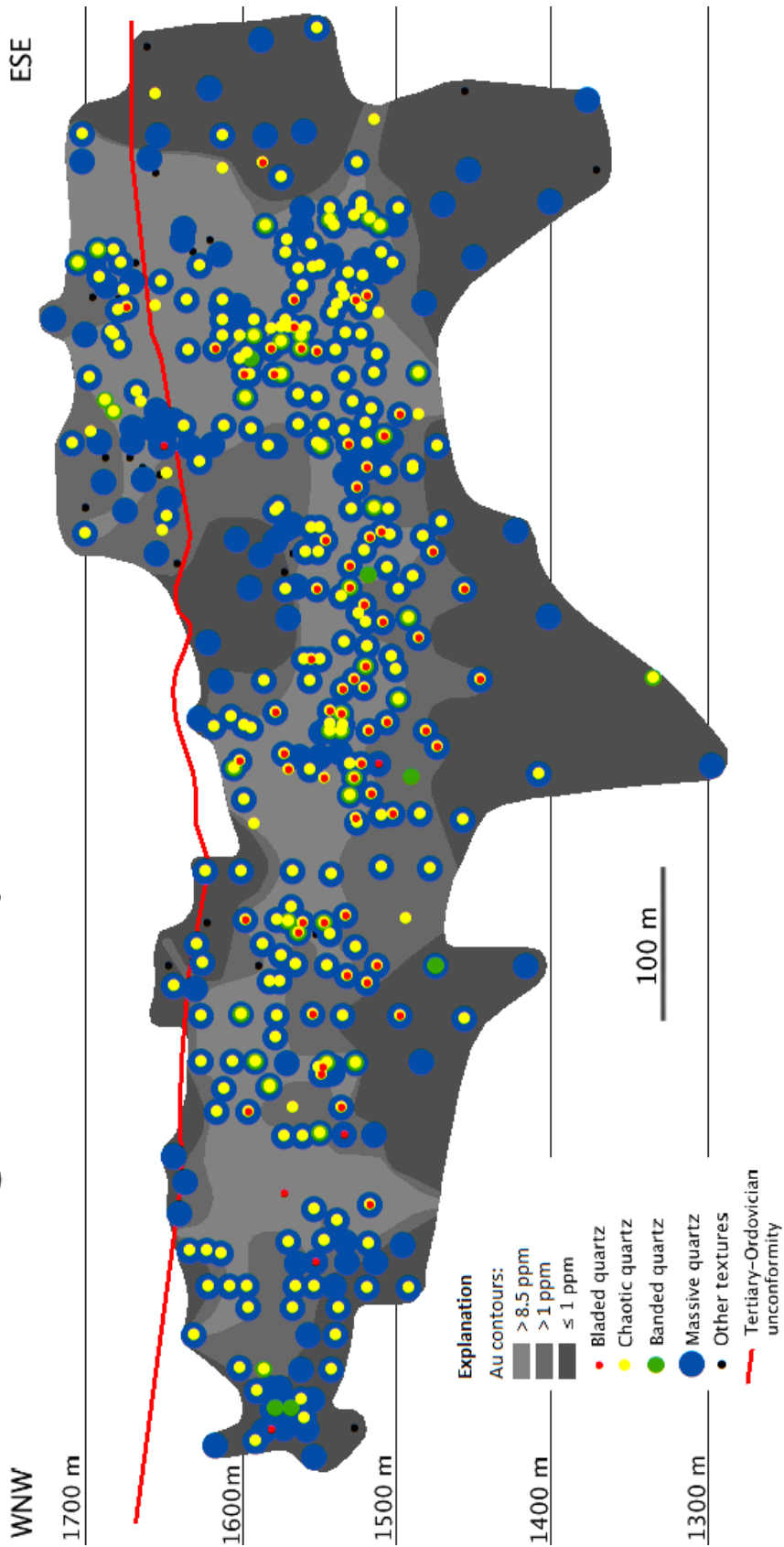
Quartz Textures as Indicators of Hydrothermal Conditions

Boiling is a fundamental process in modern geothermal systems and is important in the formation of low-sulfidation epithermal mineral deposits (Henley, 1984; Fournier, 1985; Simmons and Christenson, 1994; Hedenquist et al., 2000). In epithermal systems, the primary control on fluid pH is CO_2 concentration (Hedenquist and Henley, 1985), and to a lesser extent, H_2S concentration. As fluids boil, CO_2 and H_2S concentrate in the vapor phase, resulting in a pH increase. Increased pH leads to calcite and adularia stability, while CO_2 loss also decreases calcite solubility and causes calcite to grow as blades or plates (Simmons and Christenson, 1994). Therefore, adularia and bladed calcite are common indicators of boiling in low-sulfidation epithermal veins (Hedenquist et al., 2000).

Boiling also results in the loss of H_2 to the vapor phase, which causes oxidation, decreasing gold solubility as a bisulfide complex (Drummond and Ohmoto, 1985). As H_2S is lost to vapor, gold bisulfide complexes destabilize and fluids become supersaturated with respect to gold (Seward, 1989; Brown, 1986).

As boiling continues in epithermal systems, a significant portion of water is lost to the vapor phase, and fluids begin to cool. These changes lead to supersaturation with respect to metastable silica phases (amorphous silica, opal, chalcedony) (Fournier, 1985), which aggregate and form silica colloids (Saunders, 1994). Silica colloids deposit as bands of silica gel on vein walls or as rounded nodules that remain in the fluid. These features are commonly recrystallized to chalcedony or quartz, found as banded and chaotic quartz textures (Dong et al., 1995). For these reasons, banded and chaotic

(flamboyant) quartz are also potential indicators of boiling in low-sulfidation systems. These fluids will also typically contain gold colloids (or nanoparticles), which are physically transported and deposited. Nanoparticles deposit on the lee sides of vein wall protrusions (such as bladed quartz) to produce the "sluice box textures" that were described above (Saunders et al., 2008).

As fluids cool between boiling events, slower precipitation in open spaces likely occurs, forming textures such as massive and vuggy quartz, which are not associated with boiling (Dong et al., 1995; Moncada et al., 2012).

The paragenesis of quartz textures in four vein intercepts of Vein 18 were documented for textural parageneses. Hole HSD-202 (110 ppm Au; 1463 ppm Ag) is from the west ore shoot and displays the following textural paragenesis: vein breccia → massive quartz → banded quartz → bladed quartz. HDB-029 (96 ppm Au; 1181 ppm Ag) is from the central ore shoot and shows: vein breccia → banded quartz → massive quartz, and HDB-057 (143 ppm Au; 942 ppm Ag) is from the east ore shoot and displays: vein breccia → banded quartz → bladed quartz → massive quartz → banded quartz. Hole HSD-240 (46 ppm Au; 242 ppm Ag) is from the east ore shoot and displays: vein breccia → banded quartz → bladed quartz → banded quartz.

All four intercepts begin with vein breccia textures and display similar textural parageneses. All four contain banded quartz, and three intercepts show massive and bladed quartz as well. Similar textural parageneses between ore shoots, combined with textural patterns in other ore-grade intercepts, suggest formation of quartz textures occurred in the following sequence: vein breccia → banded quartz → bladed quartz →

massive quartz → banded quartz → bladed quartz → massive quartz. Textures showed

no evidence of a consistent "vein stratigraphy" as documented by Shimizu (2014) and

Shimizu et al (1998).

Relationship between SWIR-determined mineralogy and gold and silver grades

Short-wave infrared spectroscopic analysis of samples from Vein 18 led to the

identification of alunite, kaolinite, dickite, illite, ammonium illite, montmorillonite, and

chlorite. Clay and sulfate minerals show relationships with Au and Ag grades within

Vein 18 (Figure 28). A compilation of vein and alteration mineralogy data based on

SWIR spectral analyses and petrographic examination can be found in APPENDIX A23.

Samples which contained illite and ammonium illite were widely distributed

throughout the vertical and lateral extend of Vein 18 and coincide closely with both the

>1 ppm Au and >40 ppm Ag contours. Illite and ammonium illite are restricted to

elevations between 1445 and 1625 m, similar to the range of bladed quartz (1446-1674

m). In the eastern part of the vein, alunite accompanies high gold and silver grades (>40

ppm Au; >200 ppm Ag). Alunite was identified in 10 of 37 vein intercepts and is

restricted to elevations above 1555 m. Alunite coincides well with the large, vertically

extensive eastern ore shoot. Dickite, identified in 6 intercepts, commonly occurs with

alunite, but extends further downward, to an elevation of 1508 m. Chlorite and siderite

were only found below the zones of >8.5 ppm Au and >200 ppm Ag, occurring between

elevations of 1445 to 1535 m. The dataset shows no spatial distribution between high

grades and the distribution of kaolinite and montmorillonite, despite kaolinite occurring throughout much of the vertical and lateral extent of Vein 18, whereas montmorillonite is more common to the west and deeper in the vein, and never coexists with alunite.

Bar and whisker diagrams were constructed to assess whether Au and Ag grades were distinctly higher or lower in the presence of alunite, illite, ammonium-illite, montmorillonite, or kaolinite (Fig. 29). Grades are significantly higher where illite or ammonium illite is present. Median Au and Ag grades are 11.4 ppm and 80 ppm greater where they are present, and median Au grades are < 8.5 ppm Au where illites are absent. The same relationship, albeit not as strong, holds for alunite. The median grade for Au and Ag where alunite is present is 20.9 ppm and 131.8 ppm compared to 8.28 ppm and 93.9 ppm where it is absent. In contrast, the presence or absence of kaolinite or montmorillonite appears to have no control on Au and Ag grades. Where illite is present, it occurs as illite-montmorillonite mixtures and has not been recognized with montmorillonite. Conversely, montmorillonite occurs both with and without illite. Illite-smectite mixtures suggest temperatures between 180°C and 230°C (Reyes, 1990).

Au grades vs. vein mineralogy

Fig. 28 (above): Longitudinal section of Vein 18 showing gold grades in relation to the spatial distribution of vein minerals. Contour at < 1 ppm Au represents the extent of available drill data.
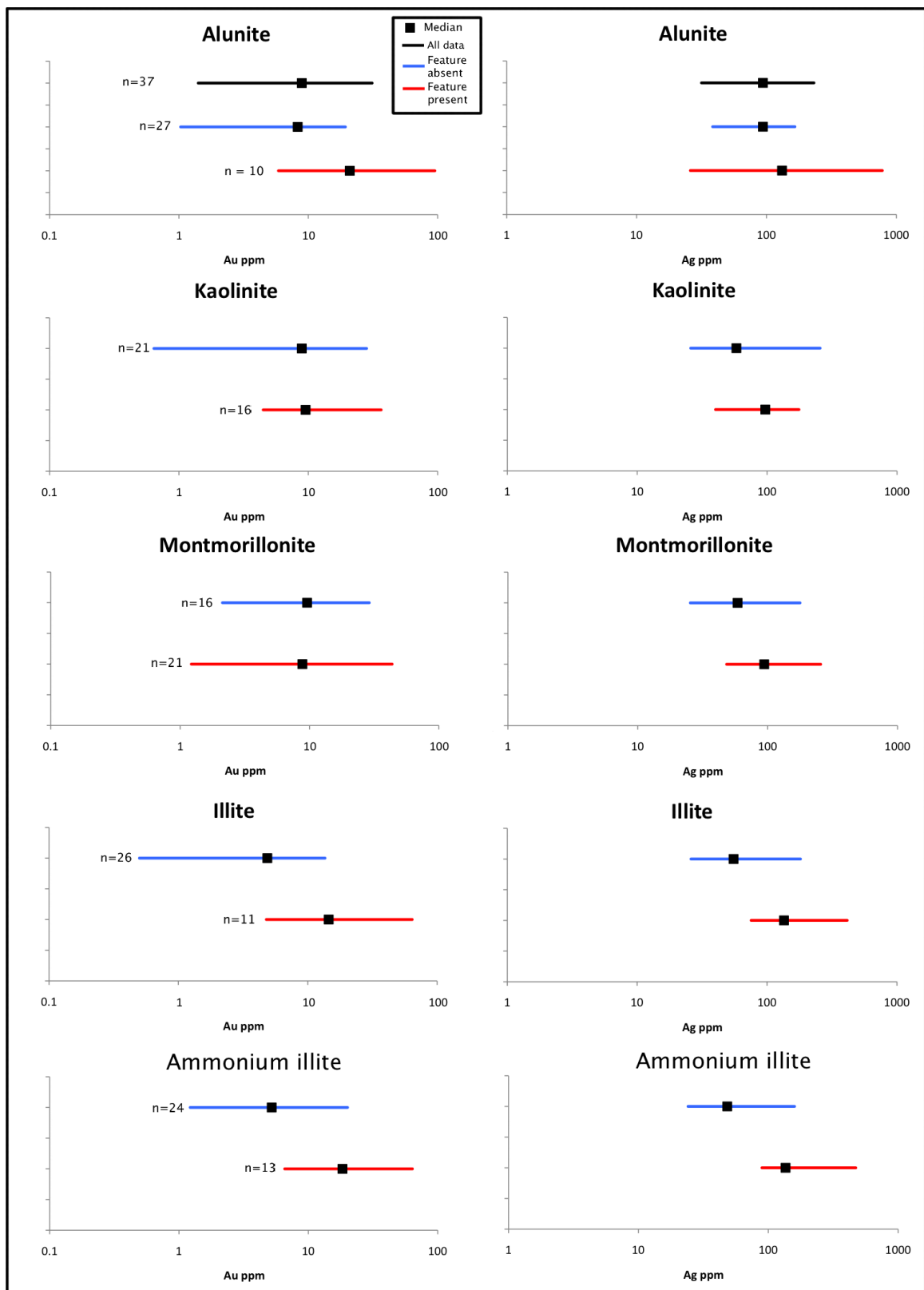
Fig. 29: (above): Bar and whisker plots comparing distributions of Au and Ag grades for alunite, kaolinite, montmorillonite, illite, ammonium illite, when those minerals are present (red lines) to when they are absent (blue lines). The black lines in the top diagrams represent all Au and Ag data. The black square represents the medians of the data populations, and the ends of the lines represent the middle fifty percent (2nd and 3rd quartiles) of the data populations.

Relationship between vein forms and gold and silver grades

Bar and whisker diagrams clearly show that grades are higher where discrete veins are present (Fig. 30). Where discrete veins occur, median Au and Ag grades are 12 ppm and 68 ppm greater than where they are absent. Where replacement veins, vein breccias, and stockworks are present, median Au and Ag grades are lower than where they are absent, although the differences are not as sharp as for discrete veins. Discrete veins are good indicators of Au and Ag grades, because they can be quite thick, and they host a wide variety of quartz textures that are less developed in other vein forms. Discrete veins, stockworks, and vein breccia forms occur throughout Vein 18 (Figure 31). Replacement veins, as described above, are restricted to volcanic rocks in the very upper parts of Vein 18 and are commonly associated with quartz-alunite steam-heated alteration.
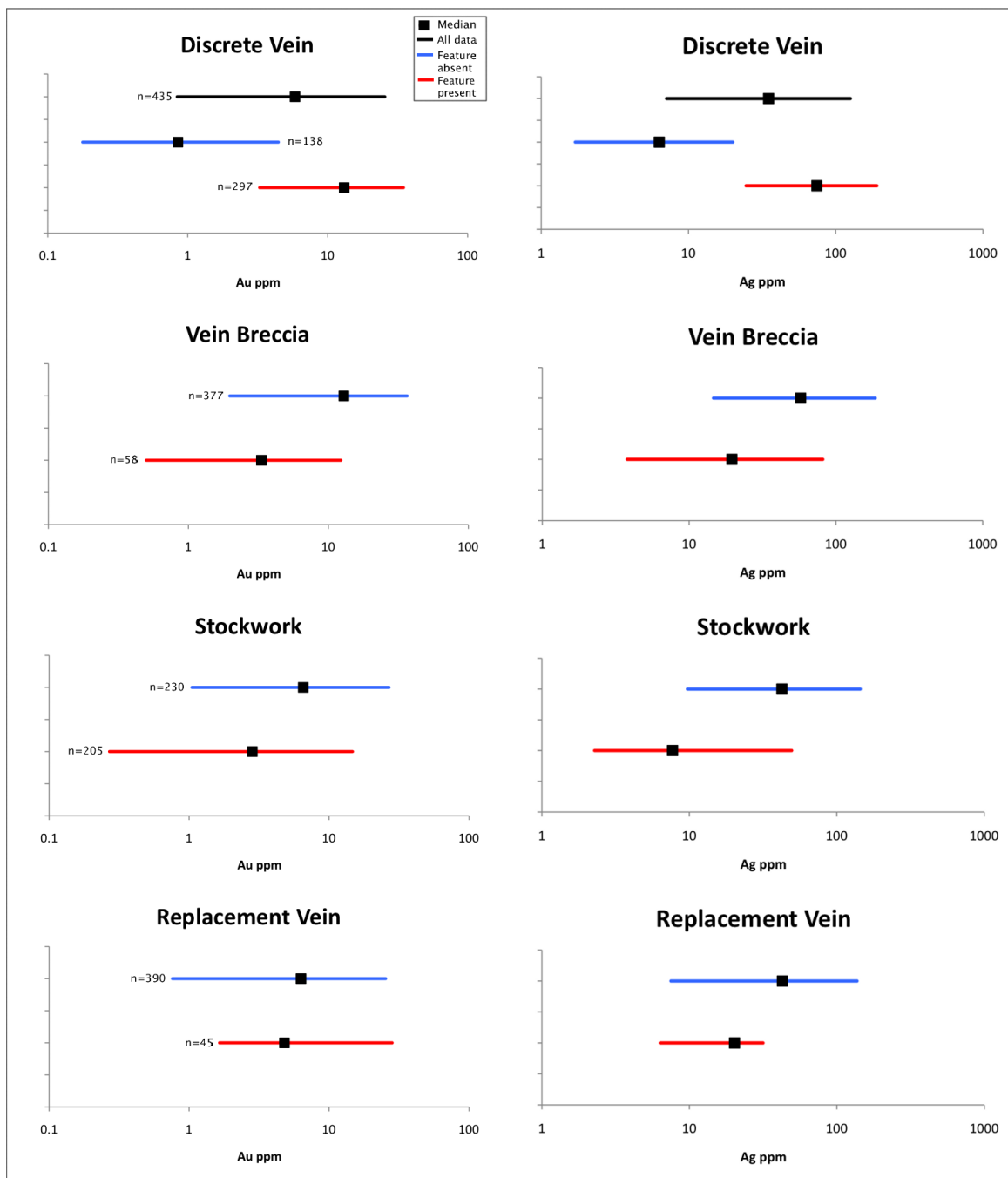
Fig. 30: Bar and whisker plots comparing distributions of Au and Ag grades for discrete vein, stockwork, and replacement veins when those veins forms are present (red lines) to when they are absent (blue lines). Blue lines represent the absence of a given vein form, while red lines represent presence of that vein form. The black lines in the top diagrams represent all Au and Ag data, respectively. The black square represents the medians of the data in the populations, and the ends of the lines represent the middle fifty percent (2nd and 3rd quartiles) of the data populations.

Au grades vs. vein form distribution
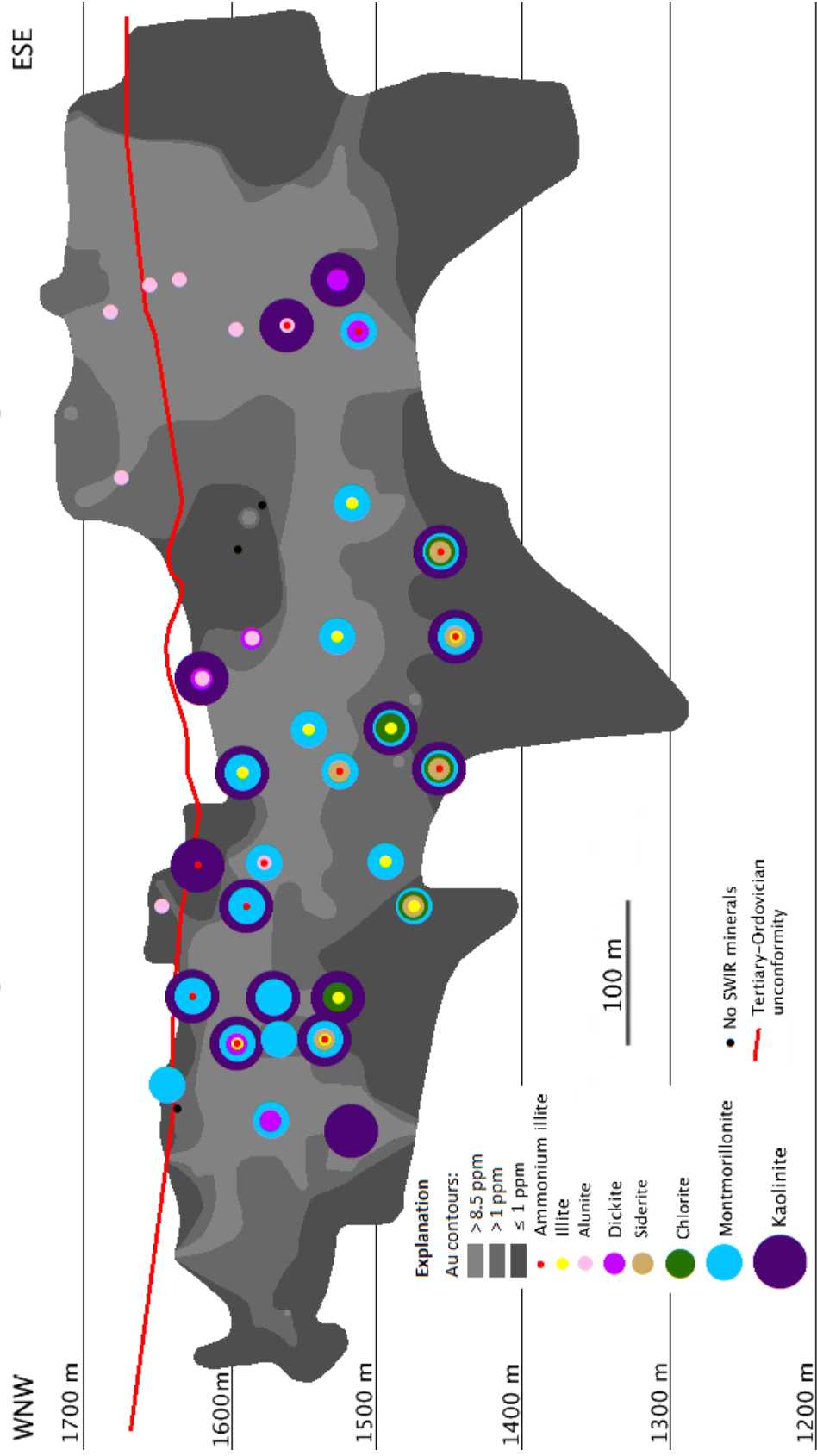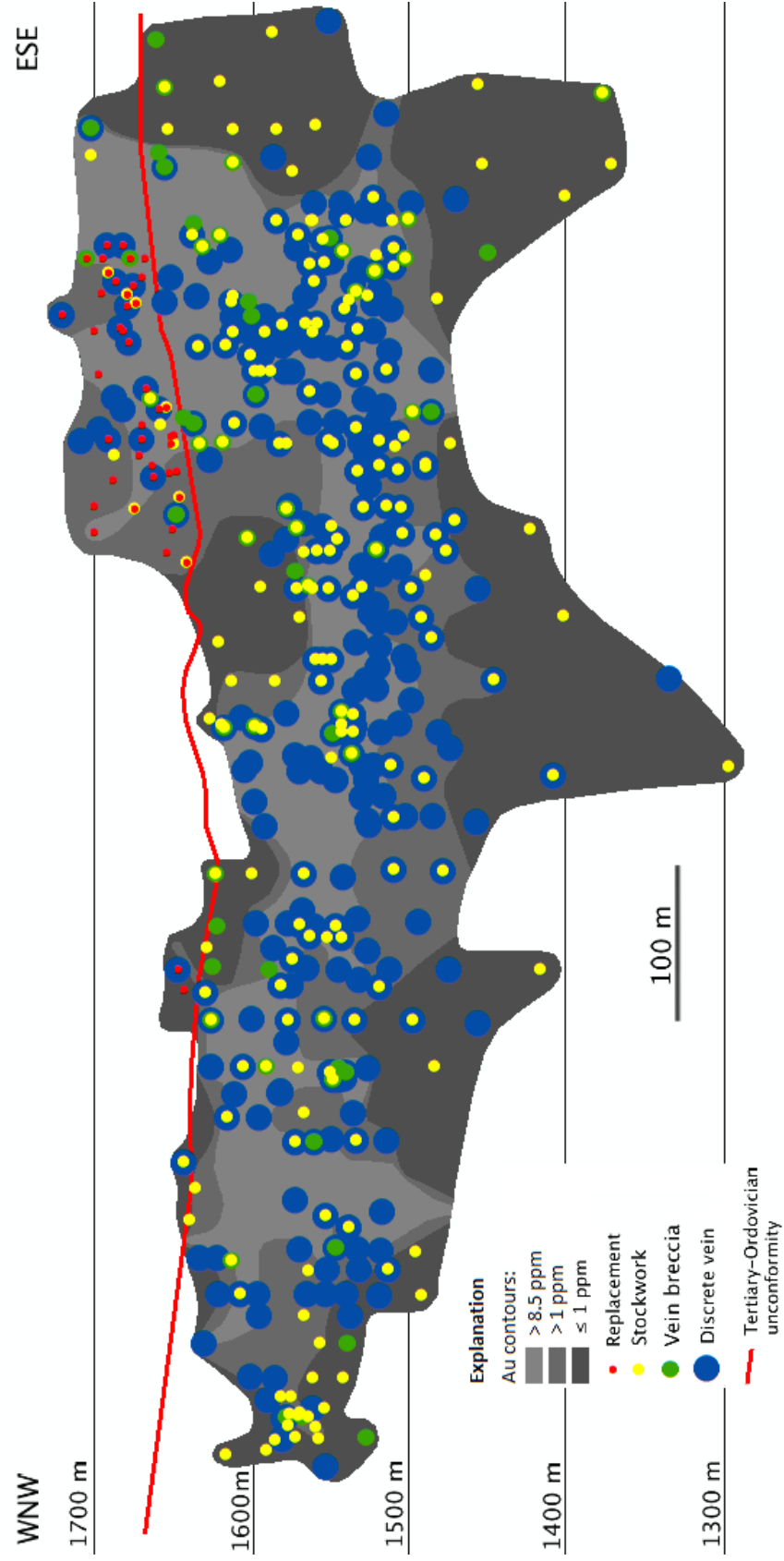
Fig. 31 (above): Longitudinal section of Vein 18 showing gold grades in relation to the spatial distribution of vein forms. Contour at < 1 ppm Au represents the extent of available drill data.

Relationship between structural trends, grade thickness variations, and gold and silver grades

High-grade ore shoots in epithermal systems are commonly developed in dilational zones caused by changes in strike or dip (Bobis et al., 1995; Christie et al., 2007). These changes suggest grades may vary with vein thickness. Traditionally, the distribution of grade*thickness values has been the way to account for variations in grade and vein thickness. Vein thickness, grade*thickness, strike, and dip in the 37 sampled drill hole intercepts of Vein 18 were evaluated using the three dimensional Leapfrog model of Vein 18, in order to assess potential structural control of high grade mineralization at Hollister.

The strike of Vein 18 ranges between 250° and 295°, while the overall trend of the vein is 280°. Graphs of Au grade vs. strike deviation show no correlation ($R^2 = -.04$) (Fig. 32), although strike variations from 0 to 15° host both high and low grades, while those that vary more than 15° host only lower grades. The surface projection of Vein 18 (Fig. 33) shows that ore shoots appear to be focused along more east-west trending portions of the vein, while the large gap between the central and east ore shoot appears to deviate more from east-west. Ore shoots in other veins may preferentially be hosted in more east-west trending portions of veins as well.

Vein 18 typically has a sub-vertical dip (90º ± 5º). Local variations in dip range to as shallow as 56° and dip both to the northeast and the southwest. Vein intercepts with grades of > 40 ppm Au have both shallow and steep dips, suggesting dip has no control on grade (Figure 34).

Gold grades do not correspond spatially with the thickest part of Vein 18 (Figures 35 and 36). Pearson correlations between Au grade and vein thickness had an $R^2 = 0.02$, while Ag grade and vein thickness had an $R^2 = -0.22$. These patterns and correlation coefficients indicate that high-grade ore shoots occur in both narrow and thick veins.
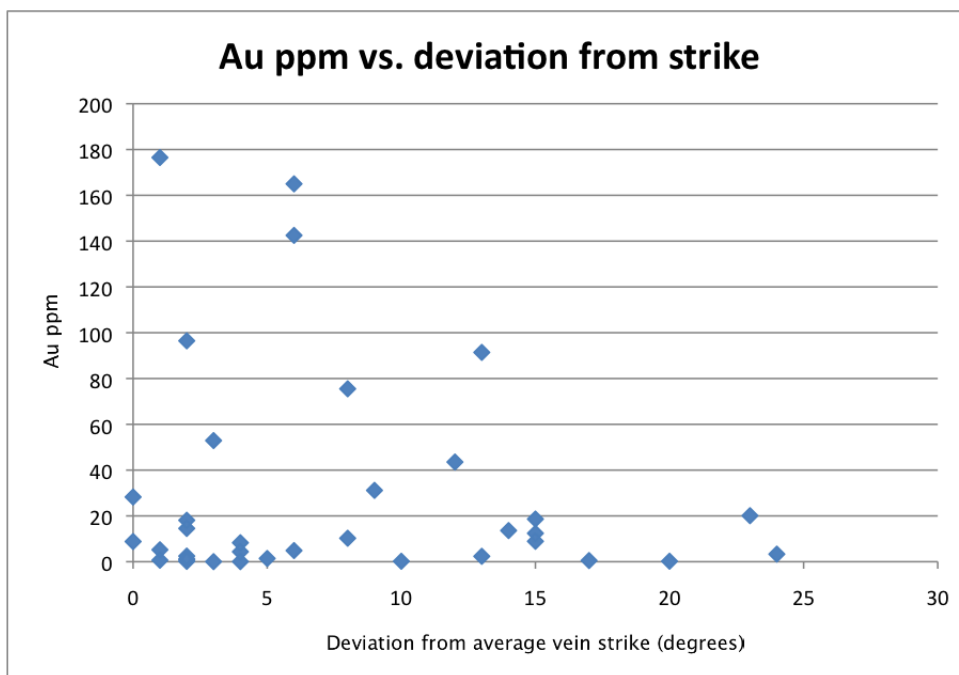
Fig. 32: Plot of Au ppm vs. deviation from average vein strike of 280°.

Surface projection of Vein 18
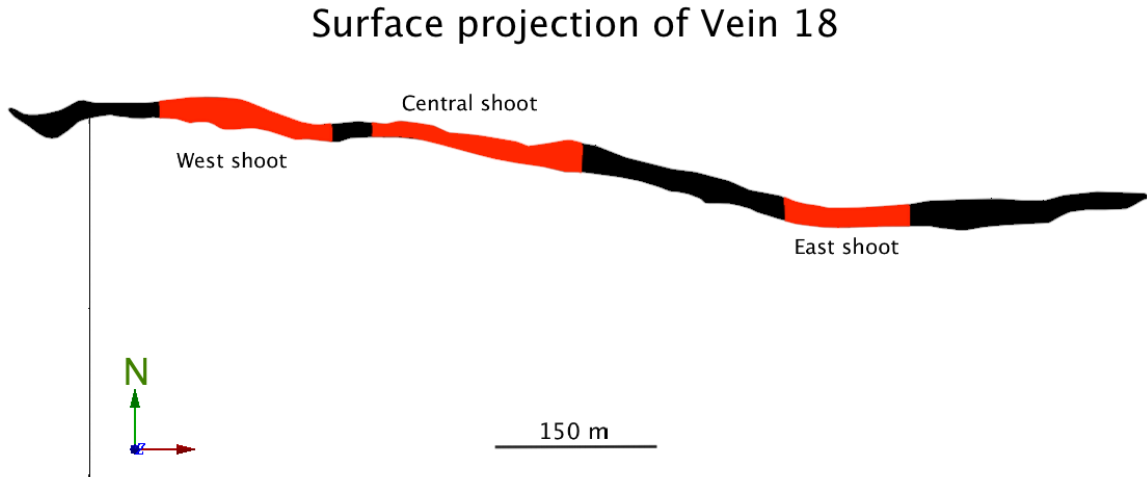
Fig. 33: Extent of available Vein 18 intercepts as projected to the surface. The west, central, and east ore shoots are highlighted in red.
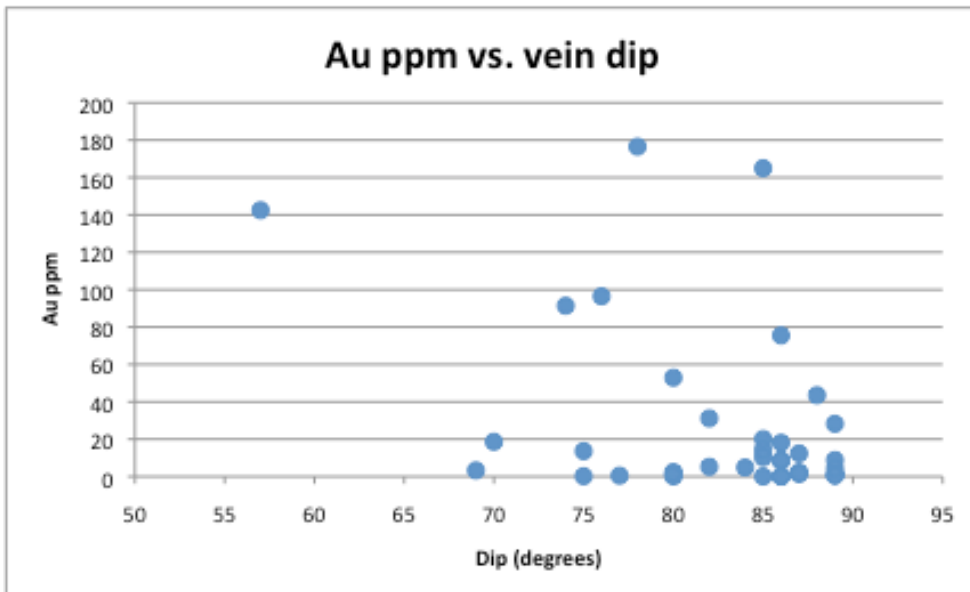
Fig. 34: Plot of Au ppm vs. vein dips.

Au grades vs. vein thickness
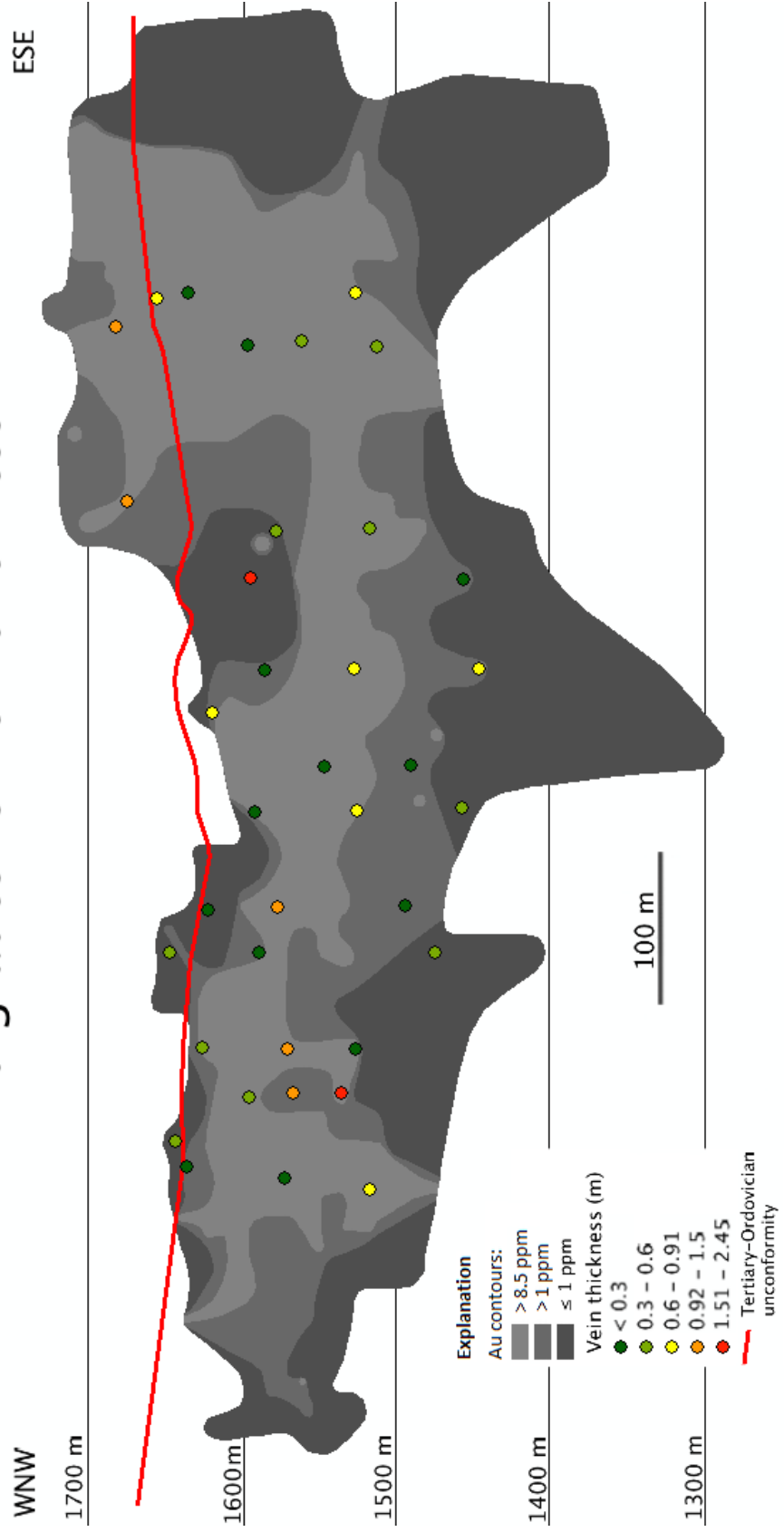
Fig. 35 (above): Longitudinal section of Vein 18 showing high-grade ore shoots in relation to the spatial distribution of vein thicknesses.
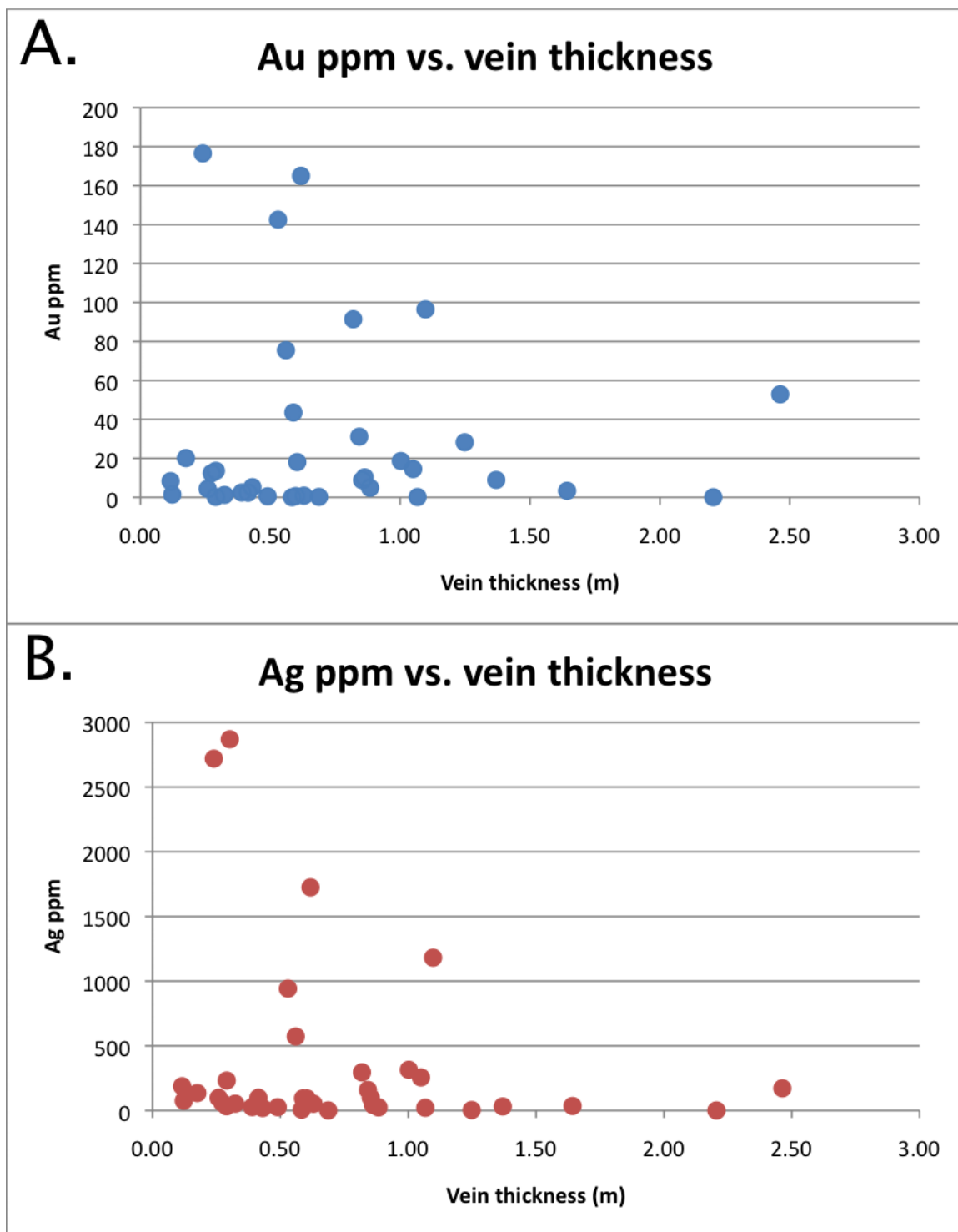
Fig. 36: Plot of A. Au ppm vs. true vein thickness, and B. Ag ppm vs. vein thickness. High grades are found in both thick and narrow veins.

Hydrothermal Features in Wall Rocks Surrounding Vein 18

Hydrothermal features in the wallrocks surrounding Vein 18 were documented to assess whether features increased in abundance with decreasing distance to Vein 18. Identification of such features could prove valuable to exploration. Features that were identified and described here include quartz vein densities, boiling indication factors, wall rock alteration, and fracture mineralogy as determined by SWIR reflectance spectroscopy. Data were collected by logging and sampling a fan of five underground core holes that were drilled along a cross-section that penetrated Vein 18 and other veins in the Clementine vein system (Figure 5). Narrow halos of $\geq$ 0.2 ppm Au surrounds individual veins 14 and 16 and coalesce around Veins 18 – 19 and Veins 20 – 22 to form wider zones.

Quartz vein densities

During the logging of the five holes, quartz vein densities were recorded by estimating the volume percentage of vein material within a given interval. Quartz veins included discrete veins, stockworks, and vein breccias and were filled with quartz and minor adularia. Veins ranged from millimeters up to about one meter in thickness. Wallrocks typically contained 1 – 2% vein material, with vein density locally reaching 30%.

A zone of >15% quartz veinlets forms an envelope around Vein 18 over much of its vertical extent (Fig. 40). At elevations below 1510 m, the envelope forms a narrow neck that extends < 5 m away from Vein 18 and into quartzite. Above 1510 m, the

envelope begins to flare out, extending up to 20 m away from Vein 18 in an overlying argillite sequence. The increase in size of the envelope could be a result of rheologic contrast between the quartzite and argillite sequences. Moreover, the size of the envelope is increasing because of potential coalescence of envelopes related to nearby parallel quartz veins. The zone of >15% quartz veins ends rather abruptly at an elevation of 1575 m. Only Vein 18 had a consistent envelope of >15% veins. The other veins (Vein 14-17, 19-22) did not exhibit consistent envelopes of increased vein density.

Quartz textures and boiling indication factors

Bladed, banded, and chaotic quartz textures are likely indicative of boiling as discussed above, and are mainly confined to elevations between 1470 and 1560 m, forming a zone that is 145 m wide and is best developed proximal to Veins 18 and 20. Massive quartz is found throughout the cross-section, in both main veins of the Clementine vein system and associated smaller veins in the wall rock.

As discussed above, banded, bladed and chaotic quartz are quartz textures that likely formed by boiling fluids. Similar to the manner of boiling intensity factors calculated by Moncada et al. (2012), boiling indication factors were calculated based on the presence of these textures. If none of these three textures was present, the boiling indication factor was zero, whereas if all three of those textures were present, the boiling indication factor was assigned a value of three. In the Clementine vein system (Veins 14-22), a boiling indication factor of 1 was measured in at least one drill intercept of each

vein. Veins 18 and 20 had the highest factors. Factors of two or higher were almost entirely confined to elevations between 1465 and 1535 m (Figure 37).
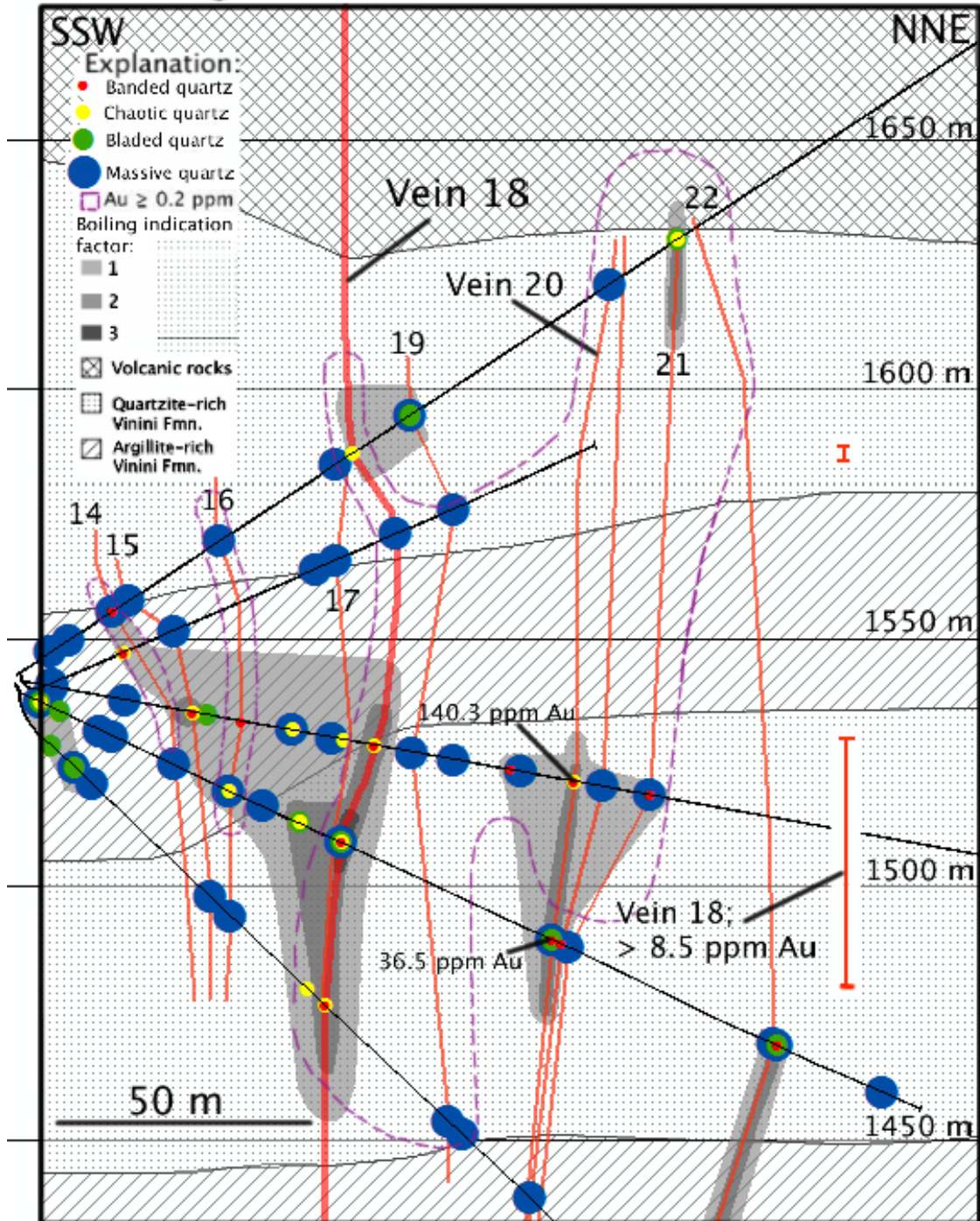
Fig. 37: Cross-section through the Hollister deposit, showing boiling indication factors in Vein 18 and other veins in the Clementine system. The red vertical line in the right portion of the image represents the elevation range in which Vein 18 is above cut-off grade (8.5 ppm Au).

Wall rock alteration

Macroscopic wall rock alteration associated with the high grade veins in relatively impermeable Vinini Formation is restricted to bleaching, which is best developed in quartzite and argillaceous siltstone. The bleaching is caused by silicification, during which interstitial clay between quartz grains was replaced by microcrystalline quartz along with very minor pyrite, resulting in a distinct lightening of the rock's color (Figures 38 and 39). Bleaching is pervasive above 1565 m elevation, where it can extend more than 60 meters from Vein 18 (Figure 40). Bleaching at depth is fracture-controlled and extends no more than 15 meters from veins. Fracture controlled bleaching takes on 3 funnel shapes around veins 14-16, 17-19, and 20-22. Deep, pervasive bleaching is typically only found near individual veins, stockworks, and breccias.
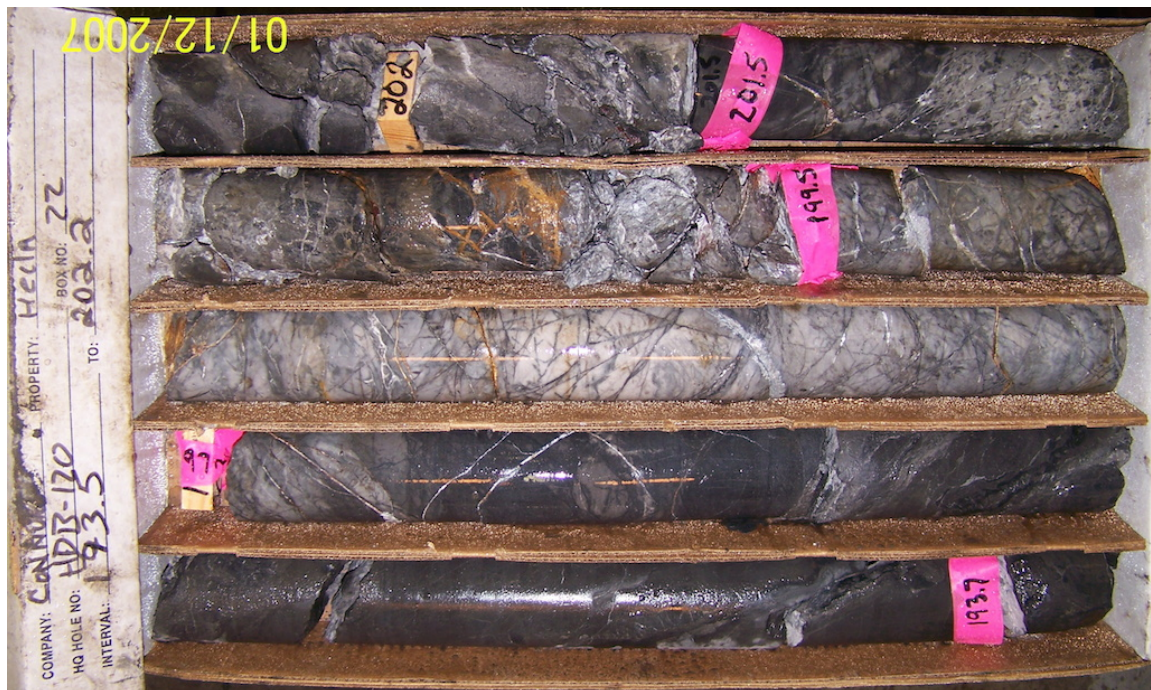
Fig. 38: Example of bleached quartzite. Intense bleaching is seen from 197 to 199.5 ft and is associated with small quartz veinlets. Weak bleaching is localized near fractures outside this interval.
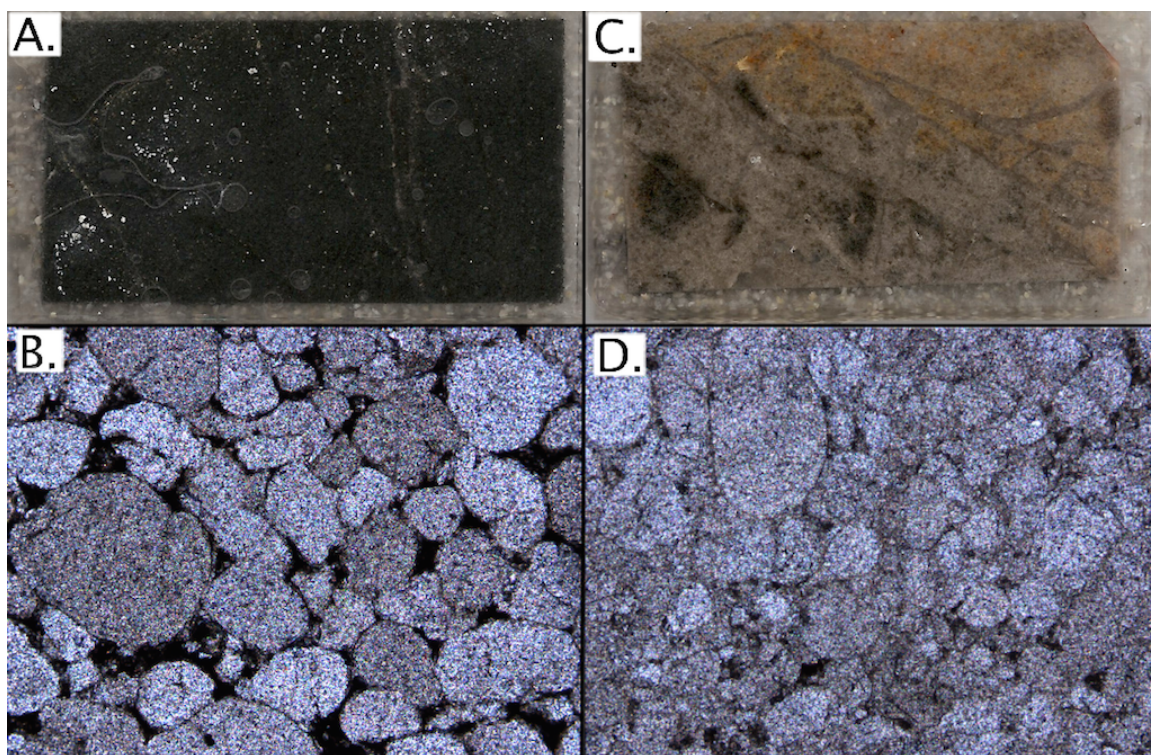
Fig. 39: Billet (A) and photomicrograph (B) of unaltered quartzites from sample 542-337, which shows a significant percentage of intergranular space filled by clays and trace pyrite (black interstices). Billet (C) and photomicrograph (D) of 536-523 represents a light gray, bleached quartzite, in which interstices between quartz grains have been replaced by hydrothermal quartz. Field of view for photomicrographs is 1.1 mm.
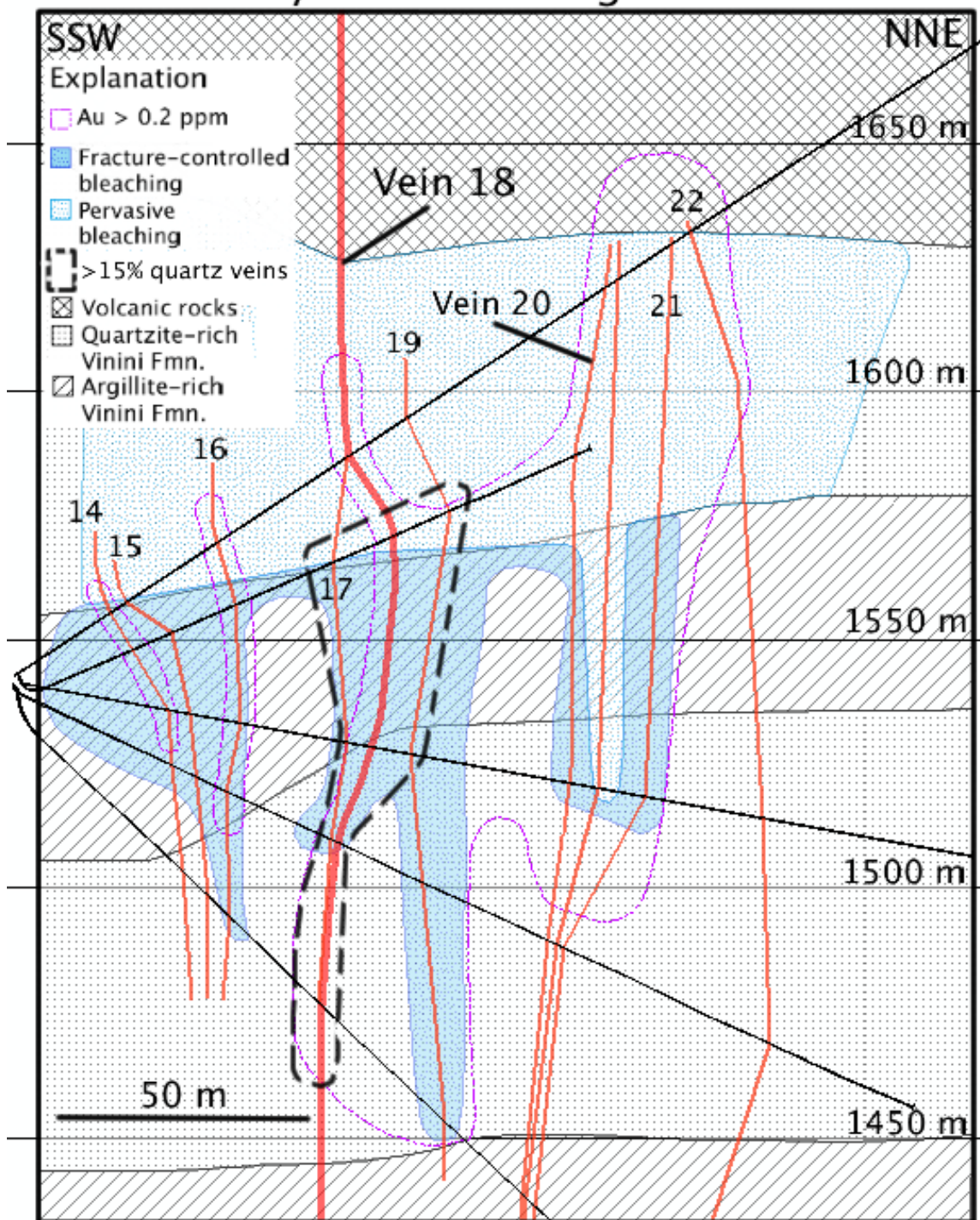
Fig. 40: Cross-section through the Hollister deposit, showing vein density around Vein 18 and other veins of the Clementine vein system.

Fracture-controlled alteration

Except for bleaching, the only other alteration recognized in the Vinini Formation were fractures coated with variable amounts of clays, alunite, siderite, and pyrite (Figure 41). These fractures are commonly filled with minor quartz and adularia, which is commonly altered to illite. The TerraSpec SWIR reflectance spectrometer was utilized to identify the clays and alunite along fractures surfaces of 156 samples along the cross section in Figures 42 and 43. Similar to the bleaching, fracture-controlled alteration is best developed along the 3 main sets of veins in the Clementine system - Veins 14-16, Veins 17-19, and Veins 20-22. Below an elevation of ~1430 m, minerals along fractures were not identifiable using the Terraspec. Only pyrite was observed along fractures and small veinlets.

Mixed clay-bearing fractures containing illite-montmorillonite and ammonium illite-montmorillonite form the widest mineralogic halo that is spatially coincident with the vertical range of high Au and Ag grades in Vein 18 (Fig. 42). The wavelength of the 2200 nm Al-OH feature showed no pattern with distance from the main veins or with elevation. Illite occurs between elevations of 1460 and 1610 m north and south of Vein 18. Ammonium-bearing illite is concentrated between elevations of 1500 and 1610 m. Both illite and ammonium illite extend up to 100 m laterally from Vein 18, but this is likely due to coalescence of separate zones of illite-bearing fractures associated with the three main vein sets. Local minor buddingtonite (ammonium-bearing feldspar) was also recognized in fractures that had ammonium illite zones. Bartlett et al. (1991) reported

buddingtonite in altered Miocene volcanic rocks in the open pit. Chlorite was detected in veins and fracture surfaces below elevations of 1510 m.

Alunite-bearing fractures occur at elevations greater than 1500 m (Fig. 43). The distribution of alunite-bearing fractures forms a funnel shape centered on Vein 18. It flares out up to 125 m from Vein 18 in the upper quartzite sequence in the Vinini. In the underlying argillite sequence, it narrows down to < 20 meters from Vein 18 in its deepest occurrence. Dickite-bearing fractures occur in a small area within the zone of alunite-bearing fractures. The dickite zone is centered on Vein 18 between elevations of 1550 and 1660 m and extends ~10-25 m from Vein 18. Kaolinite-bearing fractures are present between elevations of 1485 and 1665 m. They are laterally extensive above 1575 m and extend at least 150 meters north and 100 meters south of Vein 18. Similar to alunite, the distribution kaolinite-bearing fractures necks down with depth forming narrow halos (< 5-10 m) around the three main vein sets. Late siderite-bearing veinlets and fracture surfaces in the Vinini are found at elevations of 1510 m down to at least 1440 m. They extend north of Vein 18 at least 125 m (Figure 43), and likely extend to the south as well. Like the other minerals, this lateral extent is likely due to coalescence of the 3 main veins sets.

Fig. 41: Fracture in quartzite, coated with tan to red siderite.
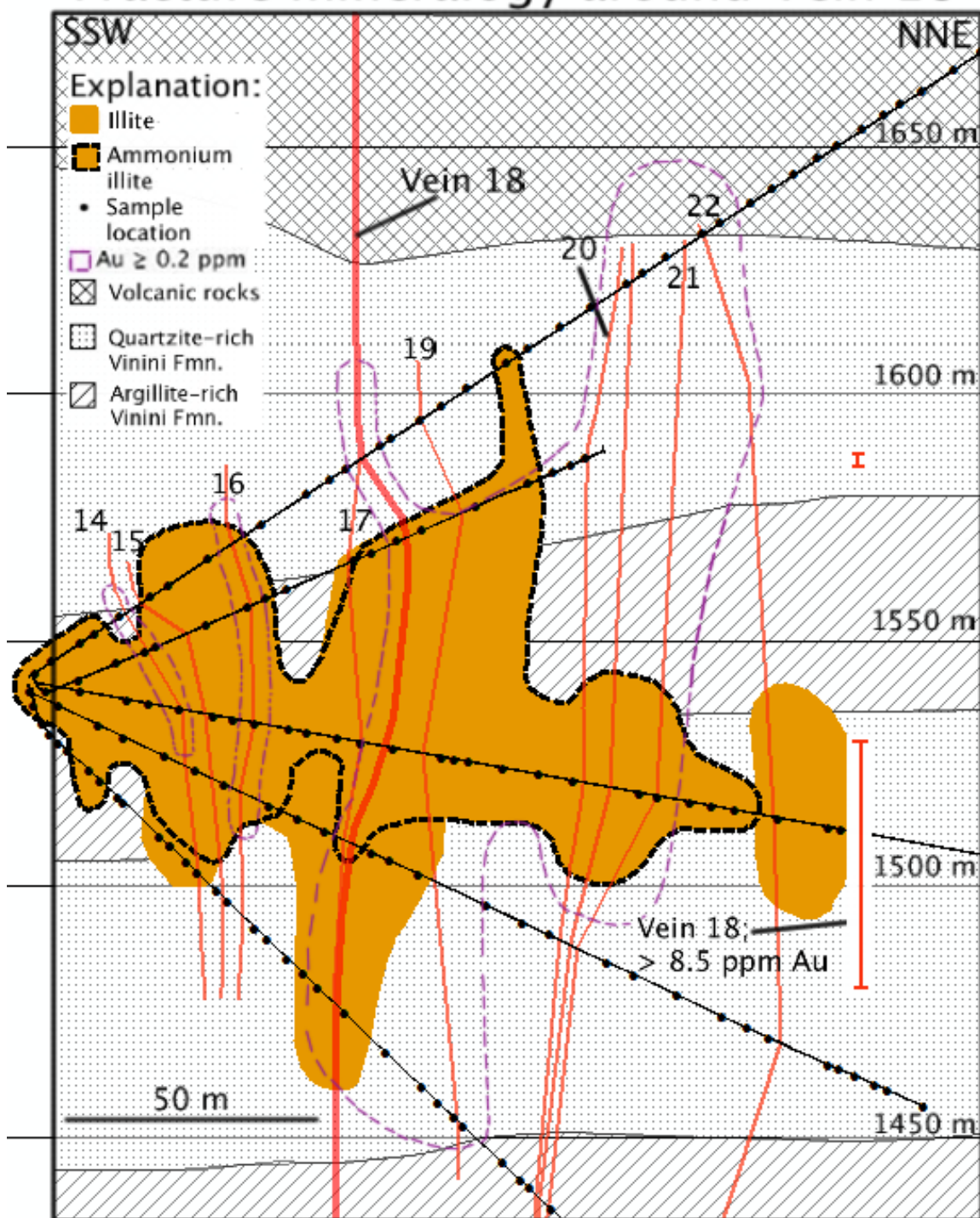
Fig. 42: Cross-section through the Hollister deposit, showing the distribution of illite-montmorillonite and ammonium illite-montmorillonite-bearing fractures around the main veins of the Clementine system. The red vertical line in the right portion of the image represents the elevation range in which Vein 18 is above cut-off grade (8.5 ppm Au).
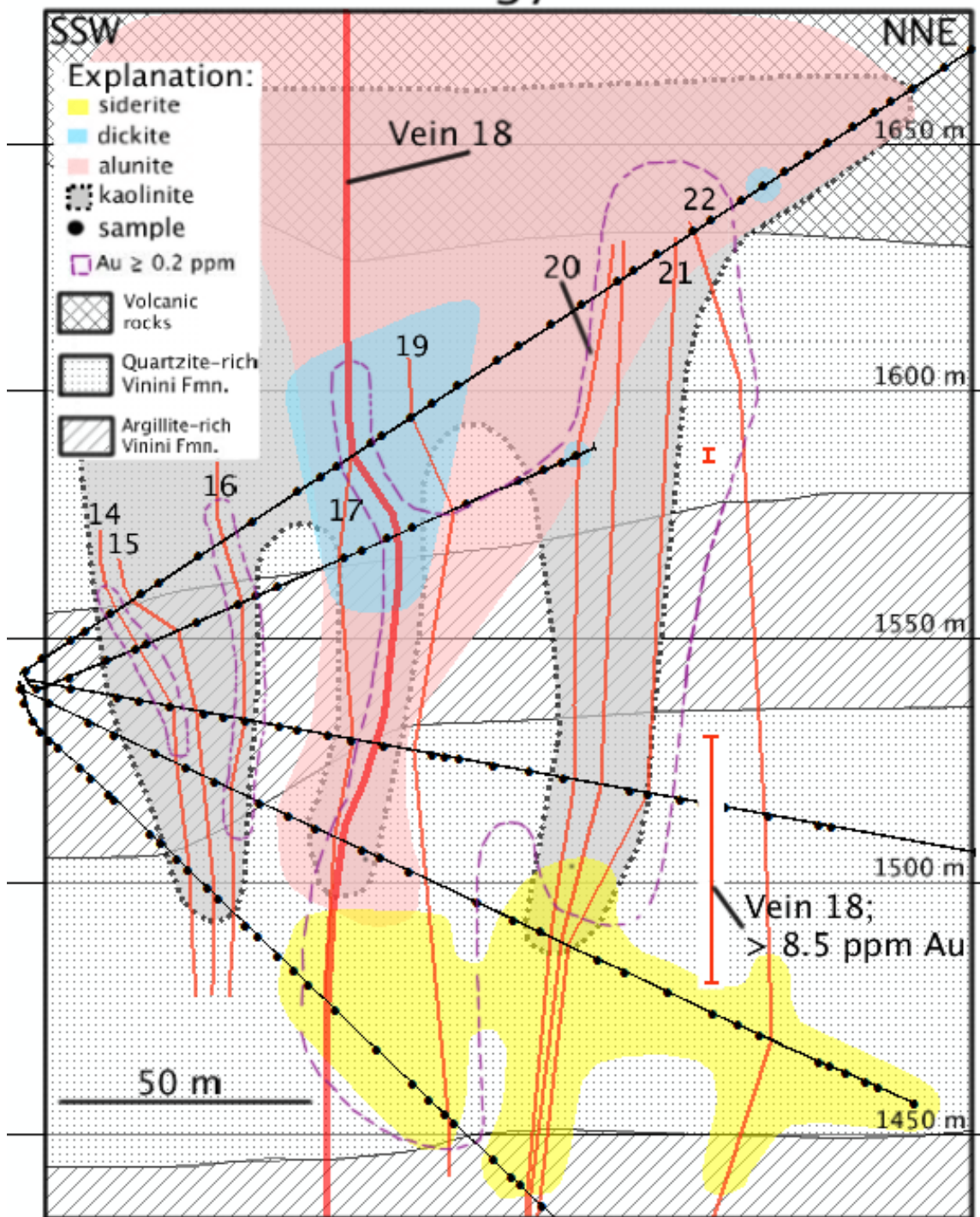
Fig. 43: Cross-section through the Hollister deposit, showing the distribution of alunite-, dickite-, kaolinite-, and siderite-bearing fractures around the main veins of the Clementine system. The red vertical line in the right portion of the image represents the elevation range in which Vein 18 is above cut-off grade (8.5 ppm Au).

Reconstruction of the Hollister Hydrothermal System in Time and Space

The main results of this paper are aimed at developing vectoring tools for the Hollister deposit and other bonanza epithermal precious metal vein deposits throughout the Great Basin and the world. A secondary result is a composite time-space reconstruction of the Hollister hydrothermal system (Figure 44), which aids in understanding the processes required to form the documented geologic features, in order to discriminate those patterns which are most useful in exploration at Hollister and other low-sulfidation systems.
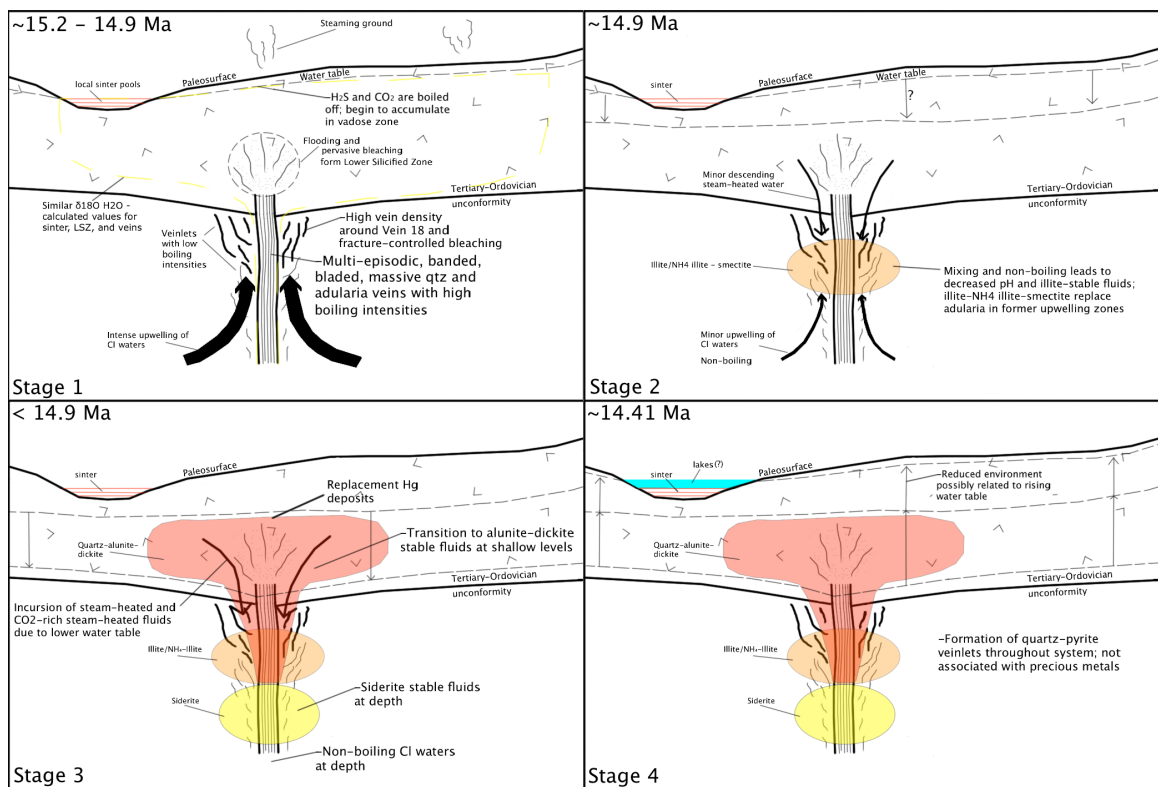
Fig. 44: Time-space reconstruction of mineralization stages at Hollister.

Formation of quartz-adularia-pyrite and deeper chlorite during Stage 1 is consistent with deposition from an upwelling, near-neutral pH, chloride water, similar to upwelling fluids in modern geothermal systems (Hedenquist and Browne, 1989; Simmons and Browne, 2000). The paragenetic sequence pyrite $\rightarrow$ base metal sulfides $\rightarrow$ Ag selenides/sulfosalts $\rightarrow$ gold/electrum at Hollister has been observed at other selenide-bearing, low-sulfidation epithemal systems. Observed mineral assemblages indicate fO_2 values below the hematite – magnetite buffer and $fSe_2{:}fS_2$ ratios < 1, which limit selenide mineralization to silver selenides in low-sulfidation epithermal deposits. The compatible nature of Se^{-2} in S^{-2} sites led to significant Se substitution in sulfide minerals. The presence of naumannite and aguilarite and the absence of acanthite, indicate formation temperatures between ~150° - 210°C (Simon et al., 1997).

Minimal offset faults (Wallace, 2003) and related fracture networks, now occupied by the mineralized veins, served as fluid pathways for upwelling, boiling Stage 1 fluids in the relatively impermeable Vinini Formation. As fluids approached the surface, they began to boil at elevations of possibly as deep as 1297 m (base of vein breccia) and certainly by 1446 m (base of bladed quartz after calcite). Increases in pH, combined with CO_2 loss, led to the deposition of bladed calcite and the deposition of adularia. Boiling also led to substantial vapor loss, leading to fluid supersaturation with respect to metastable silica phases, which caused colloidal silica to aggregate as thin bands and small nodules. As boiling continued and pyrite and base metal sulfides were deposited, the activity of reduced S in the fluid dropped, which led to increased Se/S

ratios and subsequent selenide deposition near the end of mineralizing cycles, similar to some other low-sulfidation epithermal systems (Simon et al., 1997).

Pressure, temperature, and salinity are the main parameters, which must be accounted for in a discussion of hydrothermal fluid boiling. Similar elemental associations between sinter and veins suggest that depth below sinter (1737 m elevation) is representative of depth below the paleowater table during Stage 1 vein formation. Bladed quartz after calcite, the most robust indicator of boiling in Vein 18, occurs between 291 and 63 m below the sinter. Given these depth constraints and assuming hydrostatic conditions and salinities of 2 wt.% NaCl, the calculated boiling curve (Fig. 45) indicates boiling temperatures between 227° and 165°C, which is consistent with much of the range of homogenization temperatures from Peppard (2002); however, minor CO_2 indicates that *effective* salinities were likely $0 - 1.5$ wt % NaCl equivalent (Hedenquist and Henley, 1985). Homogenization temperatures acquired from two non-boiling fluid inclusion assemblages in this study are plotted at 208 m and 228 m below the paleosurface, respectively (Figure 23) and are consistent with trapping by a non-boiling fluid.
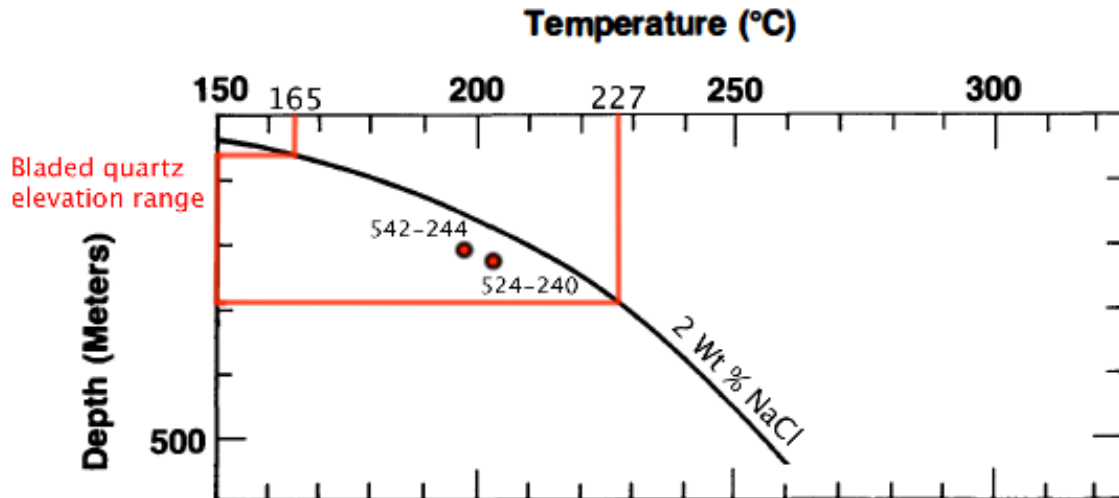
Fig. 45: Boiling point-depth curve as plotted for hydrostatic conditions at 2 wt% NaCl equivalent and 0% CO_2. Evidence for fluid boiling is recorded from 63 to 291 m below the paleosurface, marked by sinter. Homogenization temperatures of inclusions from entrapped, non-boiling fluids in drusy quartz crystals are consistent with the occurrence of fluid boiling in this interval. Modified from Loucks, 1984. Sinter depth and depositional temperatures are considered to be 0 meters and ≤100°C, respectively.

The west, central, and east ore shoots are observed to have similar textural parageneses: vein breccia → banded quartz → bladed quartz → massive quartz → banded quartz → bladed quartz → massive quartz. This progression has important implications for fluid evolution. The initial brecciation likely occurred as a variety of hydrothermal eruptions (Fournier, 1985). Hydrothermal brecciation likely increased the initial permeability, forming fluid pathways. Brecciation decreased confining pressures, leading to a time of episodic boiling and deposition of bladed and banded quartz. Separation of steam and water and decreasing pressures led to fluid saturation with respect to minerals (Fournier, 1985), and explains the association between bladed quartz, banded quartz, and gold-silver mineralization. Boiling eventually resulted in cooling and deposition of massive quartz with associated drusy quartz by non-boiling fluids. This

entire progression is observed twice at Hollister, indicating at least two periods of episodic boiling. The high-grade ore shoots preserve a greater number of these textural episodes than do more weakly mineralized portions of Vein 18, and documenting the number of generations of banding or blading may be a useful tool for exploration.

Stage 2 quartz, illite, ammonium illite, montmorillonite, and pyrite represent a time of non-boiling, cooling, and mixing of circulating chloride waters with lower pH fluids (Hedenquist and Brown, 1989), which resulted in replacement of adularia by illite-montmorillonite. Illite-montmorillonite mixed clays suggest temperatures between 180° and 230°C for stage 2, based on comparisons to the Wairakei geothermal system (Reyes et al., 1990). Ammonium illite is common in Middle Miocene low-sulfidation epithermal deposits in northern Nevada (e.g, Sleeper deposit; Corbett, 2005). Stage 2 illite and ammonium illite-bearing mixed clays form spatial patterns with gold, both in longitudinal section and cross section. Illite and ammonium illite serve as a proxy for adularia, which was originally deposited due to boiling and is associated with Au and Ag mineralization. Growth zones in Stage 2 drusy quartz hosts the majority of primary, Type I fluid inclusions.

Stage 3 alunite, kaolinite, and dickite, along with deeper siderite, resulted from steam-heated acid-sulfate and bicarbonate fluids. Steam-heated environments are common in the upper portions of low-sulfidation epithermal systems and active geothermal systems. Acid-sulfate and bicarbonate waters begin to form as H_2S and CO_2-bearing steam from underlying boiling fluids accumulates in the vadose zone, where H_2S oxidizes to form strong sulfuric acid. Accumulation of CO_2 in the vadose zone results in

the formation of steam-heated, weakly acidic bicarbonate waters. Steam-heated fluids percolate downward to mix with higher temperature hydrothermal fluids at the water table, leading to hydrolytic alteration of silicates. Steam-heated fluids, coupled with a descending water table, likely formed the replacement Hg deposits described by Wallace (2003) and Bartlett et al. (1991). Steam-heated, acid-sulfate zones are documented at Crofoot-Lewis and Buckskin, and late siderite and other carbonates at Mule Canyon also represent a CO_2-rich, steam-heated zone (John, et al., 2003). Minor naumannite, electrum, and specular hematite in Stage 3 is interpreted to have formed from dissolution and re-precipitation of stage 1 mineralization. This also required a high concentration of both selenide and sulfate in the mineralizing fluids. A $fO_2 -$ pH diagram constructed by Simon and Essene (1996) shows that at relatively high fO_2, reduced Se species (H_2Se; HSe^-) are stable in oxidized S fields (HSO_4^-; SO_4^{2-}), potentially leading to contemporaneous selenide-sulfate deposition (Vikre, 2007). Gold redistribution also supports this mechanism, as gold-bisulfide complexes are destabilized in more oxidizing environments, preferring gold deposition. Metal enrichments are not expected in steam-heated environments (Sillitoe, 1993) unless earlier mineralization is overprinted by a falling water table associated with steam-heated fluids (Ebert and Rye, 1997). Such changes in water tables are common in hydrothermal systems and was previously invoked at Hollister by Wallace (2003).

Alunite and dickite form a funnel around Vein 18. In cross section, kaolinite is more widely distributed than alunite and dickite. Siderite forms at depth as these steam-heated waters become less acidic and more reduced as they react with rock at

increasingly lower water:rock ratios. The alunite-dickite funnel centered on Vein 18 is interpreted here to result from a greater amount of H_2S flux from the boiling upwelling zone focused along Vein 18. Greater H_2S flux led to formation of more sulfuric acid and lower pH steam-heated waters that altered previously formed adularia and illite to alunite and dickite. The flanking zones of kaolinite form funnels centered on Veins 14-16 and Veins 20-22 (Fig. 44), which do not contain alunite or dickite, likely due to descending steam-heated bicarbonate waters. Therefore, in the absence of significant lateral fluid flow, alunite-bearing portions of steam-heated caps could possibly be considered more prospective than kaolinite-bearing portions because the alunite outline zones of high H_2S flux.

Stage 4, quartz-pyrite mineralization only locally occurs at Hollister, both in volcanic and sedimentary rocks. Stage 4 was likely deposited from near-neutral fluids associated with a rising water table and a transition back to a reducing environment. Peppard (2002) and Wallace (2003) reported later hydrothermal activity to the east and northeast of the Hollister veins. This activity postdated vein and disseminated mineralization by at least 0.2 Ma and likely represents a younger hydrothermal system centered to the east of the Hollister veins.

Summary of Controls on High Gold and Silver Grades

The Hollister deposit is an excellent example of a well-preserved, shallow epithermal system. The system displays a shallow hot-spring environment with abundant

sinter and silicification; disseminated gold mineralization; steam-heated zones; and

bonanza-grade veins at depth. Because of this preservation and the wealth of available

data, a variety of mappable characteristics, summarized in Table 4, act as controls on

mineralization and can be used to vector to high-grade ore shoots at Hollister. The results

of this study serve as template for not only further exploration in the Ivanhoe district, but

for other low-sulfidation epithermal deposits in the Great Basin and elsewhere in the

world. Controls on gold and silver grades in Vein 18 and features that suggest proximity

to high grade ore shoots include: 1) The presence of banded and bladed quartz and

adularia, all of which are indicative or suggestive of boiling, which is the main

depositional mechanism of high-grade ore shoots in epithermal vein deposits. 2) A

common paragenesis of quartz textures, which indicates multiple cycles of boiling, which

are commonly separated by quartz with non-boiling textures. 3) Discrete veins that

provide significant development of quartz textures; 4) Illite or illite-smectite zones that

can reflect the original distribution of adularia. 5) Discrete zones of steam-heated alunite,

that can define high H_2S flux from underlying zones of upwelling boiling fluid. The

higher the H_2S content of the upwelling fluid, the more capacity is has to transport and

deposit gold and silver. 6) Increased Se and Cu concentrations are indicative of high-

grade ore shoots, which typically contain >150 ppm Se and >250 ppm Cu; and 7) Ore

shoots are localized along the more east-west trending portions of Vein 18. These

controls should be applied below the west and east ore shoots in Vein 18, where ore

grade Au contours extend at depth, and are truncated by the extent of available data. Not

only can results from this study be used to vector to high-grade ore shoots along a known

vein, but can be used to explore for new veins by looking for many of the same features

in the wall rocks. The only recognizable pervasive wall rock alteration that appeared to be contemporaneous with deposition of ore at Hollister was silicification of clay-rich matrices of siltstone and sandstone, which resulted in a bleached appearance. Zones of bleaching at Hollister were wide in the volcanic rocks and the upper quartzite sequence of the Vinini Formation, but narrowed down to <15 m from Vein 18 in the productive depth interval. However, zones of illite and ammonium-illite-bearing fractures form a 170 m wide zone that is centered on Vein 18 and the Clementine vein system. Importantly, the vertical extent of that illite-bearing zone coincides closely with the range of elevations in which the high-grade ore shoots occur in Vein 18.

Detailed documentation of controls on high Au and Ag grades in low-sulfidation epithermal deposits of the Coromandel Peninsula (Hollinger and Mauk, 2001, 2002; Simpson and Mauk, 2007) are similar to those identified in this study at Hollister (Table 4). Like Hollister, high grade ore shoots in the vein deposits on the Coromandel Peninsula are characterized by banded and bladed quartz, adularia, and illite; ore minerals that include electrum, naumannite, chalcopyrite, and sphalerite; and high concentrations of Se. Illite alteration around deposits of the Coromandel Peninsula indicate proximity to veins, similarly to Hollister; however, Coromandel deposits are volcanic hosted and illite alteration is pervasive, whereas illite zones at Hollister are a result of altered adularia in veins and fractures. Some features of high grades at Hollister and the Coromandel deposits are different. For example, Hollister high grades are hosted in discrete veins, whereas those in New Zealand commonly occur in vein breccias; high grades at Hollister are also found in east-west portions of veins, which do not necessarily correspond to

bends in strike direction. Deposits of the Coromandel Peninsula commonly host high grades at fault intersections and bends in veins. Such fault intersections are not documented at Hollister; and Hollister high grades are associated with higher base metals and Sb, whereas New Zealand deposits are more associated with As, Mo, and Te. This association is observed in the Hollister disseminated deposit, but is not apparent in the high-grade veins. Boiling indication factors have not been documented in the Coromandel Peninsula, although such a project may prove useful and show similar patterns to those at Hollister, which increase toward better mineralized veins.

Exploration of vein systems in low-sulfidation veins should include careful mapping and logging of the distribution of banded and bladed quartz and adularia and its potential proxies (illite and ammonium illite). Identification of the paragenesis of the quartz textures with the goal of documenting the number of boiling cycles is critical, the more the better. The distribution of alunite and dickite in the veins themselves or overlying steam-heated caps should be mapped with SWIR reflectance spectroscopy, with the objective to identify discrete alunite-bearing zones that could indicate zones of increased H_2S flux. The goal in exploration should be to plot these key features on maps, level plans, cross-sections, and longitudinal sections, in order to recognize patterns than indicate proximity to high-grade ore shoots.

	Hollister	Coromandel Peninsula deposits	Source
Vein forms	Discrete veins	Vein breccias	Hollinger and Mauk (2001, 2002)
Vein textures	Banded quartz, bladed quartz after calcite, and chaotic quartz	Banded quartz, vein breccias, bladed quartz after calcite	Hollinger and Mauk (2001, 2002)
Gangue mineralogy	Quartz, adularia, illite, ammonium illite, smectite, kaolinite, alunite, dickite	Quartz, adularia, illite, smectite, kaolinite, calcite, chlorite	Hollinger and Mauk (2001, 2002)
Ore and sulfide mineralogy	Electrum, naumannite, aguilarite, pyrite, sphalerite, chalcopyrite, arsenopyrite, argentotennantite, tetrahedrite, clausthalite, giraudite	Electrum, acanthite, aguilarite, naumannite, pyrite, sphalerite, galena, chalcopyrite, tetrahedrite	Hollinger and Mauk (2001, 2002)
Trace element associations	Se, Cu, Zn, Sb, Pb	As, Sb, ± Mo, Te, Se	Mauk and Simpson (2007)
Structural controls	Ore shoots localized along east-west trending portions on vein; high grade veins strikes vary within 15° of 280°	Bends in veins; intersections with other veins and faults	Christie et al. (2007)
Alteration envelopes	Illite and ammonium illite envelopes in fractures around groups of veins	Distal illite-smectite; proximal illite	Simpson and Mauk (2007)
Boiling indicators	Increasing boiling indication factors from weakly mineralized veins to high-grade veins	N/A	N/A

Table 4: Summary of controls on high-grade ore shoots in Vein 18 at the Hollister deposit.

References

Albinson, T., Norman, D.I., Cole, D., Chomiak, B., 2001, Controls on formation of low-sulfidation epithermal deposits in Mexico: constraints from fluid inclusion and stable isotope data: Society Economic Geologists Special Publication 8, pp. 1 – 32.

Albinson, T. and Rubio, M., 2001, Mineralogic and thermal structure of the Zuloaga vein, San Martin de Bolaños district, Jalisco, Mexico; *Society of Economic Geologists*, special paper 8, p. 115 – 132.

Bartlett, M.W., Enders, M.S., and Hruska, D.C., 1991, Geology of the Hollister gold deposit, Ivanhoe district, Elko County, Nevada, *in* Raines, G.L., Lisle, R.E., Schafer, R.W., and Wilkinson, W.H., eds., Geology and Ore Deposits of the Great Basin: Geological Society of Nevada Symposium, Reno, 1991, Proceedings, p. 957 – 978.

Bobis, R., Jaireth, S., and Morrison, G., 1995, The anatomy of a Carboniferous epithermal ore shoot at Pajingo, Queensland: setting, zoning, alteration, and fluid conditions; *Economic Geology*, v. 90, pp. 1776 – 1798.

Brown, K.L., 1986, Gold deposition from geothermal discharges in New Zealand; *Economic Geology*, v. 81, pp. 979 – 983.

Buchanan, L.J., 1981, Precious metal deposits associated with volcanic environments in the southwest: Arizona Geological Society Digest, v. 14, pp. 237 – 262.

Christie, A., Simpson, M., Brathwaite, R., Mauk, J., and Simmons, S., 2007, Epithermal Au-Ag and related deposits of the Hauraki goldfield, Coromandel Volcanic Zone, New Zealand; *Economic Geology*, v. 102, pp. 785 – 816.

Coats, R. R., 1964, Geology of the Jarbidge quadrangle, Nevada-Idaho; USGS Bulletin 1141-M, 24 p.

Conrad, J.E., McKee, E.H., and Rytuba, J.J., 1993, Geochronology of the Sleeper deposit, Humboldt County, Nevada: Epithermal gold-silver mineralization following emplacement of a silicic flow-dome complex; *Economic Geology*, v. 88, pp. 317 – 327.

Corbett, G.J., 2005, Comments on continued exploration at the Sleeper gold mine and Environs, Nevada; confidential report for New Sleeper Gold, LLC, May, 2005.

Deng, Q., 1991, Geology and trace element geochemistry of the Hollister gold deposit, Ivanhoe district, Elko County, Nevada: Unpublished Ph.D. dissertation, El Paso, University of Texas, 313 p.

Dong, G., Morrison, G., and Jaireth, S., 1995, Quartz textures in epithermal veins, Queensland – classification, origin, and implication; *Economic Geology,* v. 90, pp. 1841 – 1856.

Drummond, S.E. and Ohmoto, H., 1985, Chemical evolution and mineral deposition in boiling hydrothermal systems; Economic Geology, v. 80, p. 126 – 147.

Ebert, S.W., and Rye, R.O., 1997, Secondary precious metal enrichment by steam-heated fluids in the Crofoot-Lewis hot spring gold-silver deposit and relation to paleoclimate: *Economic Geology*, v. 92, p. 578–600.

Eng, T., Boden, D.R., Reischman, M.R., and Biggs, J.O., 1996, Geology and mineralization of the Bullfrog mine and vicinity, Nye County, Nevada *in* Coyner, A.R., and Fahey, P.L., eds., Geology and ore deposits of the American Cordillera: Geological Society of Nevada Symposium, Reno, 1995, Proceedings, v. 1, p. 353 – 402.

Fifarek, R.H., Devlin, B.D., and Tschauder, Jr., R.J., 1996, Au-Ag mineralization at the Golden Promise deposit, Republic district Washington: Relation to graben development and hot spring processes, in Coyner, A.R., and Fahey, P.L., eds., Geology and Ore Deposits of the American Cordillera. Geological Society of Nevada Symposium Proceedings, p. 1063 – 1088.

Goldstrand, P.M., and Schmidt, K.W., 2000, Geology, mineralization, and ore controls at the Ken Snyder gold-silver mine, Elko County, Nevada, in Cluer, J.K., Price, J.G., Struhsacker, E.M., Hardyman, R.F., and Morris, C.L., eds., Geology and Ore Deposits 2000: The Great Basin and Beyond: Geological Society of Nevada Symposium, Reno, 2000, Proceedings p. 265–287.

Halsor, S.P., Bornhorst, T.J., Beebe, M., Richardson, K., and Strowd, W., 1988, Geology of the DeLamar silver mine, Idaho – A volcanic dome complex and associated hydrothermal system: *Economic Geology,* v. 188, p. 214 – 224.

Hedenquist, J., Arribas, A., and Gonzalez-Urien, E., 2000, Exploration for epithermal gold deposits; *SEG Reviews,* v. 13, pp. 245 – 277.

Hedenquist, J. and Browne, P., 1989, The evolution of the Waiotapu geothermal system, New Zealand, based on the chemical and isotopic composition of its fluids, minerals and rocks; *Geochimica et Cosmochimica Acta*, v. 53, pp. 2235 – 2257.

Hedenquist, J.W. and Henley, R.W., 1985, The importance of CO_2 on freezing point measurements of fluid inclusions: evidence from active geothermal systems and implications for epithermal ore deposition: Economic Geology, v. 80, pp 1379 – 1406.

Hollinger, E., and Mauk, J.L., 2002, Textures, mineralogy and geochemistry of low-sulfidation Au-Ag epithermal veins at the Favona deposit, Waihi, New Zealand;

Australasian Institute of Mining and Metallurgy New Zealand, Publication Series 6/02, p. 223 – 228.

Hollister, V., Hruska, D., and Moore, R., 1992, A mine-exposed hot spring deposit and related epithermal gold resources; *Economic Geology,* v. 87, p. 421 – 424.

Izawa, E., Urashima, Y., Ibaraki, K., Suzuki, R., Yokoyama, T., Kawasaki, K., Koga, A., and Taguchi, S., 1990, The Hishikari gold deposit: High-grade epithermal veins in Quaternary volcanics of southern Kyushu, Japan: Journal of Geochemical Exploration, v. 36, p. 1 – 56.

John, D.A., 2001, Miocene and early Pliocene epithermal gold-silver deposits in the northern Great Basin, western United States: characteristics, distribution, and relationship to magmatism; *Economic Geology,* v. 96, pp. 1827 – 1853.

John, D.A., Hofstra, A.H., Fleck, R.J., Brummer, J.E., and Saderholm, E.C., 2003, Geologic setting and genesis of the Mule Canyon low-sulfidation epithermal gold-silver deposit, north-central Nevada; *Economic Geology*, v. 98, pp. 425 – 463.

Leavitt, E.D., Goldstrand, P., Schmidt, K., Wallace, A.R., Spell, T., and Arehart, G.B., 2000, Geochronology of the Midas gold-silver deposit and its relationship to volcanism and mineralization along the Northern Nevada rift, in Wallace, A.R., and John, D.A., eds., Volcanic history, Structure, and Mineral Deposits of the North-Central Northern Nevada Rift: Geological Society of Nevada Symposium, Reno, 2000, Field Trip Guidebook 8, p. 157–162.

Loucks, R.R., 1984, Zoning and ore genesis at Topia, Durango, Mexico: Unpublished Ph.D. thesis, Harvard, 416 p.

Main, J.V., Rodgers, K.A., Kobe, H.W., and Woods, C.P., 1972, Aguilarite from Camoola reef, Maratoto Valley, New Zealand: Mineralogical Magazine, v. 38, p. 961 – 964.

Mauk, J.L. and Simpson, M.P., 2007, The Favona epithermal gold-silver deposit, Waihi, New Zealand; *Economic Geology*, v. 102, pp. 817 – 839.

Moncada, D., Mutchler, S., Nieto, A., Reynolds, T., Rimstidt, J., and Bodnar, R., 2012, Mineral texture and fluid inclusion petrography of the epithermal Ag-Au deposits at Guanajuato, Mexico: application to exploration; *Journal of Geochemical Exploration,* v. 114, pp. 20 – 35.

Nash, J.T., and Trudel, W.S., 1996, Bulk mineable gold ore at the Sleeper Mine, Nevada – Importance of extensional faults, breccia, framboids, and oxidation: Geological Society of Nevada Symposium, Reno/Sparks, Nevada, April 1995, Proceedings, p. 235 – 256.

Oelofse, J, Bentley, P., and van Heerden, D., 2011, Technical report on the update of the mineral resource and mineral reserve estimates for the Hollister gold mine, Elko county, Nevada, USA; unpublished company report.

Peppard, B., 2002, Geology and geochemistry of the Ivanhoe vein system, Elko, Nevada: Unpublished master's thesis, Ann Arbor, University of Michigan, 49 p.

Petruk, W., and Owens, D.R., 1974, Some mineralogical characteristics of the silver deposits in the Guanajuato mining district, Mexico; *Economic Geology*, v. 69, p. 1078 – 1086.

Potter, R.W., II, Clynne, M.A., and Brown, D.L., 1978, Freezing point depression of aqueous sodium chloride solutions; *Economic Geology,* v. 73, p. 284 – 285.

Reyes, A.G., 1990, Petrology of Philippine geothermal systems and the application of alteration mineralogy to their assessment: Journal of Volcanology and Geothermal Research, v. 43, p. 279 – 309.

Roberts, R.J., 1940, Quicksilver deposit at Buckskin Peak National mining district, Humboldt Country, Nevada: U.S. Geological Survey Bulletin 922 – E, p. 111 – 133.

Roberts, R.J., Hotz, P.E., Gilluly, J., and Ferguson, H.G., 1958, Paleozoic rocks of north-central Nevada: American Association of Petroleum Geologists Bulletin, v. 81, p. 2045–2060.

Rye, R., Bethke, P., and Wasserman, M., 1992, The stable isotope geochemistry of acid-sulfate alteration; *Economic Geology*, v. 87, pp. 225 – 262.

Sander, M.N. and Black, J.E., 1988, Crystallization and recrystallization of growth-zones vein quartz crystals from epithermal systems – implications for fluid inclusion studies: Economic Geology, v. 83, pp. 1052 – 1060.

Saunders, J.A., 1994, Silica and gold textures at the Sleeper deposit, Humboldt County, Nevada: Evidence for colloids and implications for ore-forming processes: *Economic Geology*; v. 89, p. 628 – 638.

Saunders, J.A., 2014, Textural and isotopic evidence for metallic nanoparticles in bonanza epithermal ores; SEG 2014 Conference, Keystone, Colorado, USA.

Saunders, J.A, Unger, D.L., Kamenov, G.D., Fayek, M., Hames, W.E., and Utterback, W.C., 2008, Genesis of middle Miocene Yellowstone-hotspot-related bonanza epithermal Au-Ag deposits, northern Great Basin region, USA: *Mineralium Deposita*, v. 43, pp 715 – 734.

Saunders, J.A., Peter Vikre, P., Unger, D.L., and Beasley, L., 2011, Colloidal and physical transport textures exhibited by electrum and naumannite in bonanza

epithermal veins from western USA, and their significance, *in* R. Steininger, and W. Pennell (eds.): Great Basin Evolution and Metallogeny, Geological Society of NV 2010 Symposium, May 14-22, 2010, p. 825-832.

Seward, T.M., 1989, The hydrothermal chemistry of gold and its implications for ore formation: Boiling and conductive cooling as examples: *Economic Geology* monograph 6, p. 98 – 404.

Shimizu, T., Matsueda, H., Ishiyama, D., and Matsubaya, O., 1998, Genesis of epithermal Au-Ag mineralization of the Koryu Mine, Hokkaido, Japan; *Economic Geology,* v. 93, pp. 303 – 325.

Shimizu, T., 2014, Reinterpretation of quartz textures in terms of hydrothermal fluid evolution at the Koryu Au-Ag deposit, Japan: Economic Geology, v. 109, pp. 2051 – 2065.

Sillitoe, R.H., 1993, Epithermal models: Genetic types, geometrical controls, and shallow features: Geological Association of Canada Special Paper 40, p. 403 – 417.

Sillitoe, R. and Hedenquist, J., 2003, Linkages between volcanotectonic settings, ore-fluid compositions, and epithermal precious metal deposits; *Society of Economic Geologists,* Special Publication 10, pp. 315 – 343.

Simmons, S., and Browne, P., 2000, Hydrothermal minerals and precious metals in the Broadlands-Ohaaki geothermal system: implications for understanding low-sulfidation epithermal environments; *Economic Geology*, v. 95, pp. 971 – 999.

Simmons, S.F. and Christenson, B.W., 1994, Origins of calcite in a boiling geothermal system: American Journal of Science, v. 294, p. 361 – 400.

Simmons, S.F., Simpson, M.P., and Reynolds, T.J., 2007, Significance of clathrates in fluid inclusions and the evidence for overpressuring in the Broadlands-Ohaaki geothermal system, New Zealand; Economic Geology, v. 102, pp. 127 – 135.

Simmons, S., White, N., and John, D., 2005, Geological characteristics of epithermal precious and base metal deposits; *Economic Geology,* v. 100, pp. 485 – 522.

Simon, G., Kesler, S., and Essene, E., 1997, Phase relations among selenides, sulfides, tellurides, and oxides: II. Applications to selenide-bearing ore deposits; *Economic Geology*, v. 92, pp. 468 – 484.

Simpson, M.P., Mauk, J.L., and Simmons, S.F., 2001, Hydrothermal alteration and hydrologic evolution of the Golden Cross epithermal Au-Ag deposit, New Zealand; *Economic Geology*, v. 96, pp. 773 – 796.

Simpson, M.P. and Mauk, J.L., 2007, The Favona epithermal gold-silver deposit, Waihi, New Zealand; *Economic Geology*, v. 102, pp. 817 – 839.

Singer, D.A., 1995, World class base and precious metal deposits – a quantitative analysis; *Economic Geology*, v. 90, p. 88 – 104

Unger, D.L., 2007, Geochronology and geochemistry of mid-Miocene bonanza low-sulfidation epithermal ores of the northern Great Basin, USA; Unpublished M.S. thesis, Auburn, AL, Auburn University, 100 p.

Vikre, P.G., 1985, Precious metal vein systems in the National district, Humboldt County, Nevada; *Economic Geology*, v. 80, pp. 360 – 393.

Vikre, P.G., 2007, Sinter-vein correlations at Buckskin mountain, National district, Humboldt County, Nevada; *Economic Geology*, v. 102, pp. 193 – 224.

Wallace, A.R., 1993, Geologic map of the Snowstorm Mountains and vicinity, Elko and Humboldt counties, Nevada: U.S. Geological Survey Miscellaneous Investigations Series Map I-2394, scale 1:50,000.

Wallace, A.R., 2003, Geology of the Ivanhoe Hg-Au district, Northern Nevada: influence of Miocene volcanism, lakes, and active faulting on epithermal mineralization; *Economic Geology,* v. 98, pp. 409 – 424.

Zubia, M.A., Genini, A.D., and Schalamuk, I.B., 1999, Yacimiento Cerro Vanguardia, Santa Cruz, *in* Zappettini, E.O., ed., Recursos minerals de la República Argentina: Instituto de Geología y Recursos Minerales SEGEMAR [Buenos Aires], Anales 35, p. 1189 – 1202.